POLISH ACADEMY OF SCIENCES – WROCŁAW BRANCH
WROCŁAW UNIVERSITY OF TECHNOLOGY

ARCHIVES OF CIVIL AND MECHANICAL ENGINEERING

Quarterly
Vol. X, No. 1

WROCŁAW 2010

EDITOR IN CHIEF

ZBIGNIEW GRONOSTAJSKI

EDITORIAL LAYOUT AND PROOF-READING

WIOLETTA GÓRALCZYK

TYPESETTING

SEBASTIAN ŁAWRUSEWICZ

SECRETARY

WIOLETTA GÓRALCZYK

Publisher: Committee of Civil and Mechanical Engineering
of Polish Academy of Sciences – Wrocław Branch,
Faculty of Civil Engineering and Faculty of Mechanical Engineering
of Wrocław University of Technology

OFICYNA WYDAWNICZA POLITECHNIKI WROCŁAWSKIEJ
Wybrzeże Wyspiańskiego 27, 50-370 Wrocław
http://www.oficyna.pwr.wroc.pl
e-mail: oficwyd@pwr.wroc.pl

ISSN 1644-9665

Drukarnia Oficyny Wydawniczej Politechniki Wrocławskiej. Zam. nr 233/2010.

Contents

Spis treści

ARCHIVES OF CIVIL AND MECHANICAL ENGINEERING

Vol. X 2010 No. 1

Using resistance spot welding for joining aluminium elements in automotive industry

A. AMBROZIAK, M. KORZENIOWSKI
Wrocław University of Technology, Łukasiewicza 5, 50-371 Wrocław, Poland.

The aluminium alloys are more frequently used in automotive industry especially as an alternative material for car-bodies.

In this article the comprehensive summary concerning technology of resistance spot welding of aluminium alloys was presented. The welding schedules, electric parameters of welding, electrodes materials and electrodes life time by resistance spot welding aluminium were described.

Few examples directly from automotive industry were presented and advantages of aluminium as a material for some vehicle parts were also discussed.

Keywords: *resistance spot welding of aluminium alloys, automotive industry*

1. Introduction

Aluminium as a pure metal is known since the beginning of the 18th century. It was extracted and isolated by Christian Oersted in 1825. Although the massive production method of extraction aluminium from its ore bauxite was discovered in the second half of 18th the century, the process in its basis is has been using until today. It consists of 2 stages: the first one – extraction of Al_2O_3 (aluminium oxide) from the ore, the second one – the electrolytic reduction of Al_2O_3 in high temperature bath of Na_3AlF_6 [1].

The mechanical strength of pure aluminium is relatively weak; this is the reason that for constructional purposes is used rarely. To increase the mechanical strength of pure aluminium some alloy elements are added, mainly silicon, magnesium, copper and zinc.

Currently, aluminium alloys are common used in aircraft, military industry and automotive industry. It is possible to join aluminium most of the known welding methods by using conventional equipment.

Today, the automotive industry struggles with weight problem, which should be taken into account by the engineers [2]. The demands of customers regarding safety and luxury cause the thicker sheets and components for more responsible parts of body like frame, chairs, reinforcement must be applied. This is the reason some parts of body are replaced by light materials (like aluminium and magnesium alloys [3]), which mechanical properties are similar or even better than steel.

The newest predictions estimate, that increasing use of light non-iron alloys like aluminium alloys decrease the total weight of vehicle. What is more, otherwise than in case of steel aluminium, and aluminium alloys are corrosion-resistance.

2. Properties of aluminium

Aluminium and its alloys are a silvery white which have density from 2.6 g/cm^3 up to 3.0 g/cm^3.

Although pure aluminium is light metal, the mechanical strength of some its alloys exceeds the strength of mild steel. It has high thermal and electrical conductivity, high reflectivity to both heat radiation and the light. It is non-magnetic material. The characteristic feature of aluminium is that there is no colour change during heating.

The melting temperature of pure aluminium is 660 ºC (1220 ºF). Aluminium alloys have approximately melting range from 480 ºC (900 ºF) up to 660 ºC (1200 ºF), it depends of the composition of alloying components.

Both high thermal conductivity and high electrical conductivity cause, the resistance spot welding requires welding higher current and shorter welding time (as compared to steel). What is more, the welding parameters must be controlled more precisely.

One of the disadvantages during welding aluminium is its oxide film – Al_2O_3 (known sometimes as alumina), which appears rapidly on the surface of aluminium. Its melting temperature exceeds 2000 ºC, so it should be removed chemically or mechanically before welding. The second disadvantage is high electrical conductivity. From the other hand aluminium oxide protects the surface of aluminium before the corrosion. This is the reason any coatings need to be used.

Physical properties of aluminium alloys and mild steel are presented in Table 1.

Table 1 . Physical properties of mild steel and aluminium alloys [4]

	Melting temperature [ºC]	Electrical Conductivity 10^6 [S·m]	Thermal conductivity [W/cm·K]	Coefficient of thermal expansion $10^{-6}\cdot$ [1/K]	Density [g/cm^3]
Mild steel	1560	5–10	0.32–0.66	11.4	7.8
Aluminium alloys	480–660	14.3–37.7	1.2–2.37	22–23	1.7–3.0

It was mentioned the pure aluminium is not used as a material for mechanical constructions. To make it stronger alloying ingredients as copper, zinc, manganese, magnesium, silicon are applied.

The designation of aluminium alloys indicates directly the form and composition of alloys and main alloying elements. The first digit identify the main alloying elements, the last three the composition of alloy. There are two forms of aluminium alloys: wrought and casting alloys. For automotive body sheet the wrought alloys mainly

5xxx and 6xxx series are used, so it will be taken into account. Designation of wrought alloys, the main alloying elements, production forms and application are presented in Table 2 [1], [4].

Table 2. Designation, product form, and application of aluminium alloys

Aluminium wrought alloy designation	Product form	Application
Pure aluminium 1XXX*	Foil, rolled plate, extrusions	Packaging and foil, roofing, cladding, low-strength corrosion resistant vessels and tanks
2XXX (Al-Cu)	Rolled plate and sheet, extrusions, forgings	Highly stressed parts, aerospace, structural items, heavy duty forgings, heavy goods vehicle wheels, cylinder heads, pistons
3XXX (Al-Mn)	Rolled plate and sheet extrusions, forgings	Packaging, roofing and cladding, chemical drums and tanks, process and food handling equipment, vehicles
4000 series (Al-Si)	Wire, castings	Filler metals, cylinder heads, engine blocks, valve bodies, architectural purposes
5000 series (Al-Mg)	Rolled plate and sheet, extrusions, forgings, tubing, piping	Cladding, vessel hulls and superstructures, structural members, vessels and tanks, vehicles, automotive body sheet
6000 series (Al-Si-Mg)	Rolled plate and sheet, extrusions, forgings, tubing, piping	High-strength structural members, vehicles, rolling stock, marine applications, architectural applications, automotive body sheet
7000 series (Al-Zn)	Rolled plate and sheet, extrusions, forgings	High-strength structural members, heavy section aircraft forgings, military bridging, heavy goods vehicle

* In case of pure aluminium the last two digits indicate the minimum purity of aluminium (e.g., 1060 is 99.60% Al minimum).

3. Applying aluminium alloys in automotive industry

Aluminium is the ideal material for future development of designing car bodies. The main purpose for applying aluminium is decreasing total weight of vehicle by assuming, that safety, and strength of constriction will be at least the same. What is more, applying aluminium as an alternative material involves the aspect of engine-load reduction and decreasing the consumption of gasoline and the reduction of exhaust emission.

Furthermore, the costs of exploitation of vehicle concerning breaks, tries, bearings and many others will decrease as well.

It was proved that the reduction the total mass of vehicle of 10% involves saving 6–8% of gasoline. Decreasing the total weight of each 100 pound causes savings 3.4–5.3 per 1000 miles [5].

Aluminium is fully recyclable. Its scarp can be easy recovered. Moreover, it can be recycled again and again without changing quality. Its properties will be the same as aluminium obtained from its ore. Even now, approximately 60–70% aluminium used

in vehicles (engine, body, wheels, etc.) comes from recycling. The cost of recycling of aluminium is considerably lower than steel due to lower than in case of steel the energy consumption.

There is one disadvantages connected with recycling of aluminium alloys. The different alloys must be selected and they cannot be mixed. It is especially important and crucial by production of sheets.

4. Resistance spot welding

The resistance spot welding is the most popular method of joining metal sheets. The connection arises by flowing the current and action of welding force. Heating of joining parts during resistance welding is an effect of heat generation on electrical resistance of welding circuit according to Joule–Lenz law:

$$Q(t) = \int_0^{\tau} I(t) \cdot R \cdot dt \tag{1}$$

where:

Q – generated heat,
I – welding current,
R – electrical resistance of welding circuit,
t – welding time.

Scheme of resistance spot welding was shown on Figure 1.

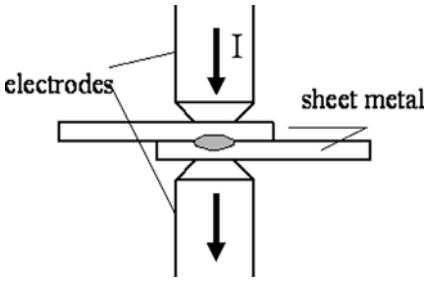

Fig. 1. Schematic view of the spot welding process [6]

Connecting 2 or 3 parts of sheets is possible by the resistance spot welding. During this process one or more welding joints can be obtained. It depends of applied welding machines.

Resistance spot welding (RSW) is the most popular method of joining parts in automotive industry, which prefers this joining method because it is low-cost, rapid, simply and easy for automation. Over 90% of spot welds of all over the world are performed by automotive industry [7]. It was estimated, that each body car and its com-

ponents contains over 50 hundred spot welds. For many years the material the car-bodies consisted of was mild steel, with or without galvanized layers. Now, the engineers try to find alternative light-materials: aluminium and magnesium alloys.

Unconformities which can appear in spot welds cause the spot welds can have less strength and can lead into total destruction of manufacturing parts of cars bodies. The typical unconformities of spot welds are [8]:

- cold weld,
- small-diameter nugget,
- bad shape of welding nugget,
- cracks inside/around welding nugget,
- deep indentation of welding electrodes in sheets.

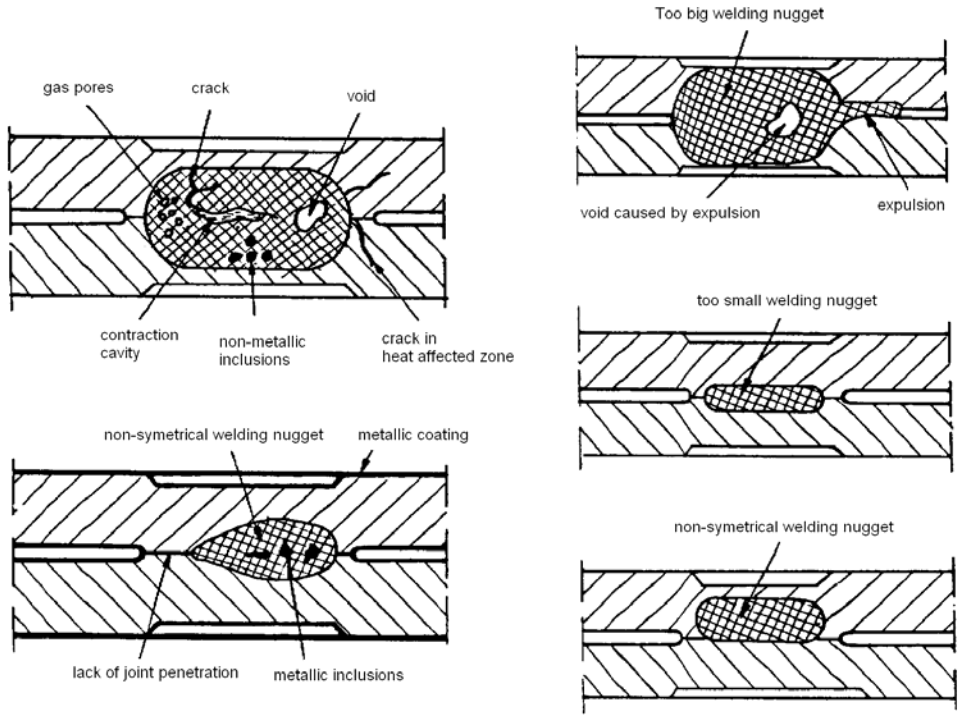

Fig. 2 Typical flaws in spot welding joints [9]

5. Resistance spot welding of aluminium

The weldability of aluminium alloys used by joining car bodies is very good but some conditions and rules must be applied. Resistance Spot Welding of aluminium and its alloys involves applying high power welding guns because welding current must be 2–3 times higher than in case of steel but the welding time is 1/3 weld time of

steel. The main of that is 3 times higher than in case of steel its thermal and electrical conductivity. It means the electric parameters (current and voltage) must be controlled more precisely in narrower window of time [10].

Sometimes the welding guns using for welding steel has not enough power to ensure required welding current, thus the sources of power are often designed for resistance spot welding of aluminium.

The comparison the typical RSW parameters for 1.0+1.0 mm mild steel and aluminium sheets are included in Table 3.

Table 3. RSW parameters for 1.0+1.0 mild steel and aluminium sheets

Material	Welding current [kA]	Welding time [periods for 50 Hz]	Welding Force [kN]
Mild steel	11	8	2.7
Aluminium alloy 5xxx, 6xxx series	25	4	2.5

6. Electrodes for resistance welding aluminium

An ideal electrode's material for RSW of aluminium should have high thermal and electrical conductivity and high hardness as well. Moreover it shouldn't tend to make alloys thus it is very difficult to find a compromise. The pure electrolytic copper has a conductivity 100% IACS (58 MS·m), however its hardness is relativity low (considerably below 100HV) and its tendency to alloying with aluminium is very high.

The main problem connected with electrodes by Resistance Spot welding of aluminium and its alloys is relatively short time of life of electrodes [11]. It can be a crucial problem especially by massive production. The rapid deterioration of tips surface is the result of high pressure, high temperature and alloying process during welding [11], which directly involves pickup effect, electrode alloying with aluminium, pitting effect and cavitations. Thus the quality of spot-welds rapidly decreases. The comprehensive numerical and experimental study, concerning pitting effect and its influence on spot-welds quality of aluminium-alloys joints were described in [12–14].

The alloying effect causes increasing resistance of contact tip-sheet. This is the reason the heat is generated in tip-sheet layer, instead sheet-sheet. To ensure the better contact between electrode and worksheet the lubricants are applied. It was investigated, that some metalworking lubricants extended the electrodes life-time and directly led to reduction alloying effect and concurrently pitting and pickup effect [15].

To avoid high costs of electrode's materials replaceable caps are used and also cleaning after at least 20 spot-welds is required as well.

It was proved, that increasing hardness of electrodes reduces mushrooming of electrodes. To achieve higher hardness pure copper is alloyed by zirconium, cadmium, chromium and also dispersion hardened with aluminium oxide is used. It was investigated that using some special copper alloys especially alloyed by gold [16–17]. This way 5 times longer time of life can be achieved.

Recommended by resistance welders manufacturing association electrodes for spot welding aluminium are group A class 1 alloys.

Group A class 1 alloys have the highest electrical conductivity thus are the best for welding pure aluminium worksheets. For Al-Mg and Al-Mg-Si alloys higher hardness is required so, electrodes A class 2 can be used. [4]. Electrodes materials properties were presented in Table 5.

Table 4. Resistance welding electrodes materials [4]

Copper alloy class	Properties	Application
A1	high conductivity 95–100% IACS (ca. 58 MS·m)	resistance welding of aluminium and aluminium alloys
A2/1 A2/2	Hardness: 130–170 HV, electric conductivity: 80% IACS (43 MS/m), softening temperature: 450–500ºC	resistance welding of mild steel, brass, aluminium alloys
A3/1	Hardness: 160–240 HV, electric conductivity: 50% IACS (23 MS/m), softening temperature: over 500ºC	resistance welding of stainless and austenitic stainless steel

The properties of copper alloys using for electrodes in automotive industry are presented in Table 5. In the columns shaded on grey, properties of copper alloys for resistance spot welding of aluminium are mentioned.

Table 5. Composition, physical and mechanical properties of electrode's copper alloys [18]

Designation of alloy	CRM16X	BICOP	CB4
Composition	Cr: >0.4% Zr: 0.3–0.15	Al: 0.6%	Co: 2.2% Be: 0.5%
Hardness [HB]	160	150	240–260
Conductivity [% IACS]	76–46	85	>43
Tensile strength MPa	480	430	700

Table 6. Electrodes diameter and recommended nugget size related to sheet thickness for mild steel and aluminium alloys series 1xxx, 3xxx, 5xxx and 6xxx [1]

Thickness of worksheets [mm]	Electrode diameter [mm]		Electrode dome radius [mm]		Nugget size [mm]	
	Al	Mild Steel	Al	Mild Steel	Al	Mild Steel
0.5	16	3.5	50	65	2.5	2.5
0.8	16	4.5	50	74	3.5	3.6
1.0	16	5	100	80	4.0	4.6
1.3	16	6	100	87.5	4.5	5.1
1.6	16	6	100	98	5.2	5.8
2.0	22	7	150	110	5.7	6.6
2.5	22	8	150	125	6.5	7.1
3.2	22	9	150	146	7.1	7.6

To maintain correctly tips condition electrodes efficient cooling must be ensured. The coolant flow rate should be of 5–10 litres per minute (more than in case of steel). Its temperature should be ca. 20 ºC in inlet area and outlet area 30 ºC. Inlet channel should be carried as close to the tips as possible by the distance 12–20 mm from outlet channel.

In Table 6 technological parameters of electrodes for welding aluminium alloys and mild steel are presented. Please notice that diameter of tips and dome radius is bigger for aluminium alloys.

6. Conclusions

According to the newest studies, automotive industry tends to use light alloys like aluminium and magnesium alloys. Companies more often use aluminium as an alternative material for vehicle body. The most popular method of joining body sheets is resistance spot welding. Aluminium and its alloys series 5xxx and 6xxx can be connected by this technique. It requires high power welding gun and precocious steering of current and time. The aspects of rapid deterioration of tips must be taken into account.

References

[1] Mathers G.: *The welding of aluminium and its alloys*, Woodhead Publishing Limited, Cambridge, England, 2002.
[2] Carle D., Blount G.: *The suitability of aluminium as an alternative material for car bodies*, Materials and Design, Vol. 20, No. 5, 1999, pp. 267–272.
[3] Kawalla, R., Lehmann, G., Ullmann, M.: *Magnesium semi-finished products for vehicle construction*, Archives of Civil and Mechanical Engineering, 2008, Vol. 8, No. 2, pp. 93–101.
[4] Welding Handbook, Vol. 3, 8th Edition, American Welding Society, 1992.
[5] The Aluminium Association, Inc.: *Aluminium industry roadmap for the automotive market: enabling technologies and challenges for body structures and closures*, May, 1999.
[6] Chertov, A.M., Maev R.G.: *A one-dimensional numerical model of acoustic wave propagation in a multilayered structure of a resistance spot weld, ultrasonics, ferroelectrics and frequency control*, Vol. 52, Issue 10, pp. 1783–1790.
[7] Papkala H., Pietras A., Zadroga L.: *Zgrzewanie rezystancyjne punktowe blach ocynkowanych*, Przegląd Spawalnictwa, No. 5–7, 2004, pp. 51–57.
[8] Ambroziak A., Korzeniowski M., Kustron P.: *Quality control of spot welds – the challenge for automotive industry, inżynieria produkcji. Wiedza – wizja – programy ramowe*, Pod red. E. Chlebusa, Wrocław, Oficyna Wydaw. PWroc., 2006, pp. 359–366.
[9] A. Klimpel: *Kontrola i zapewnienie jakości w spawalnictwie*, WPS, Gliwice, 1998.
[10] Aloca Inc.: Spinella D.J., Brockenbrough J.R., Fridy J.M.: *Trends in aluminium resistance spot welding for the auto industry*, Vol. 84, No. 1, 2005, pp. 34–40.
[11] Li Z., Hao C., Zhang J., Zhang H.: *Effects of sheet surface conditions on electrode life in resistance welding aluminium*, Supplement to Welding Journal, Vol. 86, No. 4, 2007, pp. 81–89.

[12] Lum I., Fukumoto S., Birdo E., Boomer D.R., Zhou Y.: *Electrode pitting in resistance spot welding of aluminium alloy 5182*, Metallurgical and Materials Transactions, Vol. 35, No. 1, 2004, pp. 217–226.
[13] Zhou Y., Fukumoto S., Peng J., Ji C.T., Brown L.: *Experimental simulation of surface pitting of degraded electrodes in resistance spot welding of aluminium alloys*, Materials Science and Technology, Vol. 20, No. 10, 2004, pp. 1226–1232.
[14] Chang B.H., Zhou Y., Lum I., Du D.: *Finite element analysis of effect of electrode pitting in resistance spot welding of aluminium alloy*, Science and Technology of Welding and Joining, Vol. 10, No. 1, 2005, pp. 61–66.
[15] Rashid M., Fukumoto S., Medley J.B., Villafuerte J., Zhou Y.: *Influence of lubricants on electrode life in resistance spot welding of aluminium alloys*, Welding Journal, Vol. 86, No. 3, 2007, pp. 62–70.
[16] Kumagai M., Sano H.: *Effect of Cu-Ag-O electrode on resistance spot welding of aluminium alloy sheet*, JASE Review, Vol. 17, No. 1, 1996, pp. 83–83.
[17] Elmedur X, Technical Datasheet, Thyssen Durometall.
[18] Electral, Le bronze Industrial datasheets.

Zastosowanie zgrzewania oporowego do zgrzewania konstrukcji w przemyśle motoryzacyjnym

Stopy aluminium są coraz częściej stosowane jako materiał alternatywny do budowy elementów karoserii samochodowych.

W artykule opisano technologiczne problemy podczas zgrzewania oporowego punktowego materiałów ze stopów aluminium (głównie z grupy 5xxx i 6xxx), skupiając się na parametrach elektrycznych zgrzewania, materiałach na elektrody oraz czasie ich życia.

Przedstawiono zalety zastosowania materiałów ze stopów aluminium, jako materiału, z którego mogą być wykonywane niektóre części w pojazdach samochodowych.

ARCHIVES OF CIVIL AND MECHANICAL ENGINEERING

Vol. X 2010 No. 1

Stochastic models of particle distribution in separation processes

J. DETYNA
Wrocław University of Technology, Institute of Materials Science and Applied Mechanics,
Smoluchowskiego 25, 50-370 Wrocław, Poland, phone: +48604789008, e-mail: jerzy.detyna@pwr.wroc.pl

Separation processes are important in industry. The understanding of the fundamentals of granular separation on sieve surfaces is incomplete. It results from the fact that granular matter is a system of many particles interacting via short ranged repulsive and dissipative forces, both normal and tangential to the surface of contact. We can try describing the separation processes by the Newton equations in a deterministic way. However, the models contain quite a lot of simplifications and therefore such models are not very useful. We perceive separation process as process of random character. Therefore, we can use statistical models to describe the separation process. In this article I presented the methodology of modelling and the way of using selected probability density functions. Parameters of these functions were appointed on the basis of regressive methods.

Keywords: *separation, granular matter, statistics, distribution*

1. Introduction

Modelling dynamic systems is a discipline, which immersed out of entire abundance of natural sciences, amongst which mathematics and physics are reckoned to be the most important. On the other hand, modelling is an art of competent connection of mentioned disciplines in order to fit the course of the analyzed process to the course represented by empirical data into the most optimal way.

Possibilities of their explicit deterministic description are strongly limited or simply impossible because the examined phenomena are very complicated. It refers mainly to physical systems with a large number of particles. Great number of predictive parameters connected with the number of freedom degrees for every of them makes the possibility of constructing correct equations of movement questionable. On the other hand, they may never be solved even using the newest numerical machines [17].

In such cases, statistical models (or else stochastic models) have high utilitarian significance. These methods are based on observation of the correctness, which may not appear in systems of this type. These observations are usually dependable on examination of randomization of initial variables and their description using appropriate distribution functions.

Separation process of granular particles is an excellent example of probabilistic experiment, which authors of many publications are trying to define in deterministic frames. Effects of such operations can have only fairly approximate character in the aspect of the course of the given process [6, 8]. If completely naturally, we describe this phenomenon a statistical rank (drawing particles on the surface of the discrete element) then its description will be much more complete for any number of predictive variables [11, 14].

2. Purpose of the work

Distribution of granular mixtures on discrete elements (sieves) has been described in detail in numerous academic publications [4–7, 10]. However, differential equations of the particles' movement have usually been used for the mathematical description of this phenomenon. Generated models, together with imposed initial conditions, can be used for the description of the analysed process. However, it should be rated that values appointed through such models diverge considerably from empirical data. The randomization of the given phenomenon, which results from its nature, is responsible for such "state of affairs".

Deterministic methods of description of the separation process are not possible in some model cases. This is the case when we want to connect variables with each other in the model, but then the number of preliminary conditions and equations of the given model is becoming completely impossible thus making the problem unsolvable [15–16, 18]. Generally, we can formulate every model by the functional relation in the form:

$$y_j = f(x_i, D_k), \qquad i = 1, 2, \ldots, m, \qquad j = 1, 2, \ldots, n, \qquad k = 1, 2, \ldots, o, \tag{1}$$

where y_j is j-dependent variable, x_i makes i-predictive variable, D_k depicts k-parameter of the model.

The need for the improvement of the existing construction solutions in the aspect of the quality of the process separation is mostly displayed in research on possibilities of using sieves with the variable surface geometry. In such case, (symbolically called) geometrical variables are the predictive factors. Analysis of the influence of this type of variables can be carried out using statistical methods and models. The source of inspiration for writing this publication was the attempt to use the statistical model to determine the influence of chosen predictive variables on quality of the particle separation process. Universally known probability distributions were taken into consideration in proposed models [12].

3. Methodology of research

Research was carried out on the stationary experimental stand. A blade sieve of the sectional type is a main work element of the post (Figure 1). The sieve is equipped with

the mechanism for adjustment of the angle of lowering the blind, which results in obtaining the working slit of the sieve in the range from 0 to 8 mm [2–3]. The construction of sieve basket enables to adjust the angle of section blind within limits 0–15°.

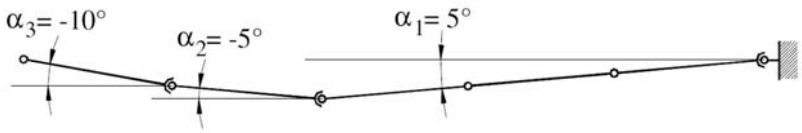

Fig. 1. Adjusting angles for the sectional sieve

An electric engine, whose rotational speed was controlled continuously by means of frequency converter, was used for the drive system. Such drive enables precise selection of kinematical parameters of active elements of the system [4].

The research was carried out on the material with the following parameters:

- spring wheat of the ETA type,
- grain humidity 12.1–12.7 (%).

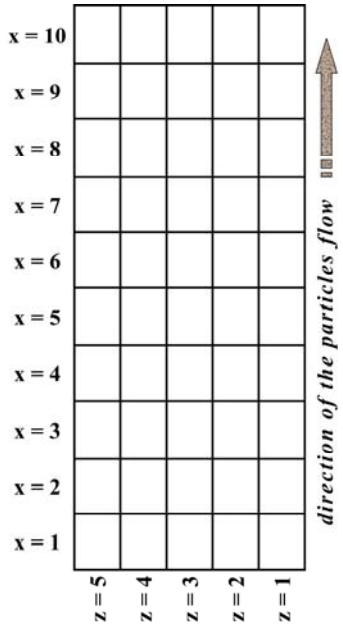

Fig. 2. The division (and label) of surface of the sectional sieve to measuring zones

While doing research we changed the adjustment of the sieve section in the crosswise surface and the angle of side inclination of the entire sieve basket [9]. We were measuring the sifting mass during research under the sieve in definite measuring zones (Figure 2). We described the cleanness of grain and we carried out the measurement of

duration of the process. A laboratory weight of high-class accuracy was the basic measuring device [4–5].

Series of preliminary observation enabled to determine variable parameters of inclination of the sieve basket and the section of the sieve before starting the fundamental research. All measurements were carried out at fixed (optimal for given material) wide opening of sieve blinds.

In order to become independent from unchecked factors (changeable humidity of cleaned material during research, different grade of pollutants changing in harmony with the certain gradient) a completely random system of experiment was chosen, in which a generator of random numbers decided about order of measurements.

An identical way of proceedings was accepted for meeting conditions of the comparability of obtained results, keeping dependences accepted in methodology.

4. Selected distributions of random variables

4.1. Gamma distribution

In literature the Gamma distribution appears in the form of the three-parametrical distribution, two-parametrical and in the standard form [1]. Three-parametrical Gamma distribution has density function of the following form:

$$f(x)=\begin{cases}\dfrac{b^{\lambda}}{\Gamma(\lambda)}(x-x_0)^{\lambda-1}\cdot e^{-b(x-x_0)} & for\ \ x\geq x_0>0\\ 0 & for\ \ x\leq 0\end{cases}, \tag{2}$$

where $b > 0$, $\lambda > 0$.

Numerical characteristics for this form of the Gamma distribution are the following:

– expected value: $EX = x_0 + \lambda/b$,

– variance: $V(X) = \lambda/b^2$,

– asymmetrical coefficient: $A_x = 2/\sqrt{\lambda}$.

In practice the two-parametric distribution is more frequent form of the Gamma distribution. This density function has the following form:

$$f(x)=\begin{cases}\dfrac{b^{\lambda}}{\Gamma(\lambda)}x^{\lambda-1}\cdot e^{-bx} & for\ \ x\geq x_0>0\\ 0 & for\ \ x\leq 0\end{cases}, \tag{3}$$

where $b > 0$, $\lambda > 0$.

This form of the Gamma distribution is characterized by the following parameters:

- expected value: $EX = \lambda/b$,
- variance: $V(X) = \lambda/b^2$,
- asymmetrical coefficient: $A_x = 2/\sqrt{\lambda}$,
- modal: $M_x = \begin{cases} 0 & for\ \ \lambda \le 1 \\ (\lambda - 1)/b & for\ \ p > 1 \end{cases}$.

Standard form of the Gamma distribution has the density function defined as

$$f(x) = \begin{cases} \dfrac{x^{\lambda-1} \cdot e^{-x}}{\Gamma(\lambda)} & for\ \ x > 0 \\ 0 & for\ \ x \le 0 \end{cases}. \tag{4}$$

Forms of the density function of the standard Gamma distribution for different value of the parameter λ is presented in Figure 3.

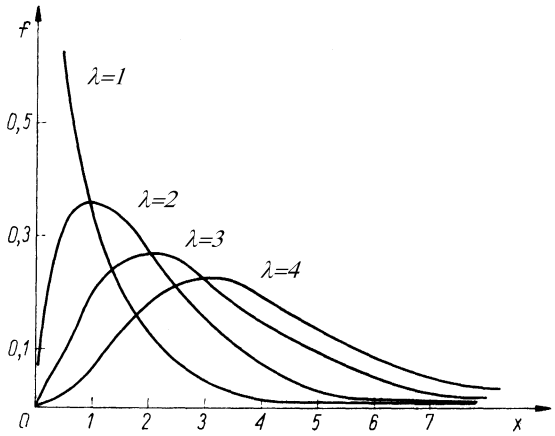

Fig. 3. Density function of the Gamma distribution according to four values of λ parameters

4.2. Beta distribution

The family of Beta distributions has the density function of general form:

$$f(x) = \begin{cases} \dfrac{1}{B(p,q)} \dfrac{(x-a)^{p-1}(b-x)^{q-1}}{(b-a)^{p+q-1}} & for\ \ a \le x \le b \\ 0 & for\ \ x < a \quad or \quad x > b \end{cases}, \tag{5}$$

where $p > 0$, $q > 0$, whereas function $B(p, q)$ is described by the formula:

$$B(p,q)=\int_0^1 t^{p-1}(1-t)^{q-1}dt=\frac{\Gamma(p)\cdot\Gamma(q)}{\Gamma(p+q)}. \tag{6}$$

Describing the standard form of the density function of the Beta distribution of I kind is possible through the relation:

$$f(x)=\begin{cases}\dfrac{1}{B(p,q)}\,x^{p-1}(1-x)^{q-1} & for\ \ 0\le x\le 1\\ 0 & for\ \ x<0\quad or\quad x>1\end{cases}, \tag{7}$$

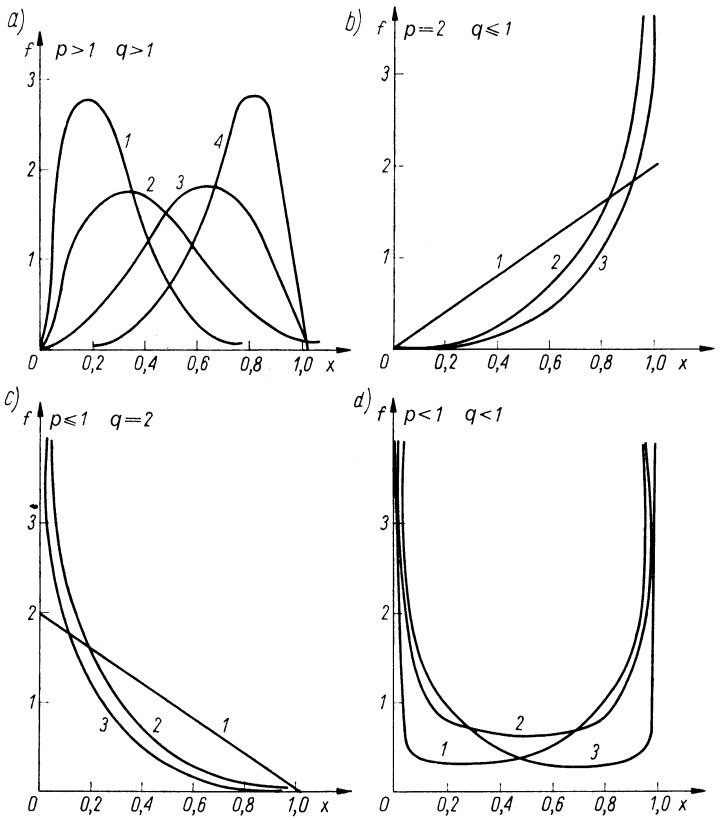

Fig. 4. Density function of the Beta distribution of I kind with several different values of p, q parameters

The form of the Beta distribution of I kind, which is described above, is characterized by the following parameters:

- expected value: $EX = p/(p + q)$,
- variance: $V(X) = p \cdot q/[(p + q)^2(p + q + 1)]$,
- asymmetrical coefficient: $A_x = [2(p - q)/(p + q + 2)] \cdot \sqrt{(p + q + 1)/p \cdot q}$,
- modal: $M_x = (p - 1)/(p + q - 2)$ for $p \geq 1$, $q \geq 1$, $(p + q) > 2$.

The plots of a density function of the standard Beta distribution of I kind, according to their parameters are presented in Figure 4.

5. Modelling the distribution of the particle concentration

The practice of statistical modelling introduces a more and more sublimated problem. It is connected with the action, which in the end leads to the generation of models tightly fitting to empirical variables [11, 13]. Above arguments and the problem of the description of separation processes analysed in this paper, it should be stated that only two-dimensional distributions, whose marginal probability density functions are characteristic of (by values of parameters) asymmetry, can challenges this task. If variables X (connected with the length of the sieve) and Y (connected with the width of the riddle) are independent, then it is possible to introduce the two-dimensional distribution density function as:

$$f(x, y) = f(x) \cdot f(y) \tag{8}$$

where $f(x), f(y)$ are distributions of random variables X and Y.

The independence of random variables was verified on the basis of the value the covariance of random variables X and Y and on the basis of the test results for independence χ^2. Results of the test did not give basis for rejecting the hypothesis about the independence X and Y [1].

The collection of asymmetrical functions for continuous random variables is large. On the basis of tests carried out earlier and on essential issues concerning the separation process, we have finally chosen the Beta and Gamma distribution. The Beta distribution describes the distribution of particles separated crosswise to the direction of their stream Y, on the other hand the Gamma reconstructs the character for the lengthwise distribution X. Functional forms of these distributions were described above in detail.

Parameters of the probability density function of the modelled random vector were appointed on the basis of the gathered empirical material, and the usage of numeric tools.

Estimated value of parameters of the Beta and the Gamma distribution determine the base for expressing the existing relations between quantities in the form of functional dependencies. Multiple regression methods were used for the identification of distributions parameters. The calculations were carried out in the Statistica® program of the StatSoft™ company.

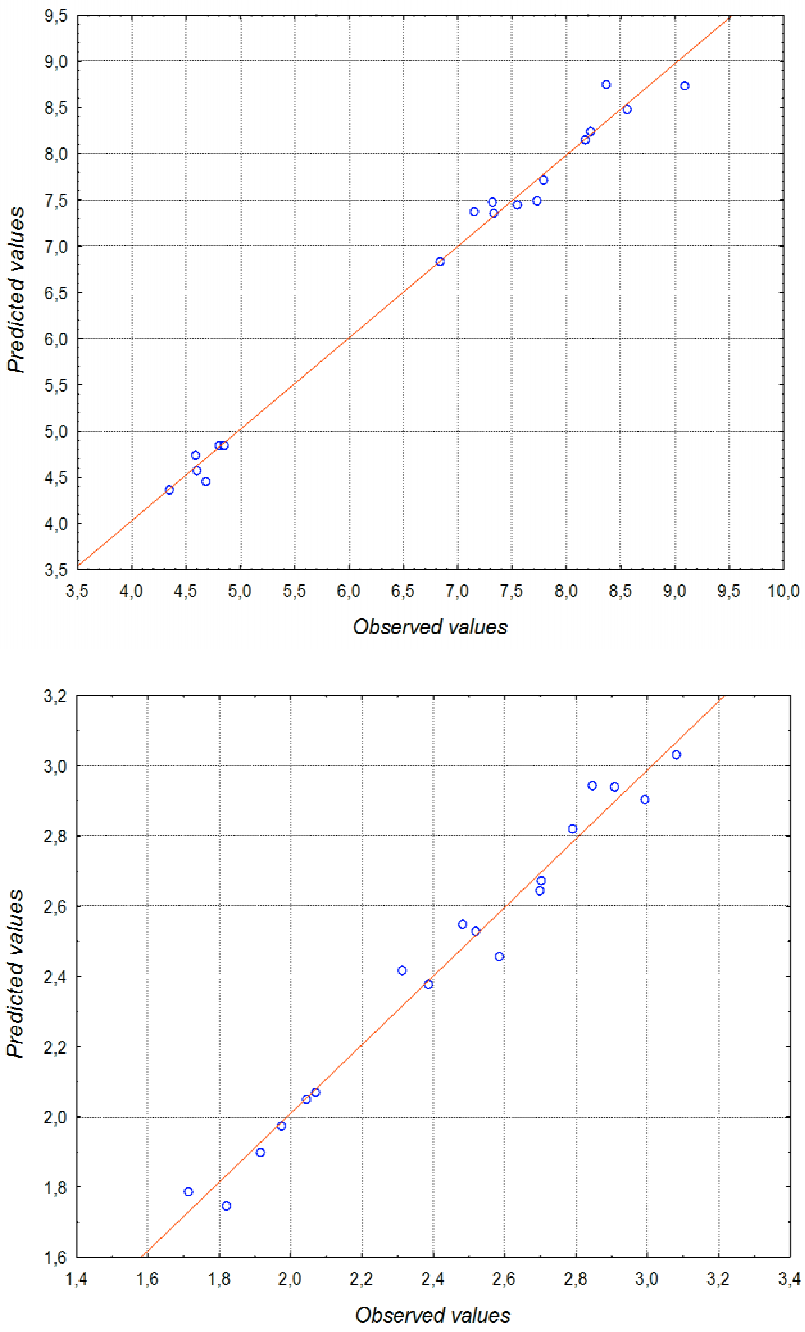

Fig. 5. Correlation graphs of observed and predicted values according to the regressions function of parameters b (above) and λ (below)

For the Gamma distribution of which the probability density is expressed with the dependence, the regression functions for parameters (b, λ) take the form:

$$b = 2.9440 - 0.0305\cdot\alpha_1 - 0.0058\cdot\alpha_1^2 - 0.0501\cdot\alpha_2 - 0.0049\cdot\alpha_2^2 + \\ + 0.0021\cdot\alpha_3 - 0.0011\cdot\alpha_3^2 + 0.0059\cdot\alpha_1\cdot\alpha_2 + 0.0022\cdot\alpha_1\cdot\alpha_3 \quad (9)$$

$$\lambda = 0.1142 - 0.0031\cdot\alpha_1 + 0.0012\cdot\alpha_1^2 \quad (10)$$

Correlation of empirical and theoretical value was presented in Figure 5 appropriately for functional relations described above.

Regressive forms of parameters for the density probability function of the Beta distribution are the following:

$$p = 1.4856 - 0.1104\cdot\alpha_1 + 0.067\cdot\alpha_1^2 - 0.0903\cdot\alpha_2 - 0.0111\cdot\alpha_2^2 - \\ - 0.0013\cdot\alpha_3 - 0.0017\cdot\alpha_3^2 + 0.0068\cdot\alpha_1\cdot\alpha_3 \quad (11)$$

$$q = 2.1439 - 0.0346\cdot\alpha_1 + 0.0188\cdot\alpha_1^2 - 0.0775\cdot\alpha_2 - 0.0082\cdot\alpha_2^2 - \\ - 0.0448\cdot\alpha_3 - 0.0022\cdot\alpha_3^2 + 0.0025\cdot\alpha_1\cdot\alpha_2 + 0.0096\cdot\alpha_1\cdot\alpha_3 \quad (12)$$

Plots of observed and predicted values for the regression function were depicted in Figure 6a, b.

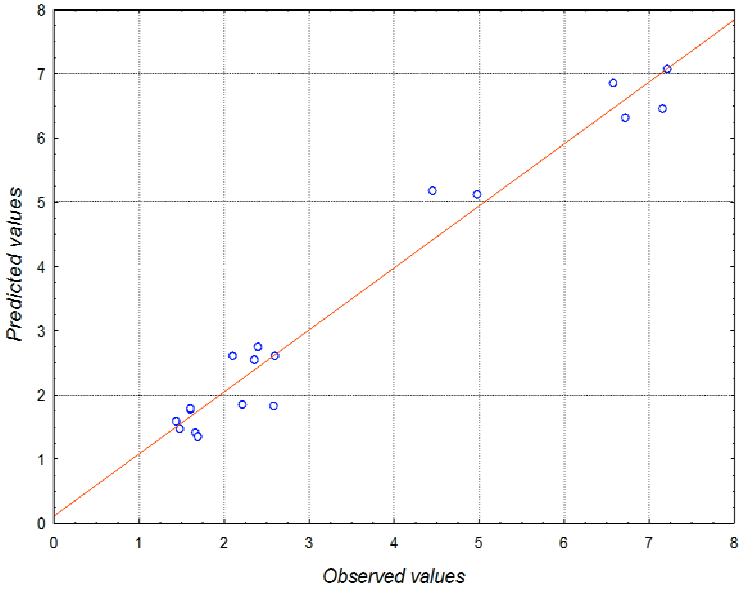

Fig. 6a. Correlation graphs of observed and predicted values according to the regression function of parameters p (above) and q (below)

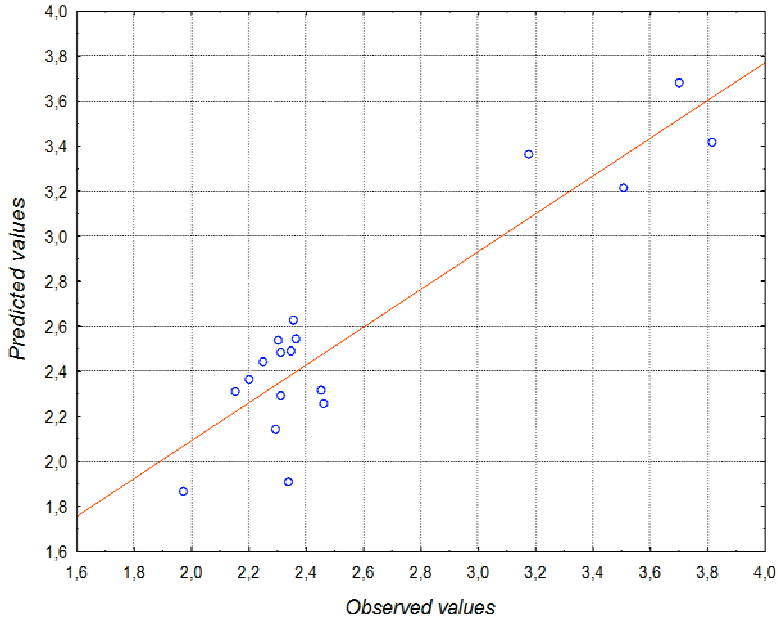

Fig. 6b. Correlation graphs of observed and predicted values according to the regression function of parameters p (above) and q (below)

6. Conclusions

In this publication we present estimation works which confirmed our assumptions concerning the connection between chosen external variables with the quality of particles distribution. Appointed regressive functions are close to empirical data. Determination coefficient R^2 for parameters b, λ, p takes value over 0.92. Only the fourth model concerning the endogenous variable q approximates its values with a little lower coefficient $R^2 = 0.84$. If we have in mind the fact that the research refers to biological material, for which the repeatability is also a random variable in the range of the separation feature, we need to assume that the quality of fitting the model is very good.

The presented procedure can successfully be applied to influence the analysis of series of other factors on the quality of the separation process. A selection of the appropriate distribution function and right random method is usually the most difficult problem. It is obvious that the quality of the modelled problem depends to a large extend on the way of carrying out the research. It concerns the cardinality of measurements and their quality mainly (accuracy).

Appointed functions of the particle distribution have high utilitarian significance in the construction aspect. It is possible to use described equations for finding optimal value of parameters α_1, α_2, α_3 in this particular case in relation to the desirable distribution of a particle. Moreover, appointed functional relations can be used for dynamic

control of predictive parameters, if one of them is subject to change according to the time function.

References

[1] Barlow R.J.: *Statistics: A guide to the use of statistical methods in the physical sciences*, "Wiley", New York, 1989.

[2] Beck F., Zhao Y., Kutzbach H.D.: *Mähdreschersimulation. Modellierung der Korn/Stroh /Spreu – Trennung*, Jahrgang Landtechnik, Vol. 4, 1997, pp. 180–182.

[3] Bieniek J., Banasiak J., Detyna J.: *Selected constructional aspects of sectional sieves with variable geometry, destined for combines-harvesters*, Systems, Vol. 8, No. 2, Publishing company of the Wrocław University of Technology, Wroclaw, 2004, pp. 141–152.

[4] Bieniek J., Banasiak J., Lewandowski B, Detyna J.: *Cleanness of the grain obtained on the sectional sieve*, Acta Agrophysica, No. 46, 2001, pp. 7–14.

[5] Bieniek J., Banasiak J., Lewandowski B., Detyna J.: *The analysis of the capacity of the sectional shutter sieve conditioned of the variable inclination*, The Agricultural Engineering Science, No. 1, 2001, pp. 27–32.

[6] Bruno L., Calvo A., Ippolito I.: *Granular Mixing and Diffusion: a 3-Dimensional Study*, International Journal of Heat Technology, Vol. 21, No. 1, 2003, pp. 67–73.

[7] Castro J., Ostoja-Starzewski M.: *Particle sieving in a random fibre network*, Applied Mathematical Modelling, Vol. 24, No. 8–9, "Elsevier" 2000, pp. 523–534.

[8] De Gennes P.G.: *Granular matter: A tentative view*, Rev. Mod. Phys., Vol. 71, 1999, pp. 374–382.

[9] Detyna J.: *Analysis of influence of the geometry of blade sieve on the course of the grain cleaning process...*, PhD thesis, Wrocław, 2000.

[10] Detyna J., Bieniek J.: *Methods of statistical modelling in the process of sieve separation of heterogeneous particles*, Applied Mathematical Modelling, Vol. 32, No. 6, 2008, pp. 992–1002.

[11] Ditlevsen O.: *Stochastic models for atmospheric particle dispersion*, Probabilistic Engineering Mechanics, Vol. 18, No. 2, 2003, pp. 97–106.

[12] Dudek D.: *Elementy dynamiki maszyn górnictwa odkrywkowego. Akwizycja sygnałów. Analiza układów*, Oficyna Wydawnicza Politechniki Wrocławskiej, Wrocław, 1994.

[13] Greenspan D.: *Computer studies in particle modelling of fluid phenomena*, Mathematical Modelling, Vol. 6, No. 4, 1985, pp. 273–294.

[14] Makse H.A.: *Continuous avalanche segregation of granular mixtures in thin rotating drums*, Phys. Rev. Lett., Vol. 83, 1999, pp. 3186–3189.

[15] Khakhar D.V., McCarthy J.J., Ottino J.M.: *Mixing and segregation of granular materials in chute flows*, Chaos, Vol. 9, 1999, pp. 594–610.

[16] Ottino J.M., Khakhar D.V.: *Open problems in active chaotic flows: Competition between chaos and order in granular materials*, Chaos: An Interdisciplinary Journal of Nonlinear Science, Vol. 12, 2002, pp. 400–407.

[17] Rusiński E., Harnatkiewicz P., Bobyr M., Yakhno B.: *Caterpillar drive shaft damage causes analysis*, Archives of Civil and Mechanical Engineering, Vol. 8, 2008, pp. 117–130.

[18] Solomon T.H., Tomas S., Warner J.L.: *Chaotic mixing of immiscible impurities in a two-dimensional flow*, Phys. Fluids, Vol. 10, 1998, pp. 342–350.

Statystyczne modele rozkładu cząstek w procesie separacyjnym

Procesy separacyjne mają istotne znaczenie w wielu gałęziach przemysłu. Jednakże z punktu widzenia teoretycznego proces separacji nie został jeszcze dokładnie rozpoznany. Wynika to m.in. z faktu, że w procesie separacyjnym mamy do czynienia z materią granulowaną, która jako system składa się z dużej ilości cząstek. Cząstki oddziałują na siebie wzajemnie oraz na elementy zespołu separującego. Pojawiające się w literaturze próby opisania takiego systemu w ujęciu deterministycznym zawierają zbyt wiele uproszczeń, a to powoduje, że predyktywne własności tak formułowanych modeli dynamicznych są nienajlepsze. Z uwagi na losowy charakter zjawisk, które zachodzą podczas separacji cząstek bardziej właściwym jest podejście stochastyczne do tego procesu. W artykule podjęto próbę skonstruowania i identyfikacji modelu statystycznego, który utożsamia ilość separowanych cząstek w danym miejscu na sicie ze zmienną losową.

ARCHIVES OF CIVIL AND MECHANICAL ENGINEERING

Vol. X 2010 No. 1

Cellular automata in nonlinear string vibration

W. GLABISZ
Wrocław University of Technology, Wybrzeże Wyspiańskiego 27, 50-370, Wrocław, Poland.

Cellular automata procedure for the analysis of nonlinear viscously damped transverse string vibrations was defined. Parameters were obtained by comparing the cellular automata defining rules with relations resulting from the discrete form of the mathematical description of the investigated phenomenon. A series of numerical tests that were run confirmed the agreement between the obtained results and the solutions found in the literature. Numerical results demonstrate that cellular automata can constitute a simple and effective tool for the analysis of a range of complex problems which have not been analyzed in this way before.

Keywords: *cellular automata, string, nonlinear vibration, dynamic loading, moving forces*

1. Introduction

Most of mechanics problems are usually mathematically modelled by ordinary differential equations, partial differential equations, differential-integral equations or integral equations. When the phenomenon being described is complex, the equations are solved by numerical methods, except for a very narrow class of problems for which closed analytical solutions can be formulated. The natural desire of researchers is to include in the description of reality the latter's complexity, which results in increasingly more complex mathematical descriptions of reality, difficult to analyze even by advanced numerical methods.

In recent decades descriptions of various physical phenomena by means of simple mathematical models called cellular automata (CA) have been intensively developed. Cellular automata constitute an alternative to describing such phenomena by complex mathematical equations. CA can be regarded as generally simple discrete dynamic systems whose evolution is described by uncomplicated local rules. Using cellular automata one can represent a given phenomenon as a synchronous mutual interaction of a discrete in time and space set of cells. The state of a cell is described by simple rules based on the state of this cell and the states of the cells in its immediate vicinity. One can say that cellular automata enable one to describe global phenomena by means of local rules of evolution and their discrete representation.

The idea and mathematical foundations of cellular automata were formulated by von Neuman and Ulam in the 1940s [1]. Although CA came within the field of interest of scientists, it was as late as in the 1970s, when John Conway presented the famous

"game of life" [2], that the interest rapidly grew and has resulted in a huge number of researches on the theory and applications of cellular automata. A broad survey of literature on the description and use of CA can be found in, e.g. [3–8]. S. Wolfram greatly contributed to the theory of cellular automata, collecting his findings in an extensive monograph [9].

In recent years cellular automata have been effectively applied to: traffic flow problems [10], the simulation of brain tumour growth dynamics [11], biochemical phenomena [12], fluid and gas dynamics and particle transport [13–14], ecological modelling [15], biological modelling [16], vegetation dynamics [17], migration problems [18], the modelling of reaction-diffusion systems [19], the modelling of water release and absorption in soils [20], soil erosion by water [21], epidemic modelling [22], forest fire modelling [23], the design of variable-stiffness composite layers [24] and many other problems. CA have also proved to be an effective tool in data compression and encryption [25], the generation of high-quality random numbers [26], cryptographic procedures [27] and the analysis of partial differential equations [28–29]. In mechanics, cellular automata have been used to describe deformations of an elastic body and the frictionless contact between the body and a rigid foundation [30], and to solve nonlinear string vibration problems [31–32], being the subject of this paper. A nonlinear model of transverse string vibration was first formulated by Kirchhoff [33], and Carrier [34–35] included the longitudinal displacement of the string in its nonlinear vibration. The theory formulated in those works has been developed in numerous publications whose survey, with regard to theoretical formulations, numerical methods and experimental tests, can be found in respectively [36–38].

The aim of this paper is to formulate an alternative, modified CA model of damped nonlinear transverse string vibration and to demonstrate that CA can constitute a simple and effective tool for the analysis of a range of complex problems which have not been analyzed in this way before.

Section 2 presents an alternative CA formulation for nonlinear transverse string vibration problems, with a modified description of the viscous damping model. In section 3, tests solutions are presented and the proposed approach is applied to nonlinear statics and dynamics problems of a string with unilateral and bilateral constraints, loaded with stationary and moving forces. In section 4 the obtained results are briefly recapitulated.

2. Cellular automata model of string vibration

Let us assume that the string model is a chain of uniformly distributed point masses (cells) connected by elastic massless elements of the string whose fragment is shown in Figure 1.

The transverse displacement of the i-th string mass over the j-th time, referred to as the cell state, is denoted by $w(i, j)$. As defined in the papers by Kawamura et al. [31–32], the evolution of the string state can be divided into two (identical in their descrip-

tion) stages. In the first stage, for example, balls marked as white in Figure 1 undergo displacement while the black balls remain stationary, whereas in the second stage the opposite happens.

Physically, this way of analysis should be interpreted as the propagation of a transverse disturbance, which in a given time interval covers a distance exactly equal to distance a (resulting from the applied uniform division of the string into n elements) between neighbouring balls, each of which can be a source of transverse vibrations. State ($w(i, j)$) of a black ball after time Δt ($w(i, j + 1)$), during which the transverse disturbance reaches the neighbouring balls and the black ball performs undamped free vibrations, can be calculated from this relation

$$w(i, j + 1) = w(i, j) + 2w_0 \tag{1}$$

where $w_0 = 1/2[w(i - 1, j) + w(i + 1, j)] - w(i, j)$ (2)

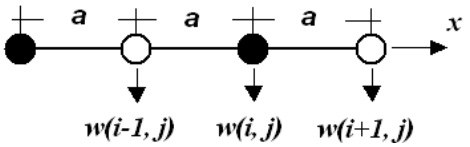

Fig. 1. String model

The relations are represented graphically in Figure 2.

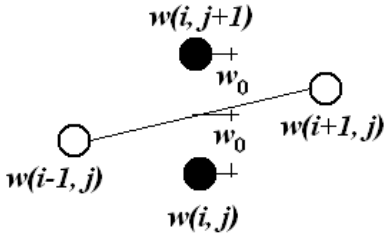

Fig. 2. Graphic representation of cell state updating

If the influence of distributed (transversely to string axis x) excitation forces $q(x, t)$ and that of viscous damping $C(x, t)$ are taken into account, then

$$w(i, j + 1) = \delta[2w_0 + \chi f(i, j)] + w(i, j) \tag{3}$$

where (for the time being undetermined) parameters δ and χ are responsible for respectively vibration damping and the influence of transverse load $f(i, j)$ on the state of displacement $w(i, j + 1)$.

Taking into account relation (2), relation (3) can be written as

$$w(i,j+1) = \delta[w(i-1,j) + w(i+1,j)] + (1-2\delta)w(i,j) + \delta\chi f(i,j), \tag{4}$$

which expresses the state of the i-th cell (its evolution procedure) at time $j + 1$ as a function of: the previous state (before time Δt elapses), the state of the neighbouring cells ($w(i-1,j)$, $w(i+1,j)$), the actual transverse load and damping.

The mathematical Kirchhoff model [33] of nonlinear transverse vibration, neglecting the displacements along the string's axis and averaging tension (N) over its length (l), can be in an elementary way derived from Newton's second law and written as

$$\rho A\frac{\partial^2 w(x,t)}{\partial t^2} + C\frac{\partial w(x,t)}{\partial t} + \left(N_0 + \frac{EA}{2l}\int_0^l \left(\frac{\partial w(x,t)}{\partial x}\right)^2 dx\right)\frac{\partial^2 w(x,t)}{\partial x^2} = q(x,t), \tag{5}$$

where ρ, E, C, N_0 and $q(x, t)$ are respectively the density of the string material, the Young modulus of the latter, the viscous damping parameter, the initial string tension value and the transverse load intensity.

Applying central difference approximation for $\partial^2 w/\partial t^2$, $\partial^2 w/\partial x^2$ and $\partial w/\partial t$ one can write Equation (5), after elementary transformations, in the form presented in the papers by Kawamura et al. [31–32]

$$w(x,t+\Delta t) = \frac{1}{\gamma+1}\left[w(x+\Delta x,t) + w(x-\Delta x,t)\right] + \frac{\gamma-1}{\gamma+1}w(x,t) + \frac{1}{\gamma+1}\frac{(\Delta t)^2}{\rho A}q(x,t) \tag{6}$$

where:

– $\gamma = C\Delta t/\rho A$,

– $1/(\gamma+1)\cdot(\Delta t)^2/\rho A = (\Delta t)^2/(C\Delta t + \rho A)$.

By comparing relations (4) and (6) one can easily determine the still unknown parameters δ and χ from this cellular automaton

$$\delta = \frac{1}{\lambda+1} = \frac{\rho A}{c\Delta t + \rho A}$$
$$\chi = \frac{\Delta t}{\rho A} \tag{7}$$

For the above relations it can be shown that $(1-2\delta) = (\gamma-1)/(\gamma+1)$, which fully agrees with the relations presented by Kawamura et al. [31–32].

Since work W of load $q(x, t)$ is a linear function of the displacements shown in Figure 2 and energy dissipation function Φ is a homogenous quadratic function of velocity (differentiation over time is marked with a dot),

$$W = 2\int_0^a q(x,t)w\frac{x}{a}dx$$
$$\Phi = \int_0^a C\left(\dot{w}\frac{x}{a}\right)^2 dx \tag{8}$$

the parameter $f(i, j)$ in relation (4) is $f(i, j) = q(x, t)$ and the damping per unit string length (in relation (7)) is $c = {}^2/_3C$. The latter relation is due to the zero velocities of the balls adjoining the ball which moves in one of the string evolution stages.

Relation (4) together with (7) and definitions c and $f(i, j)$ explicitly define the cellular automaton law for the nonlinear transverse vibration of the string.

Velocity v of transverse disturbance propagation is defined as $v = \sqrt{N/\rho A}$, and so in the nonlinear equation considered here it is

$$v(t) = \sqrt{\frac{1}{\rho A}\left(N_0 + \frac{EA}{2l}\int_0^l \left(\frac{\partial w(x,t)}{\partial x}\right)^2 dx\right)}. \tag{9}$$

According to the proposal presented by Kawamura et al. [31–32], time-variable velocity $v(t)$ is the basis for the use of time increment Δt which changes in the course of string evolution (and influences the values of δ and χ). Such a value of Δt is selected that the disturbance wave-front will cover exactly distance $a = l/n$ (constant throughout the analysis) during this time.

3. Numerical analysis

The solutions presented in this section were tested [31–32] for a string with length l = 0.8 m, cross section A = $20\cdot10^{-3}$ m × $0.5\cdot10^{-3}$ m, material density ρ = $7.8\cdot10^3$ kg/m^3, Young modulus E = 206 GPa, damping C = 0.14 Ns/m^2 and initial tension N_0 = 130 N. The string was divided into n = 100 segments (cells) each having length a = $8.0\cdot10^{-3}$ m. For these data, transverse wave propagation velocity $v_0 = \sqrt{N_0/\rho A}$ = 40.8248 m/s and the first natural frequency $f_1 = v_0/2l$ = 25.5155 Hz. In some of the solutions presented below it was assumed that load $q(x, t) = q(x) + Q\cos(\omega t)$, where $q(x)$ = 3.0 N/m, Q = 15.0 N/m ($\omega = 2\pi f$), and the load acts within the segment 0.08 m $\leq x \leq$0.15 m.

For the above data it is easy to estimate the frequency response function [39], e.g. for the string's midpoint, assuming that the displacement state can be approximated by function $\sin(\pi x/l)$ (for unmovable string ends) and that $q(x)$ = 0.0 N/m and f = 25 Hz. In Figure 3 this function (the function of fixed string response amplitude variation amp measured in meters) is marked with a solid line and dots mark the solutions ob-

tained using the linearized (neglecting changes in tension force $N(t) = N_0$) cellular automaton defined in the previous section.

The maximum difference between the solutions for the excitation frequency adopted in the considered example amounts to 13% of the exact solution and is much better than in [32]. This demonstrates the effectiveness of a well calibrated CA in such an analysis.

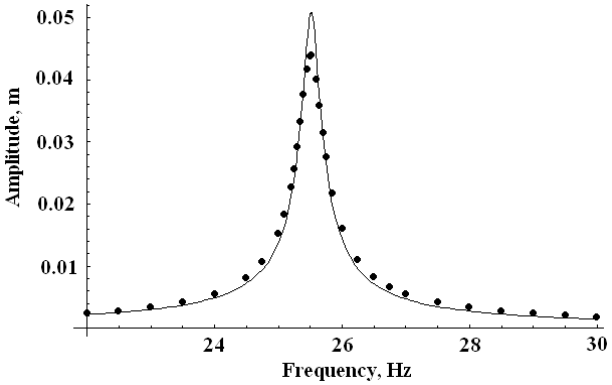

Fig. 3. Frequency response function for linear problem

Figure 4 shows selected schematics of the analyzed strings. The nonlinear transverse string vibration model was used in each of the problems.

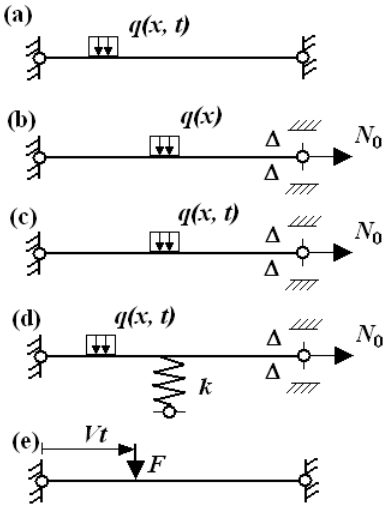

Fig. 4. Schematics of analyzed strings

Figure 5 shows a typical frequency response function at the midpoint of the string whose schematic is shown in Figure 4a, for $q(x)$ = 0.0 N/m and Q = 30 N/m in frequency range 20 Hz $\leq f \leq$ 50Hz.

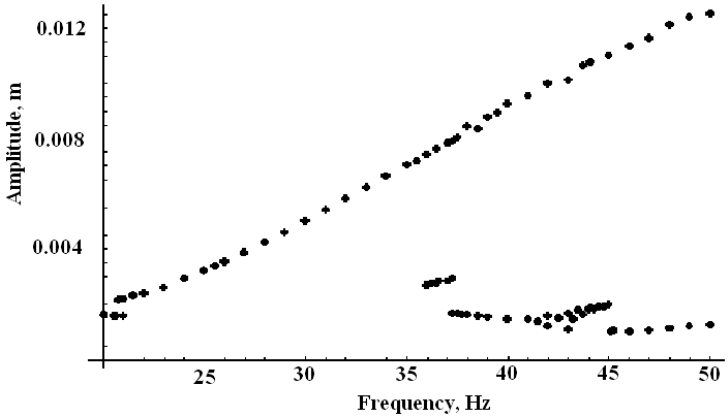

Fig. 5. Frequency response function for nonlinear problem

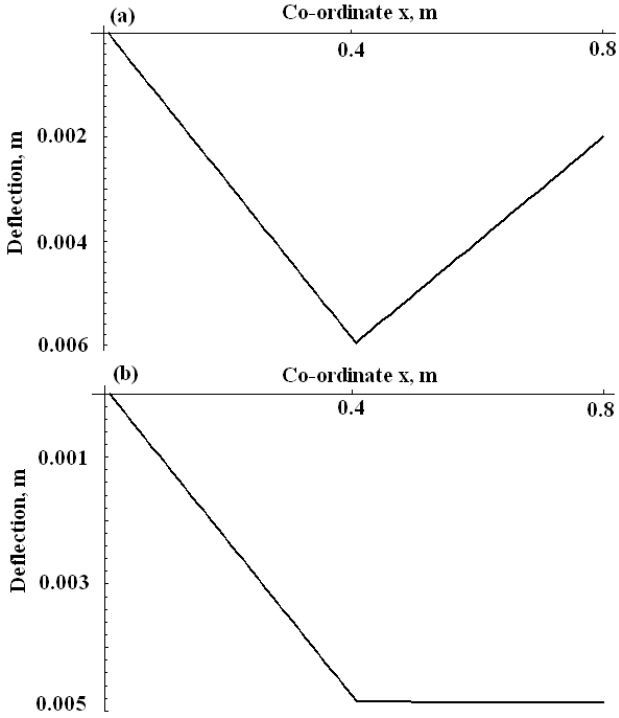

Fig. 6. Static deflections of string Δ = 0.002 m (a) and Δ = 0.005 (b)

Different string response branches can be obtained by, for example, controlling excitation function frequency f in the initial time of the analysis, after which f reaches a constant target value. The analysis of string vibration amplitude at different excitation frequencies requires (in certain ranges of the frequencies) arduous searches for possible steady string vibration amplitude values.

Interesting responses of the vibrating string are obtained under a static load when, for instance, the string's right end can freely move transversely in the parameter Δ determined range which describes a unilateral stiff constraint (Figure 4b).

Figure 6 shows lines of static string deflections under load $q(x)$ = 1250 N/m applied to segment $a = l/n$ precisely at the string's midpoint for respectively Δ = 0.002 m (Figure 6a) and Δ = 0.005 m (Figure 6b). The acting load $q(x)$ corresponds to concentrated force F = 10 N applied in the middle of the string span. As it can be easily verified (checking the current tension of the string), the static equilibrium conditions, in the form of the sum of forces projections onto the vertical axis, are satisfied here.

Under dynamic load $q(x, t) = 1250 + 1250\cos(2\pi ft)$ applied to the middle segment (a) of the string (Figure 4c) and at Δ = 0.002 m, f = 10 Hz and C = 0.6 Ns/m^2, the state of displacement of the string's midpoint and its right end over time t is shown in respectively Figure 7a and 7b.

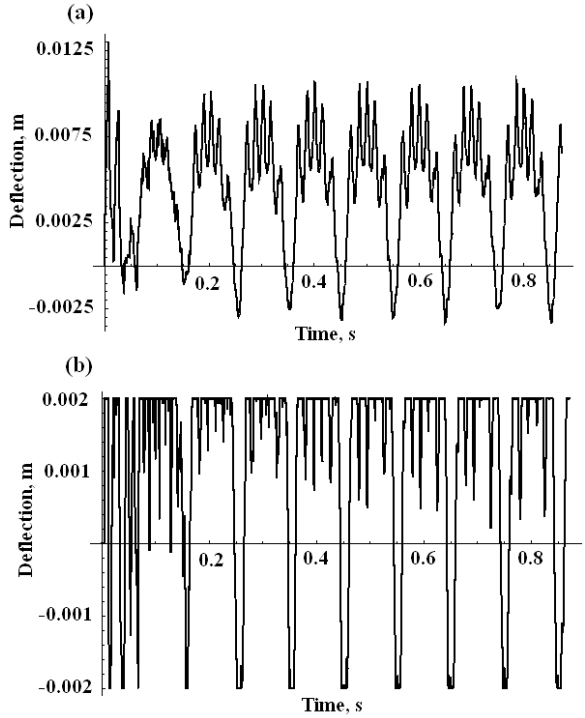

Fig. 7. Dynamic deflections of string's midpoint (a) and right end (b)

The CA algorithm allows one to easily impose arbitrary constraints on any string point. This has been confirmed by several numerical tests (not presented here). The CA algorithm can be easily generalized to cover cases with any number of bilateral elastic constraints with any (also nonlinear or time-dependent) characteristic of their stiffness (k). Bilateral constraints are taken into account by modifying node load $f(i, j)$ by adding an elastic reaction proportional to the node displacement multiplied by a function characterizing the stiffness of the added constraint.

As an example, Figures 8 and 9 show phase portraits of the vibration of points at $x = {}^3/_4\ l$ and $x = l$ of a string whose displacements are confined by a bilateral elastic constraint (with stiffness k = 400 N/m) in the middle of the string and a stiff unilateral constraint at the string's end at Δ = 0.005 m (Figure 4d). Vibration excitation load $q(x, t) = 1250 + 1250\cos(2\pi f t)$ was applied to one segment a at $x = {}^1/_4\ l$ and f = 175 Hz (Figure 8) and f = 179.9 Hz (Figure 9). It was assumed that C = 0.45 Ns/m^2 and initial tension N_0 = 2600 N.

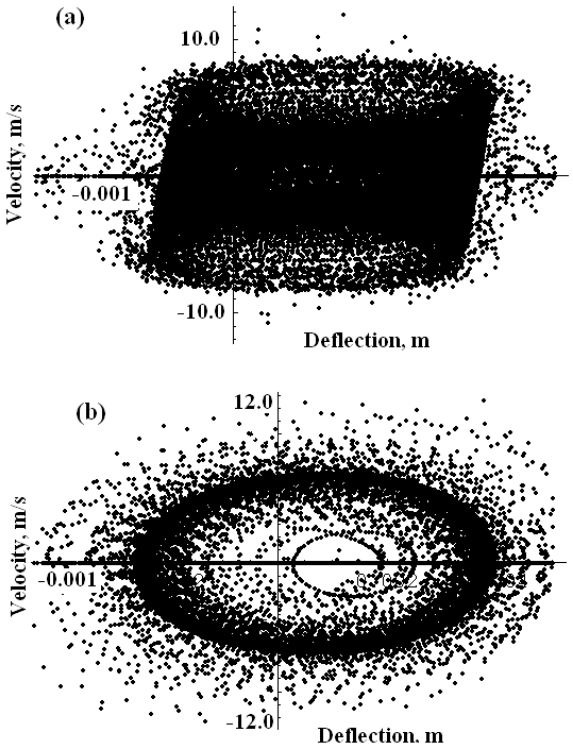

Fig. 8. Phase portraits of vibration of string points at x = 3/4 l (a) and $x = l$ (b) for f = 175 Hz

Figure 10 shows the Fourier transform $P(f)$ of string midpoint displacements at the above frequencies: f = 175 Hz (Figure 10a) and f = 179.9 Hz (Figure 10b).

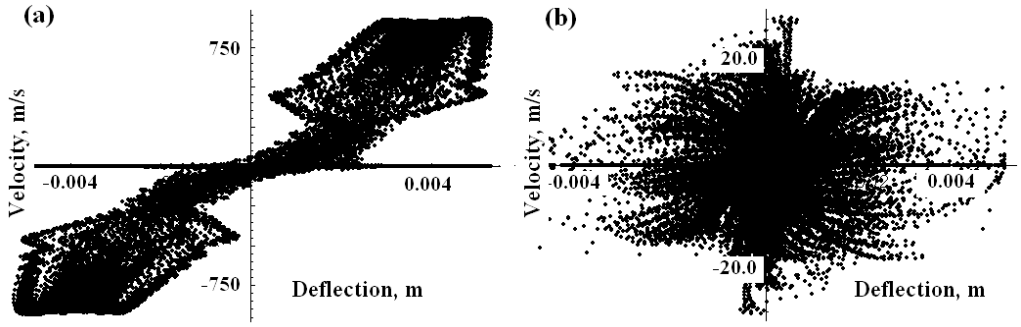

Fig. 9. Phase portraits of vibration of string points at $x = 3/4\ l$ (a) and $x = l$ (b) for $f = 179.9$ Hz

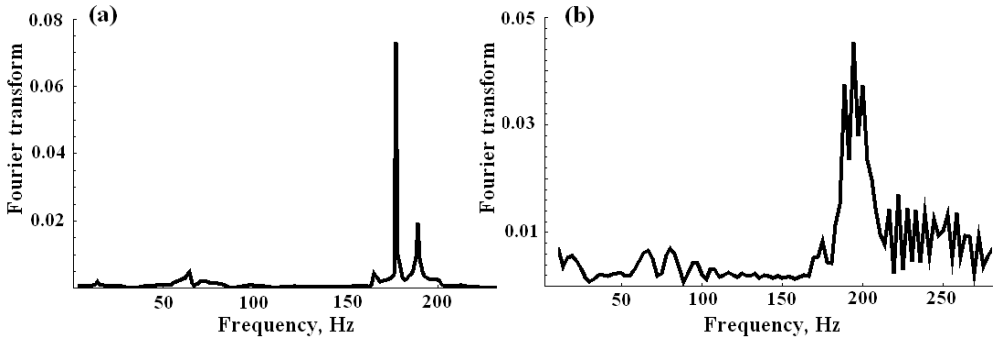

Fig. 10. Fourier transform of string response at $f = 175$ Hz (a) and $f = 179.9$ Hz (b)

The string response at frequency $f = 179.9$ Hz has the features of chaotic motion.

Ratio β of elastic wave velocity at current tension $N(t)$ to its velocity at initial tension N_0, which can be regarded as a certain measure of problem nonlinearity, was controlled in each of the solutions. Figure 11 shows the variation of β in the initial stage of analysis of the string (Figure 4d) at respectively $f = 175$ Hz (Figure 11a) and $f = 179.9$ Hz (Figure 11b).

The CA algorithm presented in section 2 has proved effective also in the analysis of the string under moving static and dynamic loads. A moving load can be realized on a string with elastic and inelastic constraints. If it is assumed that force F moves on the string with, for example, uniform motion with velocity V (this problem can be generalized to cover a case of the force moving with an arbitrary acceleration), interesting solutions can be obtained at different velocity values, particularly at critical velocities (close to elastic wave propagation velocity v). Figure 12 shows the state of displacement (a snapshot) of the string under force $F = 10$ N moving at velocity $V = 2$ m/s (Figure 4e). Figure 12a shows the deflection of the string over time $t = 0.26$ s when the force acted directly on the string. Figure 12b shows string deflection over time $t = 0.58$ s when the string's free damped vibration after the travel of force F.

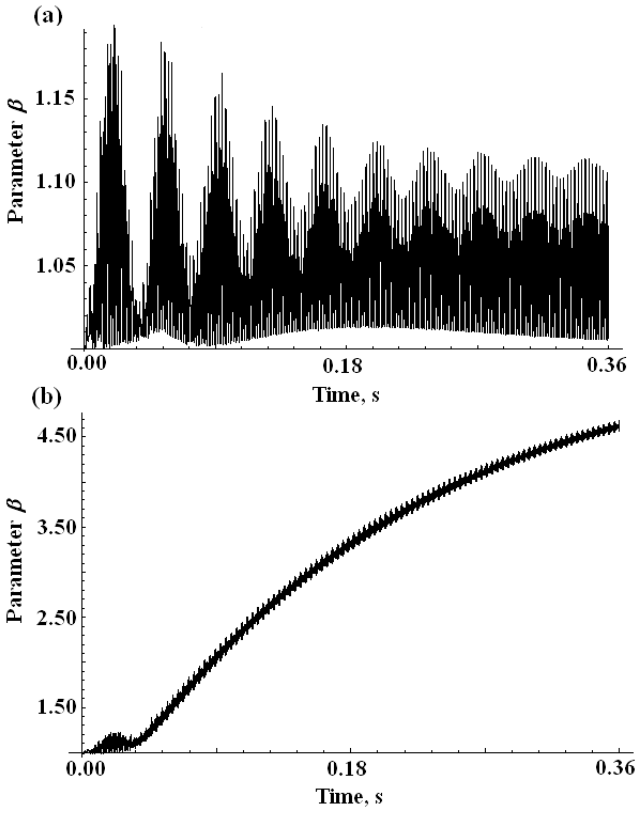

Fig. 11. Variation of parameter β at f = 175 Hz (a) and f = 179.9 Hz (b)

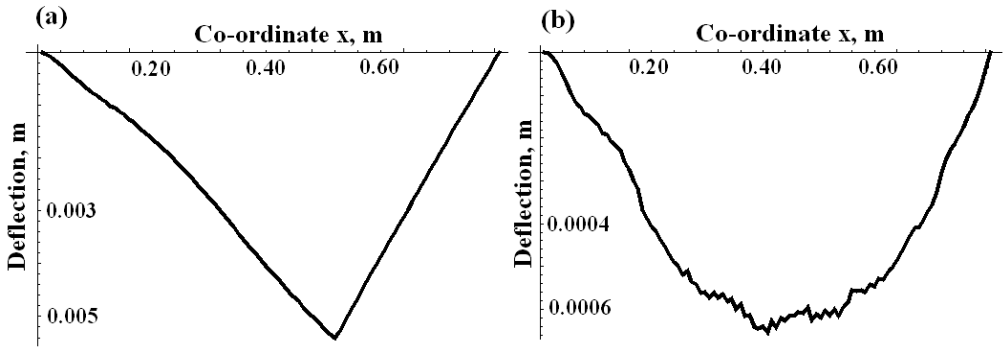

Fig. 12. String displacement state under moving load (V = 2 m/s) over t = 0.26 s (a) and t = 0.58 s (b)

The displacement state at subcritical speed V = 40 m/s as the force acted directly on the string (t = 0.009 s) and after its travel (t = 0.023 s) is shown in respectively in

Figure 13a and 13b. In the analysis it was assumed that $C = 3.0$ Ns/m^2. In Figure 13a the disturbance front preceding the force has not reached the end of the string. Figure 13b shows the wave reflected from the string's end during its free vibration.

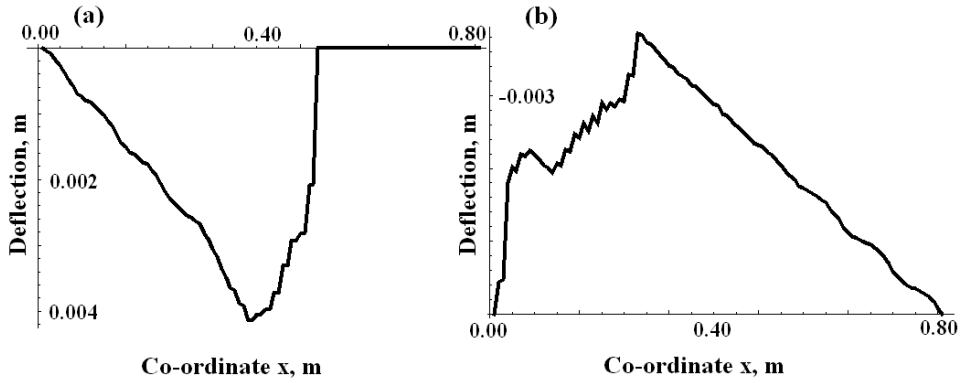

Fig. 13. String displacement state under moving load ($V = 40$ m/s) over $t = 0.009$ s (a) and $t = 0.023$ s (b)

Similarly as in Figure 13, the string responses in the linearized problem ($N(t) = N_0$) are shown for $t = 0.011$ s and $t = 0.027$ s in respectively Figures 14a and 14b.

CA were also used to good effect in problems with given kinematic excitation of an arbitrary string point and in problems with forced time-variable string tension.

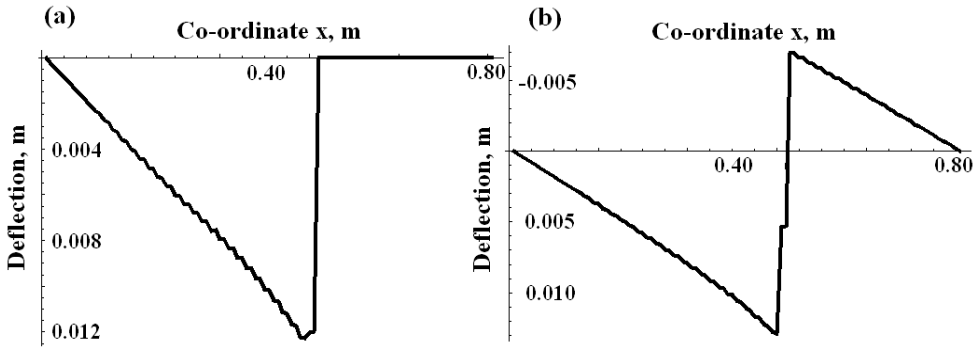

Fig. 14. Linearized string displacement state under moving load ($V = 40$ m/s) over $t = 0.011$ s (a) and $t = 0.027$ s (b)

4. Conclusion

Cellular automata, intensively developed in recent years, can constitute an effective alternative to complex mathematical descriptions of many physical phenomena. The

latter are described, as a rule, by simple, repeatable, CA-evolution-expressing formulas used in the discrete representations of the space of the phenomena. The calibration of CA's parameters is of critical importance for their effectiveness. As a rule, when CA are used, it is easier to obtain a qualitatively correct form of the sought solutions than their quantitatively correct form.

In this paper a modified CA procedure for the analysis of nonlinear viscously damped transverse string vibrations was defined. CA parameters were obtained by comparing the CA defining rules with relations resulting from the discrete form of the mathematical description of the investigated phenomenon. A series of numerical tests that were run confirmed the agreement between the obtained results and the solutions found in the literature. The CA model calibrated in this way was used in the analysis of string vibrations under arbitrary static and dynamic loads at different unilateral and bilateral constraints imposed on the motion of an arbitrary string point.

The numerical tests have shown that:

– cellular automata are simple and effective tools for the analysis of linear and nonlinear string vibrations,

– owing to the fact that the CA algorithm is easily modifiable, it can be used (usually after minor changes in its structure) to analyze various complex problems,

– in order to build a properly functioning CA, one must carefully calibrate its parameters which determine the qualitative and quantitative correctness of the results.

References

[1] Neumann J. V.: *The theory of self-reproducing automata*, A. W. Burks (ed), Univ. of Illinois Press, Urbana and London, 1966.

[2] Gardner M.: *The fantastic combinations of John Conway's new solitaire game "Life"*, Sci. Am., Vol. 223, 1970, pp. 120–123.

[3] Vollmar T.: *Cellular space and parallel algorithms: an introductory survey*, Parallel Computation-Parallel Mathematics, M. Feilmeier (ed), North Holland Publishing Co, 1977, pp. 49–58.

[4] Toffoli T., Margolus N.: *Invertible cellular automata: a review*, Physica D, Vol. 66, 1994, pp. 1–24.

[5] Mitchell M., Crutchfield J., Das R.: *Evolving cellular automata with genetic algorithms: a review of recent work*, First International Conference on Evolutionary Computation and its Applications, 1996.

[6] Chaudhuri P.Pal, Chowdhury A.R., Nandi S., Chatterjee S.: *Additive cellular automata – theory and applications*, IEEE Computer Society Press, CA, USA, Vol. 1, 1997.

[7] Sarkar P.: *A brief history of cellular automata*, ACM Computing Systems, Vol. 32, 2000, pp. 80–107.

[8] Kari J.: *Theory of cellular automata: a survey*, Theoretical Computer Science, Vol. 334, 2005, pp. 3–33.

[9] Wolfram S.: *A new kind of science*, Wolfram Media, Inc., 2002.

[10] Maerivoet S., Moor De B.: *Cellular automata of road traffic*, Physics Reports, Vol. 419, 2005, pp. 1–64.
[11] Kansal A.R., Torqato S., Harsh IV G.R., Chiocca E.A., Deisboeck T.S.: *Simulated brain tumour growth dynamics using tree-dimensional cellular automata*, J. Theor. Biol., Vol. 203, 2000, pp. 367–382.
[12] Kier L.B., Cheng Chao-Kun, Testa B., *Cellular automata models of biochemical phenomena*, Future Generation Computer Systems, Vol. 16, 1999, pp. 273–289.
[13] Chopard B., Masselot A.: *Cellular automata and lattice Boltzmann methods: a new approach to computational fluid dynamics and particle transport*, Future Generation Computer Systems, Vol. 16, 1999, pp. 249–257.
[14] Boghosian B. M.: *Lattice gases and cellular automata*, Future Generation Computer Systems, Vol. 16, 1999, pp. 171–185.
[15] Hogeweg P.: *Cellular automata as a paradigm for ecological modelling*, Applied Mathematics and Computation, Vol. 27, 1988, pp. 81–100.
[16] Bard G., Edelstein-Keshet L.: *Cellular automata approaches to biological modelling*, J. Theor. Biol., Vol. 160, 1993, pp. 97–133.
[17] Balzter H., Braun P.W., Kohler W.: *Cellular automata models for vegetation dynamics*, Ecological Modelling, Vol. 107, 1998, pp. 113–125.
[18] Schonfisch B., Lacoursiere C.: *Migration in cellular automata*, Physica D, Vol. 103, 1997, pp. 537–553.
[19] Weimar J. R.: *Cellular automata for reaction-diffusion systems*, Parallel Computing, Vol. 23, 1997, pp. 1699–1715.
[20] Townend J.: *Modelling water release and absorption in soils using cellular automata*, Journal of Hydrology, Vol. 220, 1999, pp. 104–112.
[21] Ambrosi D.D., Di Gregorio S., Gabriele S., Gaudio R.: *A cellular automata model for soil erosion by water*, Phys. Chem. Earth (B), Vol. 26, 2001, pp. 33–39.
[22] White S.H., del Rey A.M., Sanches G.R.: *Modelling epidemics using cellular automata*, Applied Mathematics and Computation, Vol. 186, 2007, pp. 193–202.
[23] Barros F.J., Mendes M.T.: *Forest fire modelling and simulation in DELTA environment*, Simulation Practice and Theory, Vol. 5, 1997, pp. 185–197.
[24] Setoodeh S., Gurdal Z., Watson L.T.: *Design of variable-stiffness composite layers using cellular automata*, Comput. Methods Appl. Mech. Engrg., Vol. 195, 2006, pp. 836–851.
[25] Lafe O.: *Data compression and encryption using cellular automata transforms*, Engng. Applic. Artif. Intell., Vol. 10, 1997, pp. 581–591.
[26] Tomassini M., Sipper M., Zolla M., Perrenoud M.: *Generating high-quality random numbers in parallel by cellular automata*, Future Generation Computer Systems, Vol. 16, 1999, pp. 291–305.
[27] del Rey A.M., Mateus J.P., Sanches G.R.: *A secret sharing scheme based on cellular automata*, Applied Mathematics and Computation, Vol. 170, 2005, pp. 1356–1364.
[28] Toffoli T.: *Cellular automata as an alternative to (rather than an approximation of) differential equations in modelling physics*, Physica 10D, Vol. 195, 1984, pp. 117–127.
[29] Doeschl A., Davison M., Rasmussen H., Reid G., *Assessing cellular automata based models using partial differential equations*, Mathematical and Computer Modelling, Vol. 40, 2004, pp. 977–994.
[30] Abdellaoui M., El Jai A., Shillor M.: *Cellular automata model for contact problem,* Mathematical and Computer Modelling , Vol. 36, 2002, pp. 1099–1114.

[31] Kawamura S., Shirashige M., Iwatsubo T.: *Simulation of the nonlinear vibration of a string using the cellular automation method*, Applied Acoustics, Vol. 66, 2005, pp. 77–87.
[32] Kawamura S., Yoshida T., Minamoto H., Hossain Z.: *Simulation of the nonlinear vibration of a string using cellular automata based on the reflection rule*, Applied Acoustics, Vol. 67, 2006, pp. 93–105.
[33] Kirchhoff G.: *Vorlesungen uber Mathematische Physik: Mechanik*, Druck und Verlag von B.G. Teubner, Leipzig, 1867.
[34] Carrier G.F.: *On the nonlinear vibration problem of the elastic string*, Q. J. Appl. Math., Vol. 3, 1945, pp. 157–165.
[35] Carrier G.F.: *A note on the vibrating string*, Q. J. Appl. Math., Vol. 7, 1949, pp. 97–101.
[36] Chen Li-Quen, Ding Hu: *Two nonlinear models of a transversely vibrating string*, Arch. Appl. Mech., Vol. 78, 2008, pp. 321–328.
[37] Bilbao S.: *Conservative numerical methods for nonlinear strings,* J. Acoust. Soc. Am., Vol. 118, 2005, pp. 3316–3327.
[38] Molteno T.C., Tufillaro N.B.: *An experimental investigation into the dynamics of a string*, Am. J. Phys., Vol. 72, 2004, pp. 1157–1169.
[39] Inman D.J.: *Vibration: with control, measurement, and stability*, Prentice-Hall, Inc., 1989.

Automaty komórkowe w nieliniowych drganiach struny

W artykule zdefiniowano procedurę automatów komórkowych, którą przystosowano do analizy nieliniowych, wiskotycznie tłumionych drgań poprzecznych struny. Parametry automatów komórkowych otrzymano porównując reguły definiujące ewolucję CA ze związkami wprost wynikającymi z dyskretnej postaci matematycznego opisu zjawiska. Przeprowadzono szereg testów numerycznych potwierdzających jakościową i ilościową zgodność otrzymywanych wyników z rozwiązaniami znanymi z literatury. Wykonane testy numeryczne pokazują, że automaty komórkowe mogą być prostym i skutecznym narzędziem analizy szeregu złożonych zagadnień dotychczas tym sposobem nie analizowanych.

ARCHIVES OF CIVIL AND MECHANICAL ENGINEERING

Vol. X 2010 No. 1

Method for approximate analysis of cracking effect on lateral stiffness of reinforced concrete framed-tube structures

S. KOBIELAK, R. TATKO
Wrocław University of Environmental Engineering and Life Science, Grunwaldzki 24, 50-375 Wrocław, Poland.

R. PIEKARZ
Wrocław University of Technology, Wybrzeże Wyspiańskiego 27, 50-370 Wrocław, Poland.

The paper presents analysis of framed-tube of tall reinforced concrete buildings subjected to horizontal loads. Authors take a cracking effect of frame spandrel girders of structure into account. Paper introduces simplified theoretical model of work of this kind of structures. The theoretical analysis and statistical multi-parameter numerical study of various framed-tube structures became the basis for developing a simplified assessment method of effective inertia moments of cracked spandrel beams.

Keywords: *lateral stiffness, reinforced framed-tube structure, cracking effect*

1. Introduction

The stiffness of structural system of a tall reinforced concrete building can be recognized as a superior criterion in its design. The stiffness measure of the structural system is a value of limit of top building deflection. The purpose of limitation of tall building drift is not only to prevent and minimize of disadvantageous influences of the second-order P-Delta effects on a building structure, as well as to prevent proper functioning of non-structural components. With regard to nonlinear material properties of concrete, the methods of structure theory based on classical assumptions of elastic theory do not reflect actual character of work under a given load. While in the phase of structure work before cracking, the dominating factor which influences the nonlinear dependence of structure deformation-load is concrete shrinkage, in the phase of structure work after cracking, the main, dominating factor affecting the nonlinear dependence of structure deformation from load is stiffness reduction of structure members [1]. In this paper, analyze of framed tube of tall reinforced concrete buildings subjected to action of horizontal loading with taking into account a cracking effect of frame spandrel girders of framed-tube structure and its simplified theoretical model of work. On the basis of theoretical analysis and statistical multi-parameter numerical study of various framed-tube structures a simplified assessment method of effective inertia moments of cracked spandrel beams has been work out. It was also suggested

to use of the above-mentioned method to assess the framed-tube structures drift with pay respect to cracking spandrel beam effect by means of the existing simplified methods for deflection calculation of framed tube systems.

2. Framed-tube system

Framed-tube structures are one of the most significant structural forms of tall buildings (Figure 1). A frame-tube structure consists of a single frame tube around the perimeter of building which is created from four orthogonal frame panels rigidly jointed in the corners. The frames consist of closely spaced columns 2–4 m between centres of joined deep spandrel girders [2]. It is assumed that the stiffness ratio of columns to spandrel beam should be not greater than 2. Floors on the each story perform the function of rigid diaphragms and connect the external frame-tube with internal core in which are given for example stairs, elevators, systems of different installations. Framed-tube structures are used in concrete tall buildings from 40 to 60 stories.

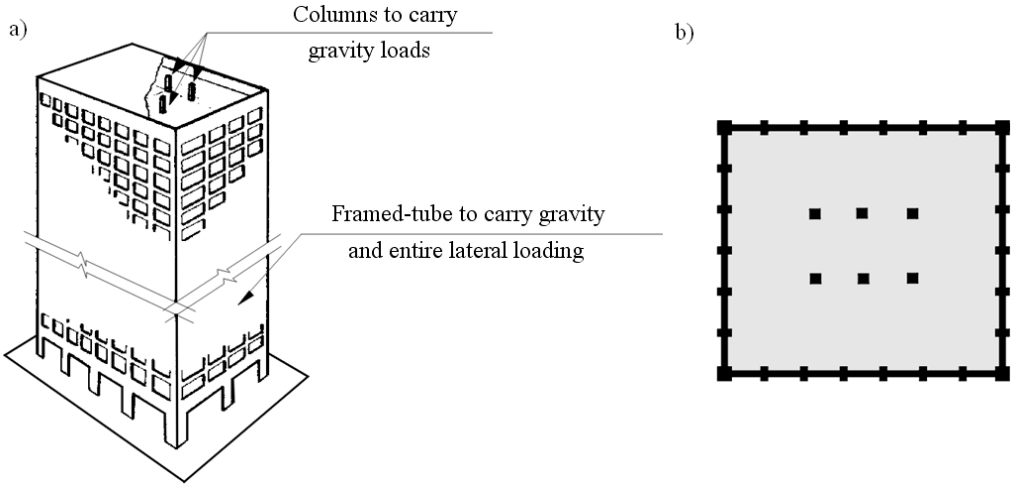

Fig. 1. Framed-tube structure [2]: a) general view of structure, b) floor plan of structure

2.1. Behaviour of framed-tube structures

Framed-tube structures under the action of horizontal load in parallel direction to one of principal axes behave like a homogeneous hollow cantilever beam, i.e. according to classical beam theory. The internal core of this structure is characterized by a comparatively small stiffness in relation to external framed-tube and does not participate in carrying out of horizontal loads. The lateral structure drift is governed by pure bending and pure shear of the structure (Figure 2). The bending of framed-tube structures induced generation of the elastic extensions and shortenings of columns of

all four perimeter frames, and arising in them of axial forces of respective signs. A non-uniform distribution of elastic extensions and shortenings in columns developed by shear lag effect produced arising of bending moments and axial forces in columns and spandrel beams of frames.

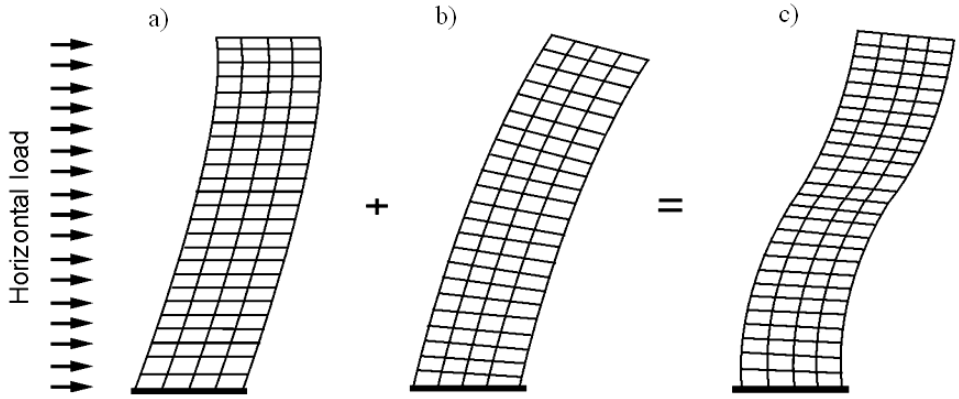

Fig. 2. Deformations of framed-tube structure caused by: a) external shear, b) external moment and c) external shear and moment

While shear lag effect being result of spandrel beams flexibility produces the increase of the axial stresses in the corner columns and reducing them in the columns toward the centre of the orthogonal frame panels, disproportional of deformations of columns successively following after them on the given story level produces arising in columns of axial forces and bending moments of small values. Shear of framed-tube structure generates flexural and shear deformations in the columns and spandrel beams of web frames aligned with the direction of the action of lateral loading.

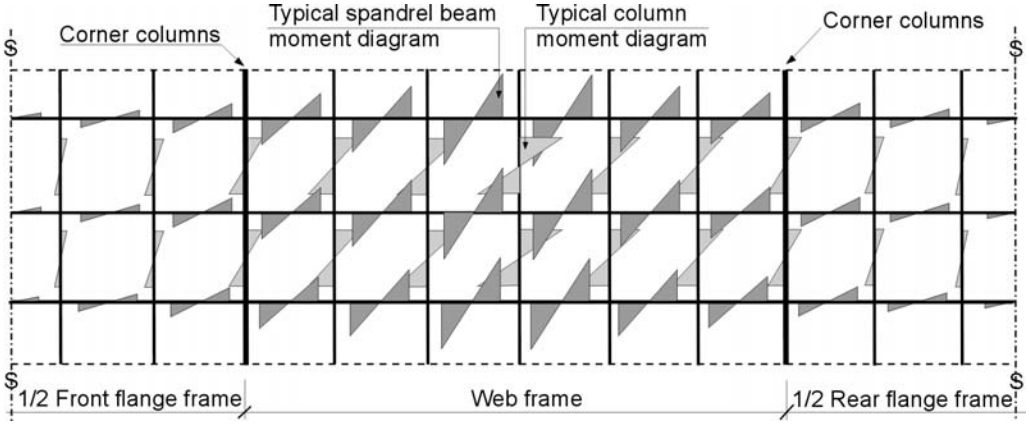

Fig. 3. Typical moment diagram caused by external shear in members of framed-tube structure

Deformations of web frames members are also induced deformations in flange frames members, which are of much lesser magnitude and are fast reduced toward the centre of these frames. In the deformed shear members of web frames bending moments are induced of significant value compared to analogical bending moments caused by bending of framed-tube structure. On Figure 3 distribution of moment in columns and spandrel beams caused by lateral loading is presented. Maximum values of bending moments appear in the mid-face web columns and spandrel beams and their minimum values have members which are near to the structure corners. The difference between both bending moment values in the centre of members of web frames is of the range of 10–20%.

2.2. Cracking in spandrel beams and columns of framed-tube structures

Generally, the compressive vertical load is opposed to generation of excessive tension stresses in the column sections as a result of biaxial bending caused by combined action of vertical and lateral loading, which prevents the column cracking. The values of compressive forces in the columns are closely conditioned by the column spacing and floor span. The combined action of vertical and lateral loading generates in the spandrel beams of web frames – the bending moments and compressive and tension forces. On account of considerable depth of spandrel beam cross section ($h_b/s_c > 5$) the live and dead loads from floors produce small tension stresses in bending spandrel sections. Considerably greater values of tension stresses in spandrel beam sections produce a bending moment caused by the action of lateral loading.

Both external shear and external moment under external horizontal load produce the bending moments in the framed-tube structure. However, considerably greater participation in bending moment values in spandrel beams of structure has external shear. From the diagram of the bending moment in spandrel beams of the structure presented on Figure 3 it can be seen that maximum bending moments appeared in the directly sheared members of web frames. The bending moments occurring in the members in the planes of web frames produce the tension stresses in the spandrel sections of significant values which conduce to cracking of members. The reduction in the frame spandrel beam stiffness caused by their cracking produce increasing structure drift, mainly by increasing of shearing action and in smaller degree as a result of the bending action and redistribution of internal forces. The bending moments in spandrel beams from the action of wind loading and reduction of their flexural rigidity caused by cracking of spandrel beam sections depend upon many complex and labour- and time-consuming factors. Besides, the applied to this purpose simplified methods of calculation of multi-story frames are often limited to the elastic range and enough high homogeneous stiffness of structure members.

3. Proposed method of analysis

Figure 4 shows deformations of web frames caused by the action of lateral shear forces. Under the action of shear forces, each joint of the frame of framed-tube struc-

tures on the *n*-th storey structure level undergoes a displacement Δ_{ni} and rotation θ_{ni}. Both quantities Δ_{ni} and θ_{ni} are variable on frame length and depend on shear rigidity GA of single frame segment mentally cut out of the frame. The shear rigidity GA of a single segment, and so the quantities Δ_{ni} and θ_{ni} depend on factors describing the geometrical and material properties of columns and spandrel beam, axial columns spacing, axial columns length l_c, sizes and areas of members cross section, members inertia moments in shear plane of frame, their longitudinal modulus elasticity, coefficient of transverse elasticity as well as number of rectangular segments of columns and spandrel beam along the axial column length, spacing of contra flexure points of columns along their height and degree of stiffening of joints.

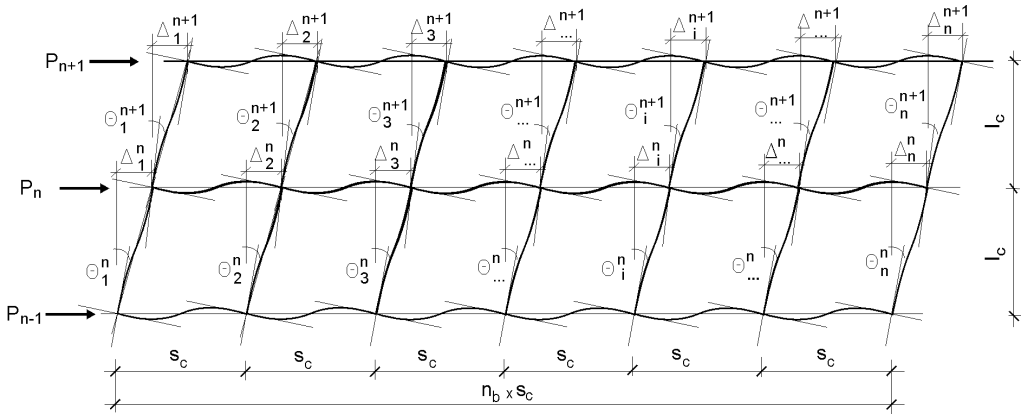

Fig. 4. Deformations caused by external shear in web frame

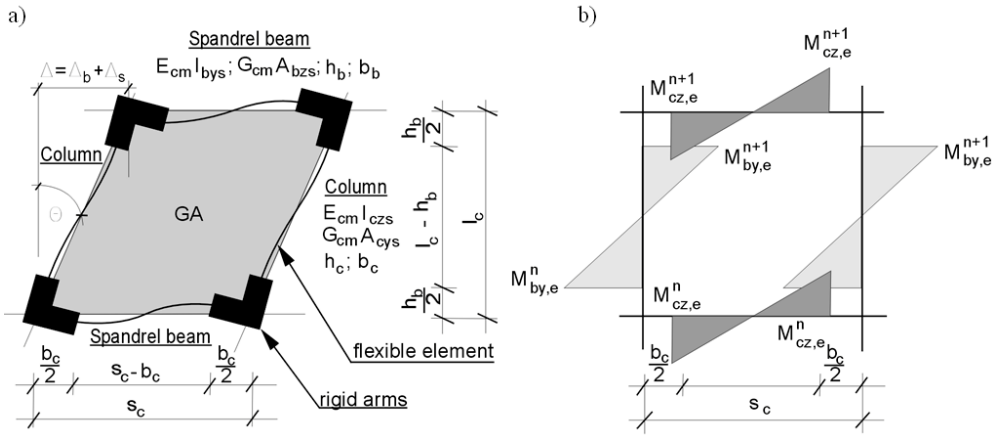

Fig. 5. a) Deformations of story-height segment, b) typical moment diagrams in its elements caused by external shear

The members of single frame segment composed of two columns and two spandrel beams under shear lateral loading undergo flexural deformations Δ_b and shear Δ_s, and their sum Δ is a value of total shear deformation of story-height segment (Figure 5a). An essential influence on shear segment deformation has stiffening of frame joints, which divides each segment member on the flexible element and rigid arms. Under the action of applied lateral load in flexible parts of members the bending moments (Figure 5b) and compressive and tension axial forces occur. In the effect of the bending moment and axial force in spandrel beam sections tension stresses can occur which can cause the cracking of the flexible part of the spandrel beam and the reduction of the flexural rigidity of the whole member.

On the account of the multi-factor problem of deformation of sheared segment members of web frame of framed-tube structures, for simplification equivalent segment was accepted in which member stiffening in frame joints and shear deformations of members were taken into account by adequate modification of inertia moment of these members in the frame plane. It was also accepted that on the level of n^{th} story, the column contra flexure points are in half of their height ($l_c/2$), and frame joints undergo equal rotations and lateral displacements of average values Δ_i^n and θ_i^n. It was also assumed that the distribution of shear lateral load on each segment on the length of sheared frame is uniform and that on each segment an equal load value falls, depending on the number of sheared segments on the frame length. It was also assumed that shear lateral load on each segment is uniformly distributed on the length of sheared frame and on each of segments is acting the same loading value depending on number of sheared segments on frame length.

On the basis of the above mentioned assumptions it was taken that lateral loading in joints of particular columns and spandrel beams of web frames on n-th story will produce the average equal bending moments M_{cz}^n and M_{by}^n. The moments M_{cz}^n and M_{by}^n for members of n story can be written as a function of the shear force $V(z)$ acted on each of web frames, number of sheared segments on frame length n_b, shear rigidity of single segment GA, height of segment l_c and rigidity ratio of the columns and spandrel beam with taking into account of no dilatational strain and stiffening in frame joints $S'_{rs,e}$. After considering the stiffening effect in the frame joints the following expressions on bending moment $M_{cz,e}^n$ in columns (1) and $M_{by,e}^n$ in spandrel beams (2) in the member faces perpendicular to them were received (Figure 5b).

$$M_{cz,e}^n = M^n{}_{cz}\left(0.5 \cdot V(z), n_b, l_c, GA, S'_{rs,e}\right) \cdot \frac{l_c - h_b}{l_c}, \tag{1}$$

$$M_{by,e}^n = M^n{}_{by}\left(0.5 \cdot V(z), n_b, l_c, GA, S'_{rs,e}\right) \cdot \frac{s_c - b_c}{s_c}, \tag{2}$$

$$E_{cm}I^{n}_{bys,eff} = E_{cm}I^{n}_{bys,eff}\left(E_{cm}I^{n}_{bys,uncr}, E_{cm}I^{n}_{bys,uncr}, \frac{M^{n}_{by,e}}{M^{n}_{by,cr}}\right). \tag{3}$$

Omitting the minimum values of axial forces occurring in spandrel beam sections of n story, this member is characterized by flexural rigidity $E_{cm}I^{n}_{bys,uncr}$ defined as for the member uncracked for a moment (of time), in which in the fixing sections in column faces, the value of bending moment $M^{n}_{by,e}$ will not reach the value of cracking moment $M^{n}_{by,cr}$. After exceeding it the member flexural rigidity $E_{cm}I^{n}_{bys,uncr}$ undergoes reduction to the value of so called effective stiffness of the cracked member $E_{cm}I^{n}_{bys,eff}$ which characterizes cracked and uncracked rigidity intervals of the member. On the account of the distribution character of bending moments along the spandrel beam length, the effective rigidity of member $E_{cm}I^{n}_{bys,eff}$ diminishes to the minimum value of effective rigidity (Figure 6), as the lateral loading increases, an so does the bending moment $M^{n}_{by,e}$. The effective flexural stiffness $E_{cm}I_{bys,eff}$ of cracked spandrel beam (3) can be written as a function of stiffness of the uncracked section $E_{cm}I^{n}_{bys,uncr}$ and the cracking section $E_{cm}I^{n}_{bys,cr}$ as well as a ratio of the bending moment $M^{n}_{by,e}$ to the cracking moment $M^{n}_{by,cr}$.

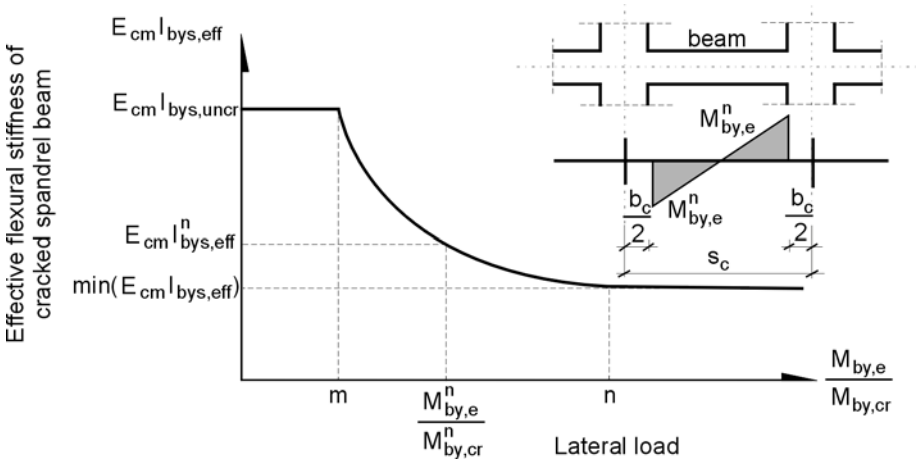

Fig. 6. Diagram of reduction of effective flexural stiffness of cracked spandrel beams in web frames of tube-framed structure (m, n – unknown values)

On the account of a significant simplification of the relationship (3) symmetric reinforcement arrangement in the spandrel beam section was assumed with the constant steel area on the spandrel length of n-th story. On this base the cracking moment $M^{n}_{by,cr}$ can be computed from the following equation:

$$M^{n}_{by,cr} = f_{ctm} \cdot \frac{I^{n}_{bys,uncr}}{0.5 \cdot h_b}, \tag{4}$$

where:

f_{ctm} – tensile strength of concrete spandrel,

$I^{n}_{bys,uncr}$ – reduced inertia moment of spandrel beam section,

h_b – height of cross section of concrete spandrel.

In the proposed model, certain quantities and relationships between them were defined which affect the values of the searched quantities of the bending moments in columns $M^{n}_{cz,e}$ (1), and in spandrels $M^{n}_{by,e}$ (2), as well as effective stiffness of cracked spandrels $E_{cm}I^{n}_{bys,eff}$ (3). A determination on relationship between these quantities on the basis of numerical study, with using of linear and nonlinear multi-factor analysis of framed-tube structures will make it possible to work-out the functions of searched quantities in statistic sense.

4. Parameter study and finite element analysis of framed-tube structures

In Table a review of geometrical and material characteristics of the executed tall buildings of framed-tube structures that were accepted in this study are presented.

Table. Parameters of executed tall buildings

	Parameter	Value 1	Value 2	Value 3
1.	slenderness ratio of tall building structure λ	5	7	
2.	maximum deflection at the top of the building	H/1000	H/1500	H/2000
3.	characteristic wind velocity pressure q_k	350 Pa	450 Pa	550 Pa
4.	axial columns spacing s_c	2.5 m	3.5 m	4.5 m
5.	axial columns height l_c	3.8 m		
6.	column cross section ratio h_c/b_c (height/width)	0.667	1.000	1.500
7.	ratio of spandrel beam cross section h_b/b_b (depth/width)	1.00	2.00	3.00
8.	stiffness ratio of concrete column cross section $E_{c-m}I_{czs}/l_c$ to concrete spandrel beam cross section $E_{c-m}I_{bys}/s_c$	0.5	1.0	2.0
9.	design compressive concrete strength, f_{cd}, mean tensile strength of concrete, f_{ctm}, concrete modulus of elasticity, E_{cm}	20 MPa 2.9 MPa 32 GPa	30 MPa 3.8 MPa 36 GPa	40 MPa 4.6 MPa 39 GPa
10.	floor spans	10 m		
11.	design yield stress of steel f_{yd}, modulus of elasticity of steel E_s	350 MPa 200 GPa		
12.	live load	2.5 kPa		
13.	floor plate thickness	0.30 m		

For the numerical study of 40-storey and 60-storey buildings of framed-tube structures of square floor plan were taken. In each of the structures six changes of cross section sizes were applied, every 10th stories and designed with satisfying con-

ditions represented by parameters 1–5, 10 and 12. In each structure a group of 10 stories mentally cut out was separately analysed which satisfy the conditions represented by parameters 6–9. For such accepted parameters on the basis of the linear analysis of MES reinforcement of spandrel beams and columns of the chosen study group of 10 storeys was determined. The combinations of variables 1–9 defined based on the study program $L_{18}(2^1 \times 7^3)$ according to Taguchi [3], which enabled the development of the population of 144 framed-tube structures. Based on the accepted parameters and on the determined reinforcement of columns and spandrel beams, ranges of quantities occurring in formulae (1–3) (see also Figures 7 and 8) were defined.

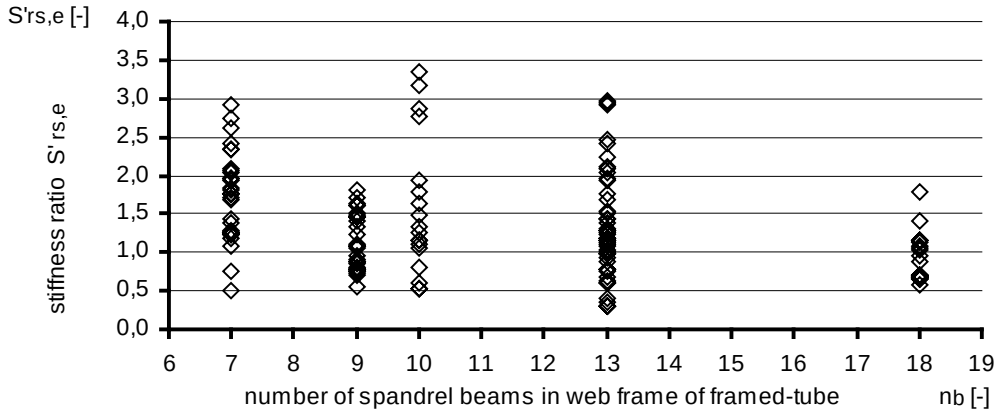

Fig. 7. Variation of stiffness ratio $S'_{rs,e}$ with number of spandrel beams in web frame of framed tube structure

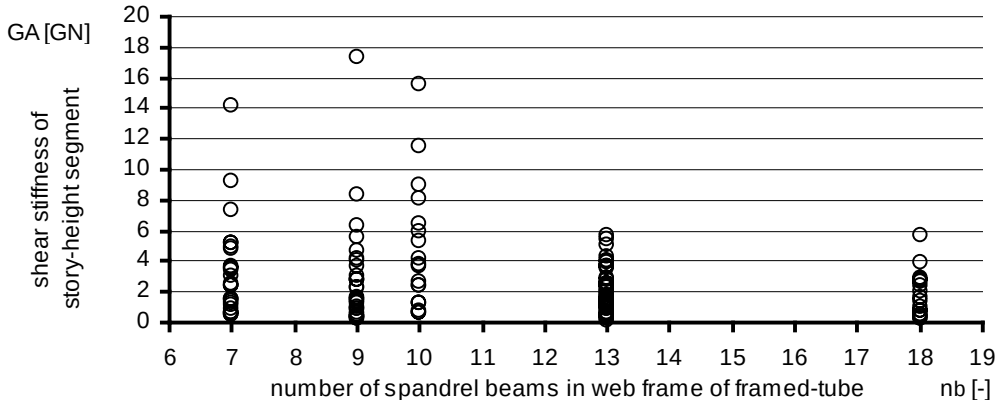

Fig. 8. Variation of shear stiffness of story-height segment with the number of spandrel beams in the web frame of framed tube structure

Nonlinear analyses of framed-tube structures with using of standard computer program supported on linear version of FEM covering of non-dilatational strains of mem-

bers were performed. The structure model was supported on bar elements generating a spatial structure of external framed-tube connected on each story level by a floor being a tube diaphragm. In the structure the frame joint stiffening were taken into account by modelling each member of columns and spandrel beams by three bar elements (two of infinite rigidity and an elastic one between them).

In the studied groups of 10 stories reduced inertia moments of bars were introduced which represent columns and spandrel beams. Spatial trapezoidal lateral load in the form of concentrated forces were applied to column joints in each level. In the model the symmetry of framed-tube structures was applied (Figure 9). The structure analysis in non-elastic phase of work was carried out applying the direct iterative method. The stiffness of cracked spandrel beams was determined on the basis of the effective stiffness presented in paper [4]. The effective stiffness takes into account uncracked and cracked intervals. The value of cracking moment $M_{by,cr}$ used in the numerical analysis was taking into consideration the actual axial compressive or tension force, occurring in particular spandrel beams of frame.

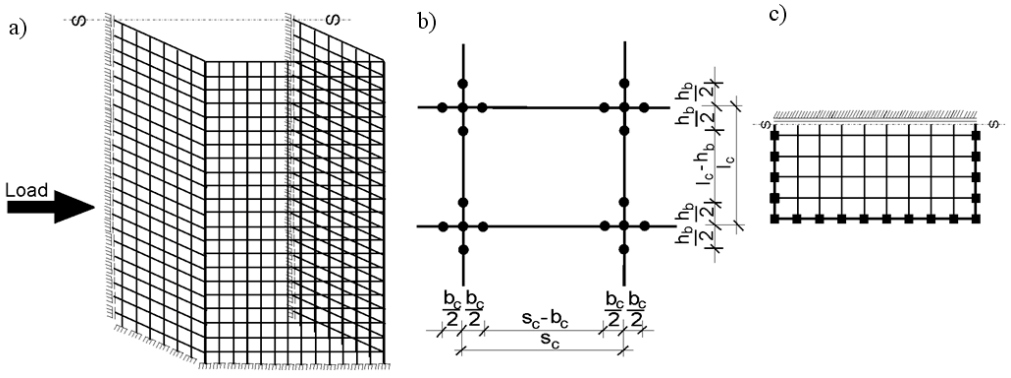

Fig. 9. Finite element idealization of symmetric framed-tube structure with symmetric loading: a) general view, b) idealization of frame members, c) idealization of floor system

5. Statistical-based analysis of flexural stiffness reduction of spandrel beams in RC framed-tube structures

On the basis of linear numerical analysis of web frames, for each examined structure level values of bending moments in spandrel beams and in columns in their fixed sections in faces of members perpendicular to them were obtained. Mean absolute values of these quantities for each story of structure were determined, which correspond to the values of bending moments in columns and spandrel beams obtained on the basis of formulae (1) and (2). Based on variance analysis of variable parameters in these formulae, the following relationships on bending moments in columns $M^n_{cz,e}$ and in spandrel beam $M^n_{by,e}$ were defined.

$$M_{cz,e}^{n} = 0.265 \cdot V(z) \cdot \frac{l_c}{n_b} \cdot \frac{l_c - h_b}{l_c} = 0.265 \cdot V(z) \cdot \frac{l_c - h_b}{n_b}, \tag{5}$$

$$M_{by,e}^{n} = 0.255 \cdot V(z) \cdot \frac{l_c}{n_b} \cdot \frac{s_c - b_c}{s_c}. \tag{6}$$

Figures 10 and 11 show a comparison of averaging values of bending moments in columns $M_{cz,e}^{n}$ and spandrel beams $M_{by,e}^{n}$ for each story, obtained by the numerical analysis and the values determined on the basis of formulae (5) and (6). The diagrams presented in these Figures confirmed the need of averaging of ratios of member stiffness $S'_{rs,e}$, the effect of segment shear stiffness GA and stiffening of members in frame joints on the distribution of lateral loading on individual members of frames parallel to action direction of this lateral loading, which enabled to obtain simple and effective formulae on averaging values of bending moments in columns $M_{cz,e}^{n}$ (1) and spandrel beams M_{by}^{n} (2).

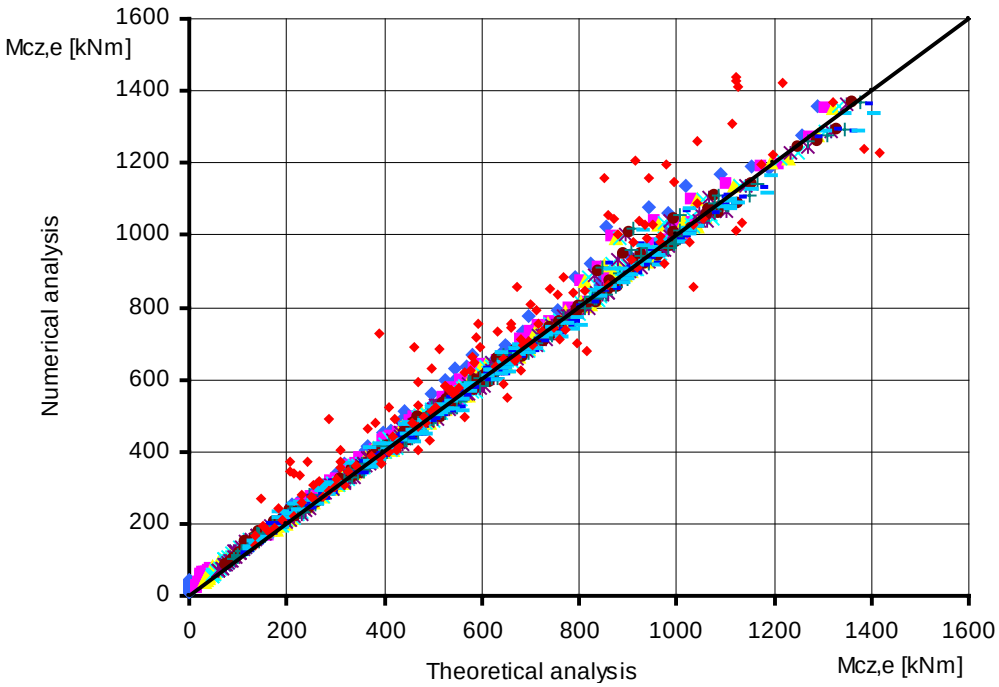

Fig. 10. Comparison of theoretical analysis (5) to numerical analysis of framed-tube structures

Having in mind the scatter of the above mentioned quantities caused by their averaging and the actual moment distribution on the length of the frame, increase corrections should be taken into account of the values of both quantities in middle members

of these frames for about 15–20%, and decrease corrections of the values of bending moments in side members of frames for about 15–20%.

This operation enables simplified determinations of the values of both quantities in particular members of the frames parallel to the direction of action of the lateral loading and it can be effectively applied in the initial conceptional stage of designing framed-tube structures or for verifications of the calculations obtained on the basis of computer programs. In this place it should be mentioned that the values of bending moments in columns and spandrel beams perpendicular to lateral loading of (web) frames, determined during numerical analysis were many times smaller in comparison with the moments in members of web frames on which longitudinal reinforcement in columns and spandrel beams should be calculated. On the basis of nonlinear numerical analysis on each considered story of the structure, the values of effective stiffness of cracked spandrel beams in web frames were defined. Mean values of the reduction of stiffness of cracked spandrel beams in the form of the ratio of effective stiffness of cracked spandrel beams $E_{cm}I^{n}_{bys,eff}$ to the values of stiffness of the spandrel beams defined as non cracking ones $E_{cm}I^{n}_{bys,eff}$ were defined.

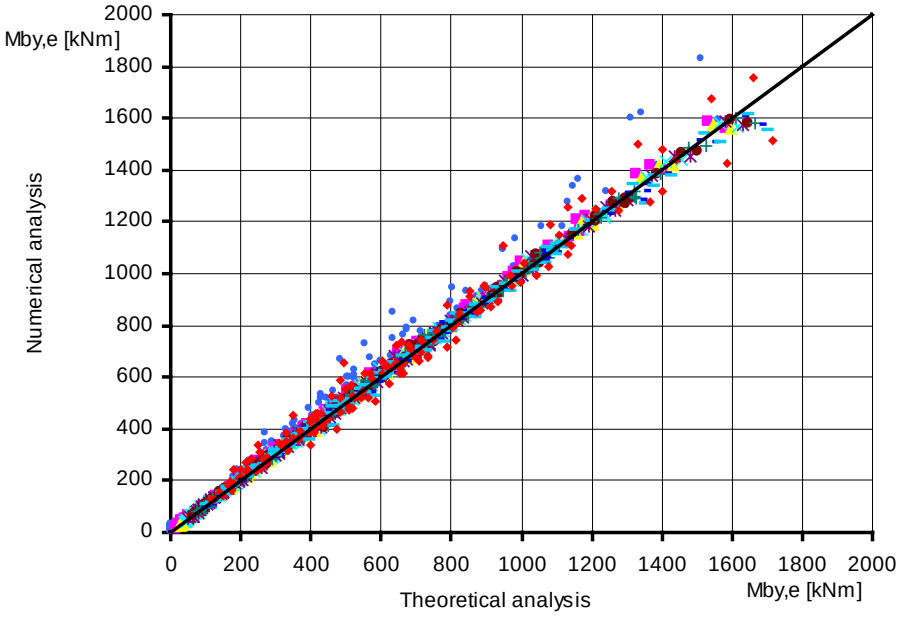

Fig. 11. Comparison of theoretical analysis (6) to numerical analysis of framed-tube structures

In Figure 12 presented was a distribution of the relationship of stiffness reduction of cracked spandrel beams $E_{cm}I^{n}_{bys,eff}/E_{cm}I^{n}_{bys,uncr}$ on each considered story of particular framed-tube structure in the dependence on the ratio of averaging values of bending moments defined by means of formula (6) to the value of cracking moment $M_{by,cr}$ de-

fined by means of formula (4). On the basis of the relationship of the distribution of the values between these variables following formulae and ranges of their applicability were defined.

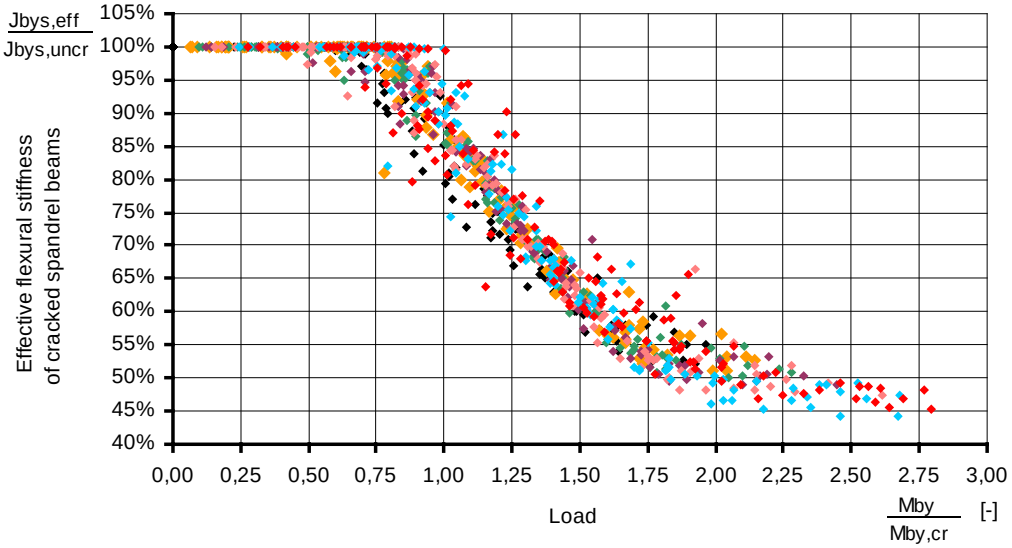

Fig. 12. Flexural stiffness reduction of spandrel beams in web frame with increasing lateral load

For the ratio of $m = (M^n_{by,e}/M^n_{by,cr}) < 0.86$ the averaging effective stiffness $E_{cm}I^n_{bys,eff}$ of n-th story of web frame of framed-tube structures subjected to action lateral loading corresponds to the stiffnesses of non cracking member $E_{cm}I^n_{bys,uncr}$ (7)

$$E_{cm}I^n_{bys,eff} = E_{cm}I^n_{bys,uncr}. \tag{7}$$

For range of $0.86 \le (M^n_{by,e}/M^n_{by,cr}) \le 1.93$ the averaging effective stiffnesses of nth story of framed tube structures can be described by using of following relationship:

$$E_{cm}I^n_{bys,eff} = 0.88 \cdot \left(\frac{M^n_{by.e}}{M^n_{by,cr}} \right)^{-0.86} \cdot E_{cm}I^n_{bys,uncr}. \tag{8}$$

For ratio of $m = (M^n_{by,e}/M^n_{by,cr}) > 1.93$ the averaging effective stiffnesses $E_{cm}I^n_{bys,eff}$ of spandrel beams of n^{th} story of web frames of framed-tube structures subjected to lateral loading action are corresponding to half a value of stiffness of the uncracked member:

$$E_{cm}I^{n}_{bys,eff} = \min\left(0.88 \cdot \left(\frac{M^{n}_{by,e}}{M^{n}_{by,cr}} \right)^{-0.86} \right) \cdot E_{cm}I^{n}_{bys,uncr} = 0.5 \cdot E_{cm}I^{n}_{bys,uncr}. \tag{9}$$

In Figure 13 a comparison of averaging effective stiffnesses $E_{cm}I^{n}_{bys,eff}$ of spandrel beams for each story numerically obtained to the values defined on the basis of the formulae (7–9) was presented. The above diagrams show a great convergence of the obtained theoretical and numerical effective inertia moments $E_{cm}I^{n}_{bys,eff}$ of the cracked spandrel beams, despite wide ranges of the parameters $S'_{rs,e}$ and GA, which were not directly taken into account in the formulae. The greatest departure from this convergence are the values close to 100% and 50% of the values of inertia moments $E_{cm}I^{n}_{bys,uncr}$ defined as for non-cracked sections, i.e. in the places of the changes of the monotonic intervals of data distribution. This should be explained by the effect of the averaging of the bending moment in the spandrel beams $M^{n}_{by,e}$ and by not regarding the direct influence of the ratios of inertia moments $I_{bys,cr}$, defined as for totally cracked sections to the corresponding to them inertia moment values determined as for non-cracked sections $E_{cm}I^{n}_{bys,uncr}$.

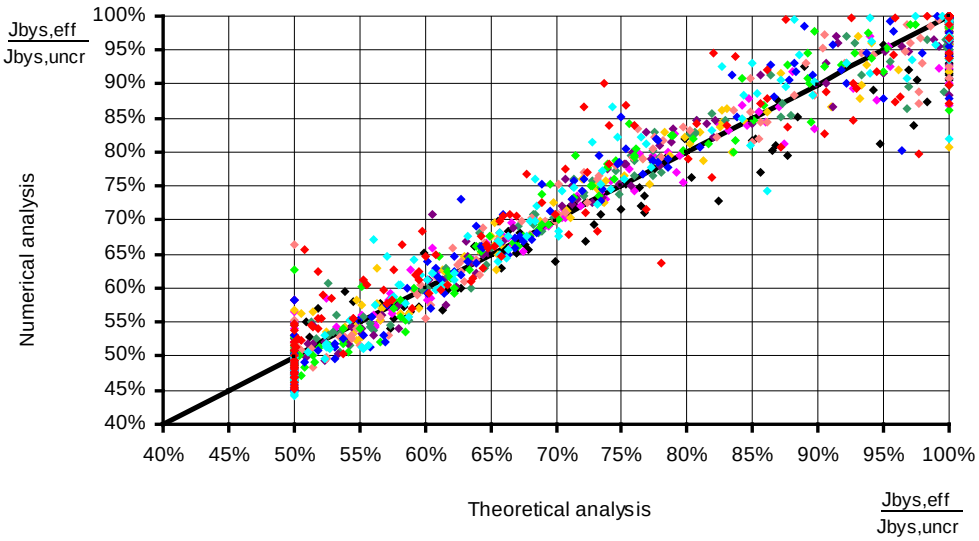

Fig. 13. Comparison of theoretical analysis (7–9) to numerical analysis of framed-tube structures

6. Conclusions

The presented formulas (5–9), worked out on the basis of the suggested frame model and of statistic data of the applied ranges of the parameters mentioned in Table made it possible to define simple relationships between bending moments $M_{by,e}$ and $M_{cz,e}$ in

the members of the web frames of framed-tube structures and the external lateral loading.

On the basis of the formulae (4) and (6) and of statistic data worked out with the use of a non-linear analysis of the population of 144 structures of 40- and 60-story tall buildings simplified formulae (7–9) defining the relationship of the value of effective stiffness of the spandrel beams to the mean bending moment in spandrel beams in the column faces $M_{by,e}$ to the value of the cracking moment of spandrel beams $M_{by,cr}$ on the n-th story were developed. On the basis of the diagrams presented in Figure 10–13 it can be evaluated that despite many changeable parameters these diagrams are characterized by simplicity and effectiveness, and they can be used in the initial stage of design of the evaluation of numerical results within the range of the presented values of these parameters. The application of formulae (7–9) in one of simplified methods of the estimation of framed-tube structure drift [5] will allow a quick evaluation of the behaviour of the cracked structure of a tall building under lateral load.

References

[1] Vecchio F.J., Balopoulou S.: *On the nonlinear behaviour of reinforced concrete frames*, Canadian Journal of Civil Engineering, Vol. 17, No. 6, 1990, pp. 698–704.

[2] Stafford Smith B., Coull A.: *Tall building structures: analysis and design*, John Wiley & Sons Inc., New York, 1991.

[3] Taguchi G.: *System of experimental design, engineering methods to optimize quality and minimize costs*, Unipub, Kraus International Publications, White Plains, New York, 1987.

[4] Chan Chun-Man, Mickleborough N.C, Ning F.: *Analysis of cracking effects on tall reinforced concrete buildings*, Journal of Structural Engineering, Vol. 126, No. 9, 2000, pp. 995–1003.

[5] Kwan A.K.H.: *Simple method for approximate analysis of framed tube structures*, Journal of Structural Engineering, Vol. 120, No. 4, 1994, pp. 1221–1239.

Metoda przybliżonej analizy wpływu zarysowania na sztywność poprzeczną konstrukcji budynku wysokiego o ramowo-powłokowym ustroju nośnym

W artykule zaprezentowano metodę przybliżonej analizy żelbetowych ramowo-powłokowych konstrukcji nośnych budynków wysokich poddanych obciążeniom poziomym. Rozpatrywano skutki zarysowania rygli ram konstrukcji. Artykuł przedstawia uproszczony teoretyczny model pracy konstrukcji tego typu. Analizy teoretyczne i wieloparametrowe analizy statystyczne różnych konstrukcji szkieletowych stały się podstawą do opracowania uproszczonej metody wyznaczania efektywnych momentów bezwładności dla zarysowanych rygli konstrukcji tego typu.

ARCHIVES OF CIVIL AND MECHANICAL ENGINEERING

Vol. X 2010 No. 1

Acceleration wave in a thin segmental hyperelastic rod

M. MAJOR, I. MAJOR
Technical University of Częstochowa, Akademicka 3, 42-200 Częstochowa, Poland.

The problem discussed in this paper runs on propagation of disturbances in the segmental rod of slowly varying cross-section area. The rod is made of three homogeneous and isotropic hyperelastic materials. This paper employs an approximate form of analysis based on the assumption of one-dimensional stress to find the transport equation for the intensity of the incident, reflected and refracted acceleration wave. Moreover, the numerical analysis of the problem of propagation of the acceleration wave in the thin segmental elastic rod of slowly varying cross-section was made. Results are illustrated for Murnaghan's nonlinear elastic materials.

Keywords: *segmental rod, acceleration wave, wave intensity*

1. Introduction

In this paper, the authors consider the propagation of acceleration waves (incident, reflected and transmitted) along the straight thin rods in which the diameter is much smaller than its length and the area of cross-section varies slowly with the length (Figure 1).

Acceleration wave propagation has been examined in detail by Bailey and Chen [1–2], and also by Chen [3–4]. From Jeffrey [5], and Jeffrey and Gilbert [6] results that for a medium in which the strain energy function $\Sigma(p)$ is such that $\partial^3\Sigma / \partial p^3 \neq 0$, ($p$ is the displacement gradient) the intensity of acceleration wave is governed by a Bernoulli equation. The basic equations for the case of rod with varying cross-section were described by Jeffrey [5]. The author showed that the transport equation for the wave intensity in the case of propagation of acceleration wave in the rod with varying cross-section, composed of the hyperelastic material, is a generalized Riccati`s equation.

In paper by Major [7] for a nonlinear compressible Murnaghan's material, the author proved that for the rod with a growing cross-section the acceleration wave intensity decreases, while for the rod with the decreasing cross-section along the rod the wave intensity grows. Based on present work, the authors put forward a proposal that the analysis showed in References [5–7] could be used for the cases of rod composited of plane segments normal to acceleration wave propagation direction. This problem could be a base to analysis of hybrid string constructions for example as a transmitting loads component of steel constructions of bridges and footbridges.

2. Basic equations

The authors consider the axis-symmetric segmental rod with slowly varying area of cross-section (in such way that S is at least a twice differentiable function of position in the rod), made of three homogeneous and isotropic hyperelastic materials of length l_i (i = 1, 2, 3). The density of medium is ρ_i, whereas the speed of propagation of longitudinal waves is c_i, for i = 1, 2, 3. The bottom indices are related to respective sections of the rod (Figure 1).

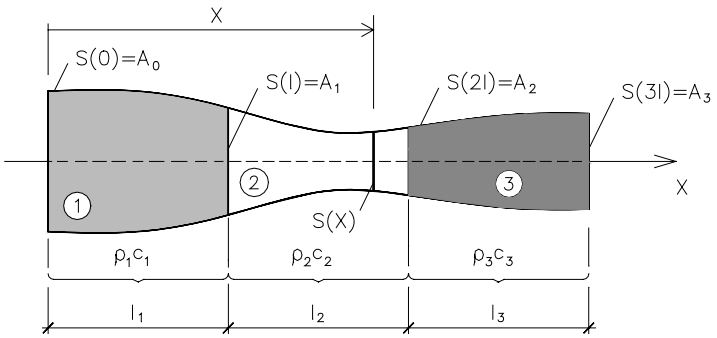

Fig. 1. The axis-symmetric segmental rod with slowly varying area of cross-section

It is assumed that the cross-section $S(X)$ varies slowly along the length of the rod. The Cartesian system of material coordinates $\{\mathbf{X}\}$ and the Cartesian coordinate system in space $\{\mathbf{x}\}$ describe the same space and covers mutually. The deformation can be denoted by (compare with [5])

$$x = u(x, t) + X, \tag{1}$$

where $u(x, t)$ is the displacement of a particle along the rod relative to an axis coinciding with the axis of the rod. In terms of these coordinates, the displacement gradient and the velocity are

$$p = \frac{\partial u}{\partial X} = u_X, \qquad v = \frac{\partial u}{\partial t} = u_t. \tag{2}$$

The authors assume that the nominal stress T at the cross-section is axial only and constant along the rod's cross-section. Then this assumption allows to propagation of the plane waves only, i.e.

$$T = \frac{\partial \Sigma}{\partial p} \neq 0, \tag{3}$$

where Σ is the strain energy function for hyperelastic materials (in this study it is assumed for Murnaghan's material (7)).

Moreover, the authors assume that there are no stresses at the lateral surface of the rod, so they defined the boundary conditions as approximated. The above assumptions exclude precise description waves' propagation in the rod at the longitudinal direction.

For the deformation (1) the equation of motion has the form (compare with [5])

$$\frac{\partial v}{\partial t} - c^2 \frac{\partial p}{\partial X} - \frac{T}{\rho}\frac{d}{dX}\ln S(X) = 0, \tag{4}$$

where

$$c = c(p) = \left(\frac{1}{\rho}\frac{\partial^2 \Sigma}{\partial p^2}\right)^{\frac{1}{2}} \tag{5}$$

As Equation (4) involves the two variables v and p, an additional equation is needed in order to close the system. This equation follows from the equality of mixed derivatives (compare with [6])

$$\frac{\partial p}{\partial t} = \frac{\partial v}{\partial X} \tag{6}$$

The basic equations governing one-dimensional acceleration wave propagation for the discussed case of the rod are thus Equation (6) and (4).

3. Propagation of acceleration wave in segmental rod

The authors assume that a wave propagating along the rod in the positive X direction starts from the end of the rod corresponding to $X = 0$ at time $t = 0$. The area before the wavefront remains at rest. The functions v and p are continuous, whereas their second derivatives experience at most a jump discontinuity. Then the wavefront, which propagates, is an acceleration wave.

The acceleration wave is propagating at the compressible elastic material determinated by Murnaghan's potential [8]

$$\begin{aligned} W(I_1, I_2, I_3) = \rho\Sigma(I_1, I_2, I_3) = \frac{l+2m}{24}(I_1-3)^3 + \frac{\lambda+2\mu+4m}{8}(I_1-3)^2 + \\ + \frac{8\mu+n}{8}(I_1-3) - \frac{m}{4}(I_1-3)(I_2-3) - \frac{4\mu+n}{8}(I_2-3) + \frac{n}{8}(I_3-1) \end{aligned} \tag{7}$$

where I_1, I_2 and I_3 are the invariants of the left Cauchy-Green deformation tensor. The hyperelastic Murnaghan's material describe five constants of elasticity – l, m, n, λ, μ. The l, m, n are the constants of second-order elasticity, and λ, μ are the Lamé constants. For the analyzed material one obtains [9]

$$\Sigma_1 = \frac{1}{\rho}\left[\frac{l+2m}{8}(I_1-3)^2 + \frac{\lambda+2\mu+4m}{4}(I_1-3) + \frac{8\mu+n}{8} - \frac{m}{4}(I_2-3)\right],$$

$$\Sigma_2 = -\frac{1}{\rho}\left[\frac{m}{4}(I_1-3) + \frac{4\mu+n}{8}\right], \quad \Sigma_3 = \frac{1}{\rho}\cdot\frac{n}{8}, \tag{8}$$

$$\Sigma_{11} = \frac{1}{\rho}\left[\frac{l+2m}{4}(I_1-3) + \frac{\lambda+2\mu+4m}{4}\right], \quad \Sigma_{111} = \frac{1}{\rho}\left(\frac{l+2m}{4}\right)$$

where

$$\Sigma_K = \frac{\partial\Sigma}{\partial I_K}, \qquad \Sigma_{KL} = \frac{\partial^2\Sigma}{\partial I_K \partial I_L}, \qquad \Sigma_{KLM} = \frac{\partial^3\Sigma}{\partial I_K \partial I_L \partial I_M}, \quad K, L, M = 1, 2, 3. \tag{9}$$

For the deformation (1) the invariants of deformation tensor are

$$I_1 = p^2 + 2p + 3, \qquad I_2 = 2p^2 + 4p + 3, \qquad I_3 = p^2 + 2p + 1, \tag{10}$$

while the coordinate of stress tensor is equal

$$T = 2\rho(1+p)(\Sigma_1 + 2\Sigma_2 + \Sigma_3). \tag{11}$$

For the initial value, when $p = 0$, the invariants of deformation tensor (10) are equal

$$I_1 = I_2 = 3, \qquad I_3 = 1. \tag{12}$$

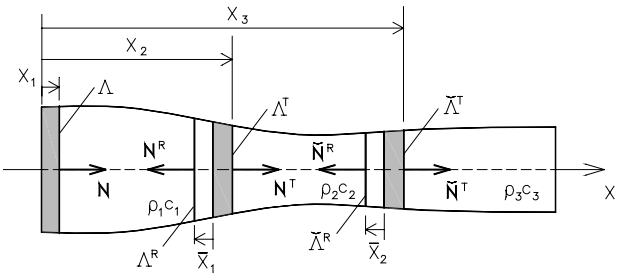

Fig. 2. Following position of discontinuity surface Λ (incident, reflected and transmitted) for X_i (i = 1, 2, 3) propagating in **N** direction in the thin segmental rod ($\bar{X}_i$ (i = 1, 2) denotes following position of the reflected wave and $\breve{N}^R$, $\breve{N}^T$, $\breve{\Lambda}^R$, $\breve{\Lambda}^T$ denotes quantities at the second surface of the segments contact)

The quantities with superscripts *R* and *T* (Figure 2) will be used to denote the reflected and transmitted wave, respectively.

4. Intensity of acceleration wave for researched cases of segmental rod

After denote by $\sigma(X)$ the intensity of the propagating acceleration wave at a point X of the considered rod ($\sigma^T(X)$ – the intensity of the transmitted wave, $\sigma^R(X)$ – the intensity of the reflected wave), based on [4] we have the following conditions at the surface of the layers contact (Figure 3), results of continuity stress and displacements X^+ will be used to denote the value of a quantity at the discontinuous surface Λ immediately ahead of the wavefront, and X^- – to denote its value at the same discontinuous surface Λ immediately behind the wavefront.

$$\begin{aligned}
\frac{\sigma^T(X^+)}{\sigma(X^-)} &= \frac{2\rho_1 c_1}{\rho_1 c_1 + \rho_2 c_2}, \qquad \frac{\sigma^R(X^-)}{\sigma(X^-)} = \frac{\rho_1 c_1 - \rho_2 c_2}{\rho_1 c_1 + \rho_2 c_2}, \\
\frac{\breve{\sigma}^T(X^+)}{\breve{\sigma}(X^-)} &= \frac{2\rho_2 c_2}{\rho_2 c_2 + \rho_3 c_3}, \qquad \frac{\breve{\sigma}^R(X^-)}{\breve{\sigma}(X^-)} = \frac{\rho_2 c_2 - \rho_3 c_3}{\rho_2 c_2 + \rho_3 c_3},
\end{aligned} \tag{13}$$

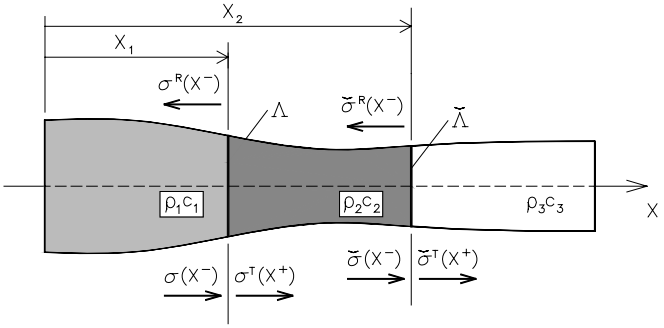

Fig. 3. Incident, transmitted and reflected acceleration wave propagating in segmental rod

Assuming that the cross-section of considered rod is equal: $S(X) = Ae^{\gamma x}$, the intensity of acceleration wave $\sigma(X)$ equals [7]

$$\sigma_1(X) = \sigma(0)\frac{e^{-\frac{Q(X)\cdot X\cdot\gamma}{2}}}{1-\sigma(0)\left[2\left(e^{\frac{Q(X)\cdot X\cdot\gamma}{2}}-1\right)\frac{\beta(X)}{Q(X)\cdot\gamma}\right]}, \tag{14}$$

where

$$Q(X)=\left[1-\frac{T_o}{2\rho^2 c_o{}^4}\left(\frac{\partial^3\Sigma}{\partial p^3}\right)_o\right],\qquad \beta(X)=-\frac{1}{4\rho c_o{}^4}\left(\frac{\partial^3\Sigma}{\partial p^3}\right)_o. \tag{15}$$

and

$$c_o{}^2=\left(\frac{dX_a}{dt}\right)^2 \tag{16}$$

is the speed of propagation of the acceleration wavefront in position $X = X_a$. Quantities with subscript o denotes values before wavefront.

For the cross-section of considered rod: $S(X) = Ae^{-\gamma x}$ [7], the intensity of acceleration wave $\sigma(X)$ is equal

$$\sigma_2(X)=\sigma(0)\frac{e^{\frac{Q(X)\cdot X\cdot\gamma}{2}}}{1+\sigma(0)\left[2\left(e^{-\frac{Q(X)\cdot X\cdot\gamma}{2}}-1\right)\frac{\beta(X)}{Q(X)\cdot\gamma}\right]}. \tag{17}$$

The authors assume for the analysis the two cases of the segmental rod:
a) with a growing cross-section and
b) with a decreasing cross-section along the rod.

5. Numerical analysis

The numerical analysis is based on Equation (13). For the considered Murnaghan's material the materials constants (7) for the steel are equal [10]

$$\begin{aligned}&\lambda=111\cdot10^{-9}\ N/m^2,\qquad \mu=82.1\cdot10^{-9}\ N/m^2,\\ &l=-459\cdot10^{-9}\ N/m^2,\qquad m=-461\cdot10^{-9}\ N/m^2,\qquad n=-358\cdot10^{-9}\ N/m^2.\end{aligned} \tag{18}$$

For the aluminium

$$\begin{aligned}&\lambda=57\cdot10^{-9}\ N/m^2,\qquad \mu=27.6\cdot10^{-9}\ N/m^2,\\ &l=-299\cdot10^{-9}\ N/m^2,\qquad m=-311\cdot10^{-9}\ N/m^2,\qquad n=-228\cdot10^{-9}\ N/m^2.\end{aligned} \tag{19}$$

It is assumed that at the beginning the considered material of the segmental rod is undeformed, then $T_o = 0$.

According to [11], the values of dynamical deformations in the propagation of acceleration waves processes in the metals include at the interval between 10^{-2} s^{-1} to

10^2 s^{-1}. Then the authors assume that the quantity of initial intensity $\sigma(0)$ (Equations (14) and (17)) according to [11] is equal 10^{-2} m/s^2.

The authors assume for the segmental rod with slowly varying cross-section the γ coefficient needed to describe variability of the cross-section and this coefficient is $\gamma = 0.5$ m^{-1}.

For the considered rod whose the first and the third segments are composed of the aluminium, while the second one of the steel, for the intensity of acceleration wave is obtained the following diagrams.

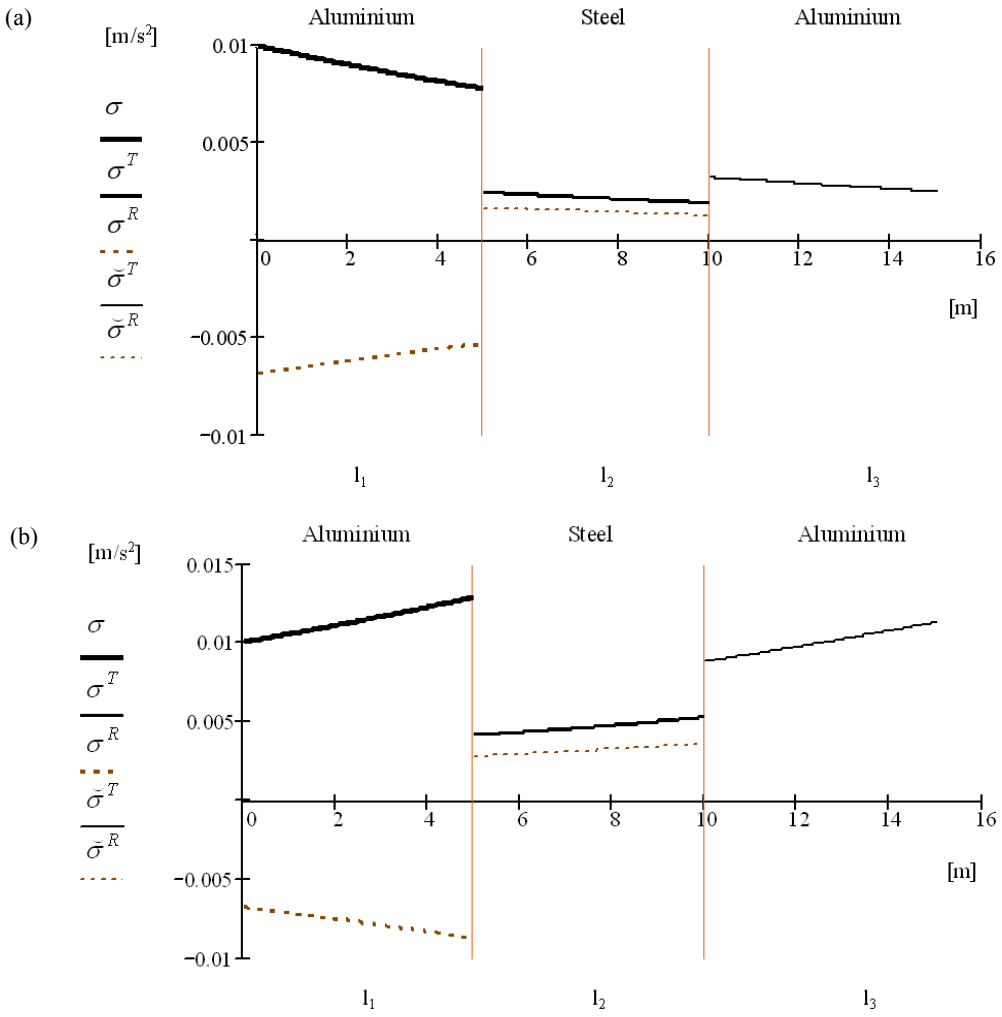

Fig. 4. Diagrams of intensity of acceleration wave propagating at segmental rod's intervals l_1, l_2, $l_3 = 5$ m: (a) for $S(X) = Ae^{\gamma x}$, (b) for $S(X) = Ae^{-\gamma x}$

6. Summary

The numerical analysis shows that for the thin segmental rod with slowly varying cross-section the propagating incident, reflected and transmitted wave intensity changes.

For the case of a segmental rod with slowly growing cross-section along its length (X value), both incident and transmitted acceleration wave intensity decreases while the reflected wave intensity grows (Figure 4a). For the inverse case, i.e. for the rod with slowly decreasing cross-section along its length, the incident and transmitted wave intensity grows, while the reflected wave intensity decreases (Figure 4b).

There are the jumps of propagating acceleration wave intensity at the plane of contact of considered thin rod segments. The transmitted acceleration wave intensity is smaller then incident during the transition from the first segment (aluminium) to second segment (steel). Transitioning to the third segment (aluminium) the transmitted wave intensity is bigger then incident acceleration wave intensity from the second segment (compare with Figure 4a, b).

In the case of a segmental rod whose first and third segments are made of steel and second of aluminium (Figure 1), the dependences between propagating acceleration wave intensity jumps at the contact of each segments are reverse to those presented in this paper. The difference between propagating acceleration wave intensity results from diversification of medium density (Figure 1), in which the wave propagates.

During transition from the denser medium to the lighter medium the propagating acceleration wave intensity increases, whereas in the reverse case (i.e. the transition from the lighter medium to the denser medium) the propagating acceleration wave intensity decreases.

References

[1] Bailey P.B., Chen P.: *On the local and global behavior of acceleration waves*, Arch. Rat. Mech. Anal., No. 41, 1971, pp. 121–131.
[2] Bailey P.B., Chen P.: *On the local and global behavior of acceleration waves: addendum, asymptotic behavior*, Arch. Rat. Mech. Anal., No. 44, 1971, pp. 212–216.
[3] Chen P.J.: *Selected topics in wave propagation*, Noordhoff, Layden, 1976.
[4] Chen P.J.: *The growth of acceleration waves in arbitrary from in homogeneously deformed elastic materials*, Arch. Rat. Mech. Anal., No. 30, 1968, pp. 81–89.
[5] Jeffrey A.: *Acceleration wave propagation in hyperelastic rods of variable cross-section*, Wave Motion, No. 4, 1982, pp. 173–180.
[6] Jeffrey A., Gilbert R.P.: *On the approximation of acceleration waves in rods*, Int. J. Non-Linear Mechanics, Vol. 22, No. 3, 1987, pp. 209–215.
[7] Major I.: *Propagacja fali przyspieszenia w pręcie o zmiennym przekroju*, Zeszyty Naukowe Politechniki Śląskiej, No. 1559, 2002, pp. 379–386.
[8] Wesołowski Z.: *Zagadnienia dynamiczne nieliniowej teorii sprężystości*, Warszawa, PWN, 1974.

[9] Kosiński S.: *Odbicie i ewolucja fali uderzeniowej w wybranych materiałach hipersprężystych*, Warszawa, IPPT PAN, 1995.
[10] Porubov A.V.: *Amplification of nonlinear strain waves in solids*, Singapore, World Scientific Publishing, 2003.
[11] KLEPACZKO J.: *Doświadczalne badania sprężysto-plastycznych procesów falowych w metalach*, Warszawa, IPPT PAN, 1970.

Fala przyspieszenia w cienkim segmentowym hipersprężystym pręcie

Zagadnienie omawiane w pracy dotyczy propagacji zaburzenia wzdłuż długości prostego cienkiego warstwowego pręta, którego powierzchnia przekroju poprzecznego powoli się zmienia. Pręt wykonany jest z trzech jednorodnych i izotropowych materiałów hipersprężystych na odcinkach o długości l_i każdy. W pracy użyto przybliżonej formy analizy przy założeniu jednoosiowego naprężenia w celu określenia równania transportu energii dla fali padającej, odbitej i transmitowanej. Ponadto została przeprowadzona analiza numeryczna dla propagacji fali przyspieszenia w cienkim sprężystym warstwowym pręcie o wolno zmieniającym się przekroju poprzecznym. Wyniki zostały przedstawione dla hipersprężystego materiału Murnaghana.

ARCHIVES OF CIVIL AND MECHANICAL ENGINEERING

Vol. X 2010 No. 1

Problems of identification of strength properties of rubber materials for purposes of numerical analysis: a review

D. MAZURKIEWICZ
Lublin University of Technology, Nadbystrzycka 36, 20-618 Lublin, Poland.

Proper selection of elements of an industrial-grade adhesive joint consisting of various types of rubber materials, supported by a detailed analysis of the phenomena occurring within the joint, especially with respect to fatigue performance, is still a very difficult and largely unresolved issue. Only single studies using FEM numerical modelling have made attempts at assessing and analyzing the phenomena occurring within the joining area of a rubber conveyor belt. This has been caused by a number of problems that have made obtaining reliable and repeatable results impossible, including the problem of defining appropriate material models for the rubbers of the individual layers of the belt and the joint, which introduce strong non-linear effects into the calculations. Rubber as an adhesive base and a construction material is unique, and its properties can be quite diverse dependent on its composition, content of additives, etc. A vulcanized rubber composition, for instance, consists of one or more rubbers and different types of additives which shape its future properties. That is why solution of the problem of identification of the strength properties of this type of materials for developing an adequate numerical model of an adhesive joint is an important issue from the point of view of industrial application of this method of bonding rubber materials; and especially so that expertise in proper use of appropriate adhesives and appropriate joining parameters is indispensable for obtaining optimal properties and maintenance characteristics of the joint. A typical error in preparing material models of rubber is that strength tests for determining stresses and strains are conducted with reference to the initial value of a specimen's cross-section. A large, unanalyzed reduction in the area of the specimen during a strength test has a significant effect on the precision of a FEM model of the analyzed structure. This article analyzes this problem with regard to the modelling of adhesive bonding of rubber materials with a rubber adhesive by presenting a mode of action to be adopted in identifying the strength characteristics of the analyzed materials which eliminates the imprecision of the FEM model.

Keywords: *adhesive joint, strength properties, rubber materials, FEM numerical modelling*

1. Introduction

Elastomers have been among the group of commonly used construction materials since 1850, when natural rubber was first used to make energy-absorbing rings in railway buffers [1]. For almost 160 years that have passed since that event, construction elements made from natural as well as synthetic rubber have been an inseparable part of nearly every machine or technical device. This fact is, among others, a consequence of the exceptionally dynamic development of methods of producing those synthetic polymers. Owing to constant improvements in processing methods and development of new and more effective vulcanizing agents, fillers and other additives,

the types of rubber used are constantly being modified. New products, with properties often tailored to the special requirements of users, are also developed.

The popularity of elastomers as construction materials is not merely a result of the dynamic development of the rubber industry and its wide product range. A more relevant cause here are the unique properties of rubber, including, in particular, its large deformability and the possibility of producing materials of diversified properties thanks to the use of a rich set of different types of additives including activators, inhibitors and accelerators of vulcanization as well as anti-reversion agents and plastifiers [1–2]. The possibility of developing such great wealth of rubber construction materials with varied properties imposes the necessity of using laboratory durability, reliability, or quality tests conducted according to normalized methods. This is of fundamental significance both for the design of rubber materials and the assessment of the usefulness of structural elements made from them.

The methods of studying physical characteristics of rubber have over the recent years been significantly improved and standardized. Most of them are based on international norms, in particular with reference to basic and applied research. The goal of normalization was, in the first instance, the necessity to guarantee comparability of results of quality control tests. When using data obtained in that manner for numerical modelling, and in particular for representing strength properties of the modelled rubber materials, one has to be aware of the limitations following from this fact. Problematic here, from the point of view of numerical modelling, are the standard-conforming simplifications that are used in such studies. They follow mainly from the limitations of laboratory conditions, the necessity to use complicated and expensive measurement apparatuses or a lack of the need for more precise analysis. Although data obtained in that manner do allow a reliable comparison of results in instances such as the already mentioned quality control, they are not suitable for use in subsequent studies of operational features carried out using numerical methods, in particular the finite element method. A case in point is, among others, the necessity to properly specify the full range of strength properties of rubber materials during tension for the purposes of their modelling in finite element method analysis of rubber structures. The arbitrariness of strength characteristics or their elements adopted in modelling or errors made in the course of laboratory tests of rubber materials result in low reliability and low usefulness of the results of numerical modelling obtained in this way.

In view of the above, the goal of the present publication is to analyze the causes of mistakes made in this area and to indicate a solution to the problem of accurate identification of strength properties of rubber materials using an example of the construction of a numerical model of an adhesive joint joining segments of a rubber fabric conveyor belt. This specific example of different uses of rubber materials in one structure as two types of layers of a conveyor belt with fabric interlayer and, additionally, as a joint made using a rubber adhesive is an important constructional and operational problem. At the same time, it is a representative example of the importance of the analyzed problem for appropriate reliability and repeatability of results of laboratory

tests and numerical analyses based on them that assess the strength, quality or usefulness of a rubber product.

2. Rubber materials in the construction of conveyor belts

Deformability of elastomers, i.e. their ability to return to the original size after removal of load, which may have the character of repeated loading cycles, with their simultaneous resistance to the action of aggressive conditions of the surroundings make them a basic material for the construction of conveyor belts. Available on the market are a number of conveyor belts of various structures, sizes, properties and applications. For instance, one of the leading Polish manufacturers – the Conveyor Belt Factory STOMIL Wolbrom plc offers, among others, flame-resistant, non-flammable, normal, and high-temperature resistant belts, belts with steel cables, belts with profiled working surface and food transportation belts.

Flame-resistant rubber-fabric belts, most frequently used in industrial practice, are intended for transportation of loose materials with a wide range of granule sizes, at the range of working temperatures from –5 ºC to +60 ºC. A multi-ply rubber-fabric belt has a core composed of several (2 to 6) layers of technical fabric impregnated with a rubber-to-fabric adhesion promoter. The individual plies are interlaid with core rubber. The number and kind of plies determine the strength of the belt. A ply consists of warp threads running lengthwise and transverse weft threads. The most frequently used fabrics are polyester, polyamide, cotton, viscose and aramid. The core, which is responsible for the strength properties of a belt, is protected by a rubber bearing cover that interacts with the transported material and a rubber running cover that comes in contact with the load-bearing structure. Thus, the basic elements of such a belt are the rubber-fabric composite constituting the core, which is the vehicle of the belt's strength, and rubber covers and rims. Belt covers can be produced from rubbers of different grades and properties. As a standard, belt covers are made from normal, flame-resistant, non-flammable, high-temperature resistant (up to 250 ºC at points), or oil and grease resistant rubbers.

Such a large diversity of belt types, their parameters and uses makes it necessary to select them to match the planned working conditions and loading. A conveyor belt, then, is chosen so that it can transmit, with an appropriate safety coefficient, the largest possible tensile forces occurring in the different states of conveyor operation. The structure of a belt and the materials from which it is made endow it with particular physico-mechanical features, which have to match a given conveyor structure, the type of material to be transported, the operating conditions and the type of the surroundings in which the belt is to be operated. A conveyor belt, then, should be appropriately elastic and should be characterized by a high coefficient of friction between the belt and a drive pulley as well as between the belt and the transported material.

Rubber conveyor belts may then have different structures, widths, strengths, and cover thicknesses, as well as different properties of the layers of rubber and protective

plies or special bearing cover profiles. For their proper use resulting in an appropriate reliability, belts have to be properly selected, since their durability to a large extent depends not only on their proper structure with respect to the operational conditions but also on a sensible choice of the type of rubber and of appropriate constituents of compositions [3].

Belt conveyors are devices that, due to the character of their operation and varying length, must be made by joining many sections. Typical belt joints are made with the cold bonding method using a rubber adhesive. Among the significant drawbacks of this type of joints, one should count their low tensile strength compared with the tensile strength of the belt itself. As an effect of this, in operating conditions conveyor belt joints are frequently ruptured without any prior symptoms that might testify to the near occurrence of this type of failure. Obviously, this is a circumstance that is highly undesirable in every respect [4–6]. That is why the majority of current research and implementation studies on multiply conveyor-belt joints are aimed at increasing the strength and reliability of the different types of joining. One direction of research in this case is an analysis and assessment of the distribution of stresses in the joint and an analysis of the effect that the very structure of the belt, including the properties of the constituent materials, has upon it. Identification of stresses in the adhesive joint makes possible its proper structural modelling as well as proper selection of materials, their properties, and the mode of making a durable joint.

Because of the complexity of the structure of a rubber-fabric belt and its lap joint as well as the difficulties in correct modelling of the properties of the individual layers, which often have non-linear characteristics, the models developed include a number of simplifications. The accompanying laboratory verification studies, on the other hand, are often conducted in a rather cursory and fragmentary manner, which in turn results from technical difficulties, the necessity to possess specialist laboratory equipment and the associated very high costs, constituting the major limitation in this case [6].

Basic assessment of the quality of both the belt and the joining of its sections can be performed in a simple way in laboratory conditions. However, comprehensive analysis aimed at a proper selection of the elements of the joint (its structure and the properties of the materials used), additionally supported by a detailed analysis of the phenomena taking place within the joint, especially in terms of fatigue performance, is still a very difficult and largely unresolved issue. Of help here might be numerical analysis using the finite element method (FEM) – which is the most widely used method of computer-aided calculation and engineering analysis in mechanical engineering [7–11]. Although this method is successfully used in research on adhesive joints, especially that regarding joining of metal materials [12–13], so far only few research studies using FEM modelling have made an attempt to assess and analyze the phenomena taking place in the joining area of the conveyor belt. This results from a number of associated problems that make obtaining reliable and repeatable results impossible, such as, among others, defining the appropriate material models of the individual layers of the belt and the joint, which introduce non-linear effects into the calculations.

3. The effect of errors in identification of the properties of conveyor belt materials on the precision of the FEM model

The use of FEM for an analysis of stresses within the joining area of a conveyor belt was, among others, an element of research carried out by Błażej [14], the aim of which was to compare elongation and stress values in an adhesive joint determined with the use of video recording. The numerical analysis conducted for that purpose involved development of an appropriate geometric model and a corresponding discrete model of a conveyor belt, determination of the external loads acting on the belt, and making numerical calculations. The numerical calculations were made with a view to determining the stress and elongation in the joining area of the conveyor belt for different combinations of fabrics and rubber compositions analyzed in the study. The obtained results, however, are rough and preliminary, and more precise values of the analyzed quantities would be obtainable with the use of actual, laboratory-determined strength properties of the constituent parts of the joint instead of the adopted approximate coefficients. In the studies, the material constants and their strength characteristics, which are extremely important for the final result, were specified in an approximate manner and burdened with additional errors influencing the final outcome of modelling.

Defining the strength parameters of the constituent materials of a conveyor belt joint in approximate terms or their adoption on the basis of universal charts are some of the causes of the later imprecision of the FEM models being developed. Another source of imprecision of the stage of numerical modelling is construction of material models for rubber on the basis of classical uniaxial tensile tests.

In standard applications, calculations of tensile strength conventionally adopt the area of the specimen's initial cross-section, which is larger than the actual cross-section at a given moment of specimen deformation. This way, by dividing force by the initial cross-sectional area, the value of engineering or nominal stress is obtained. To determine the value of true stress, i.e. one that would take into account the deformation of the specimen during the test, actual values of the cross-sectional area corresponding to the value of the acting force should be adopted for calculations. This is possible only when the reduction in the cross-sectional area is taken into consideration, which, apart from the standard measurement of force, requires an additional, integrated measurement of the changes in specimen geometry at an appropriate sampling frequency.

This customary norm-conformant simplification affects in a significant manner the subsequent imprecision of a strength-test based FEM model of a rubber structure, because the analyses adopt stress values that are lower than actual ones. Therefore, it is important that identification of the strength properties of rubber materials be carried out using a method guaranteeing measurement of the actual value of the specimen's cross-section at a given moment of its deformation.

Certain complications or errors in preparing a set of data for numerical modelling of conveyor belts and their joints may also result from using values stated in quality

certificates coming from certification tests conducted by laboratories of companies producing conveyor belts. These tests, performed on the basis of norms replacing the earlier branch standards, are suited to the specific requirements of quality and acceptance testing of finished rubber products in a given industrial sector. In conformity with norm [15], when determining, for instance, the tensile strength of a conveyor belt, one should express the result of the measurement in kN/m, dividing tensile force by specimen width and not by its cross-sectional area. A procedure for preparing strength data of rubber materials for FEM modelling that is devoid of the described errors is presented below.

4. Need for numerical modelling of belt joints

In all types of structures that use adhesive bonding as an element-joining method, the durability of the joint should be treated as one of the basic indexes of its operational usability. Unfortunately, the issue of durability of adhesive joints is often almost completely ignored by constructors and technologists. This is also the case with rubber adhesives used in conveyor belt joints, for which there are no available research results specifying in what manner the properties of an adhesive and the type of joint influence the latter's durability. This is one of the reasons why theoretical values of tensile strength of conveyor belt adhesive joints and its actual values still strongly diverge [16]. A potential solution to this problem is to obtain the indispensable information by carrying out analyses of stress and strain distribution in the joining area using numerical methods. An analysis of this sort can be performed by means of numerical modelling using the classical method of finite elements, which is believed to be of constantly growing significance, especially in designing rubber construction elements [1, 11, 17]. The relation between force and displacement is expressed in this method by means of the stiffness matrix, whose constituent elements include material constants describing the mechanical properties of the modelled materials.

As shown earlier, their inaccurate or imprecise definition is the primary cause of errors and divergences in the results of conducted analyses. This is particularly important in the case of modelling a joint of a conveyor belt that consists of different types of rubber, plies of fabric, and a rubber bonding adhesive. The values of the individual parameters adopted in, say, strength analysis of conveyor belts and their joints differ [14, 18–21], and in the case of the value of Young's modulus for a layer of fabric ply the difference may frequently be as high as 100%. It can, therefore, be stated that, despite the large number of publications in that field in the recent years, proper, accurate and reliable determination of the mechanical properties of materials, especially those made of rubber, is still a fairly complex issue [22–25].

Thus, adequate determination of the features of the materials used in the analyzed joint requires laboratory studies, the aim of which is to determine the strength properties of the materials that make up the analyzed joint. The present work analyzes and models a joint of a four-ply rubber-fabric belt, as one that is most frequently used in

industrial conditions [19, 20, 26–27]. The laboratory research work described in the subsequent part of this paper as well as the identification of the material features for purposes of FEM numerical modelling were performed using belt specimens and specimens of belt and joint constituent materials used in the production of a flame-resistant belt (type 1600) listed in a product catalogue, including specimens of this type of belts used by the Lublin coal-mining company Lubelski Węgiel "Bogdanka" plc [11].

The aim of numerical analysis here is, among others, to estimate the possibility of using the developed FEM model of a joint for predicting the durability and strength of the joint, as well as using it at the stage of designing the geometry of the joint. It is expected that use of FEM-based numerical simulation in this case will enable precise analysis of stress distribution in the joining area of the selected conveyor belt, this way making possible the determination of areas of stress concentration or an unfavourable character of the stresses from the point of view of joint durability. It is believed [28–29] that this method can be treated as a significant expansion and supplementation of the analytical methods for assessing the state of stress and strain, which simultaneously makes possible reliable and precise determination of the share of individual stress components, which, as a rule, constitutes important information in the design and optimization of adhesive joints. Of no mean significance is also the possibility this type of modelling gives of predicting the strength of adhesive joints of different geometry and different constituent material parameters without the need to use troublesome and, in the case of conveyor belts, expensive destructive tests.

5. Laboratory tests of the constituent materials of a joint

The constituent materials from which the conveyor belt and the joint are assembled, like all other construction materials, are characterized by mechanical properties that are interesting for strength-related reasons [11]. These values are well represented by stress-strain curves or the dependencies of stress on strain associated with those curves. A correct characterization and description of the modelled materials is always a basis for creating a precise FEM model of the analyzed object.

In the case of the adhesive joint of a conveyor belt regarded as an anisotropic body, strength tests of the materials that make up the joint had to be carried out to prepare appropriate input data into the FEM model. This necessity resulted from the earlier described lack of reliable data regarding the materials used in making the joint.

On account of this, four types of materials that make up a typical industrial-grade joint of the analyzed 1200 mm four-ply belt were subjected to experimental studies. These were appropriately prepared specimens of the external layer rubber (1.322 g/cm^3 thick) and the rubber of the interplay layer (1.505 g/cm^3 thick), the fabric making up the ply layers, and specimens of the Nilos TL-T70 adhesive. The laboratory tests were performed at a test stand equipped with a Zwick universal testing machine (Model Z100/SN3A, 1st class precision), extended with the Aramis 3D optical system of deformation

analysis, the use of which enabled 3D analysis of strain in the tested specimens of the rubber materials (Figure 1). The testing method conformed to standards [30–31].

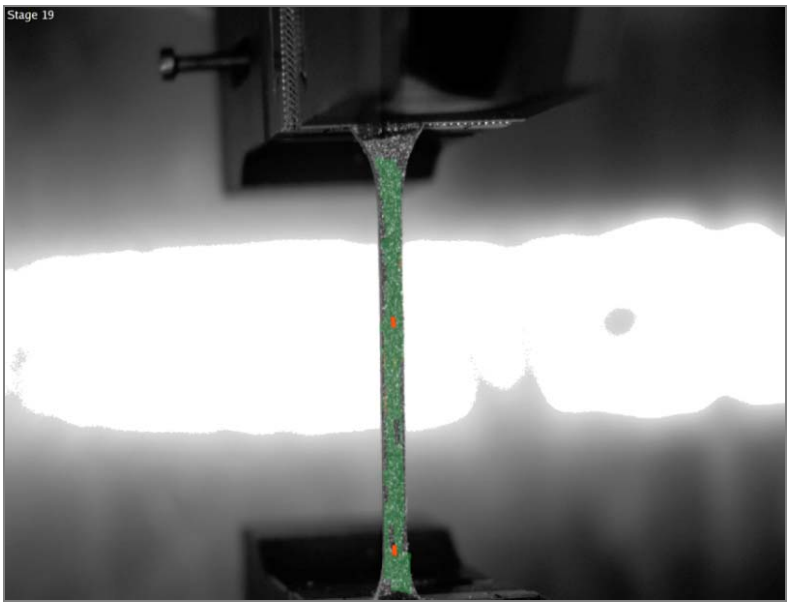

Fig. 1. A camera image from a tensile test – the tested specimen is secured with clamps against the background of reflexes of lighting on the test stand case

On the basis of the conducted tests, after appropriate processing of the measurement data, stress-strain graphs of the analyzed materials were drawn ($\sigma = f(\varepsilon)$, stress as a function of strain) with reference to the actual value of the cross-sectional area of a specimen at any given moment of the tensile test. This was of particular importance in the case of rubber materials.

Rubber, like all construction materials, is characterized by physical properties that specify its quality and operational usability [1–2, 32], however, in engineering practice there often is no possibility to determine those physical properties or to estimate them accurately without using simplifications.

An example of a typical problem in FEM modelling of rubber materials is direct adoption of strength characteristics coming from classical tensile tests which allow calculation of tensile strength, relative elongation at break, the value of breaking force, and stress at a given elongation. In this last case, making calculations solely on the basis of the initial value of the cross-section of a specimen, instead of its actual values at each moment of the tensile test, though in conformity with standards, from the point of view of the requirements of FEM is a simplification that has an important influence on the final result of the analysis due to the specific character of rubber materials, which undergo considerable elongation during tension, and, by the same token, a significant

change in the cross-sectional area of the specimen. That is why it has become necessary to specify the method of measuring the actual cross-section at each moment of a tensile test. Such tests can only be carried out using an optical system recording the changes in specimen geometry during a tensile test (Figure 2).

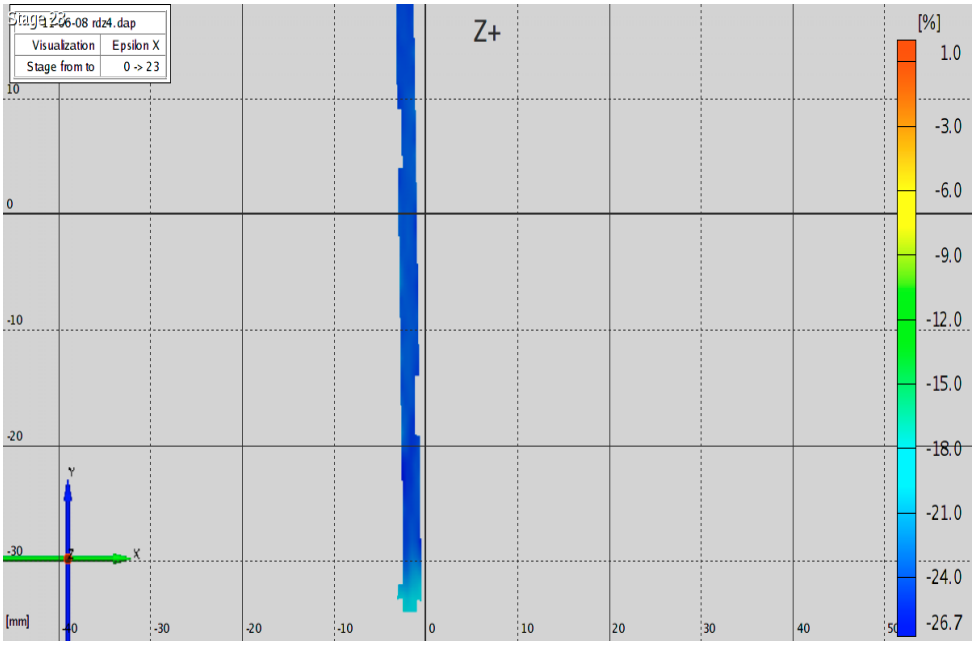

Fig. 2. A percentage change in the specimen's width during tension of rubber at the 25th second of the measurement (the narrowing of the specimen in relation to the initial value is, according to the scale, ca. 27%)

The results obtained during the laboratory tensile tests of the external and internal layer rubbers and the ply fabric of the conveyor belt, to be used in developing a FEM model of the adhesive joint, were first compared and verified using data received from the manufacturer of the belt and were related to the characteristics of the analyzed materials presented in available publications [14, 18, 20–21, 33–34]. Strength tests, analogous to those described earlier, had to be conducted for specimens of the rubber adhesive used in making the joints of the analyzed conveyor belt to specify the features of this material that constituted indispensable input data for the FEM model (Figure 3).

The stress-strain curve obtained for the specimens of the adhesive (Figure 4) during the laboratory tests allowed categorization of this material, according to the characteristics of this type of materials having different mechanical properties [28], within the group of adhesives that are in a state close to high elasticity, which is a typical feature of rubber adhesives.

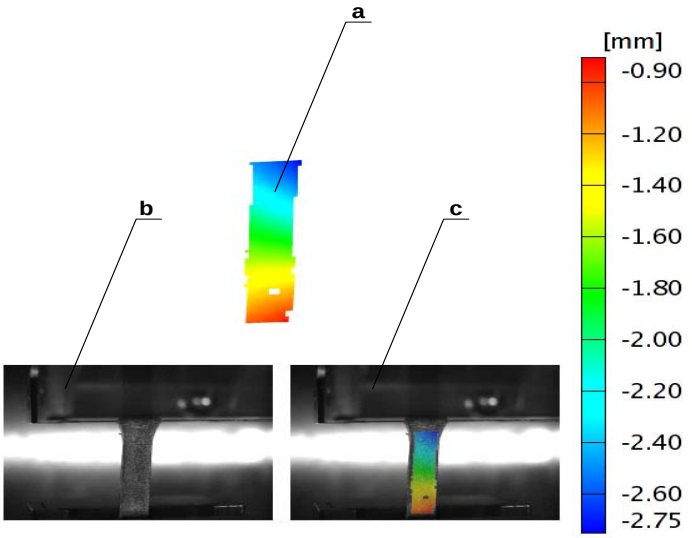

Fig. 3. A visualization of the results of a tensile test of a specimen of an adhesive (an analysis of the elongation of points on the specimen surface in the 23rd second of the test): a) a graphical image of specimen elongation, b) a camera image (specimen between the clamps of the strength-testing machine), c) a graphically transformed camera image

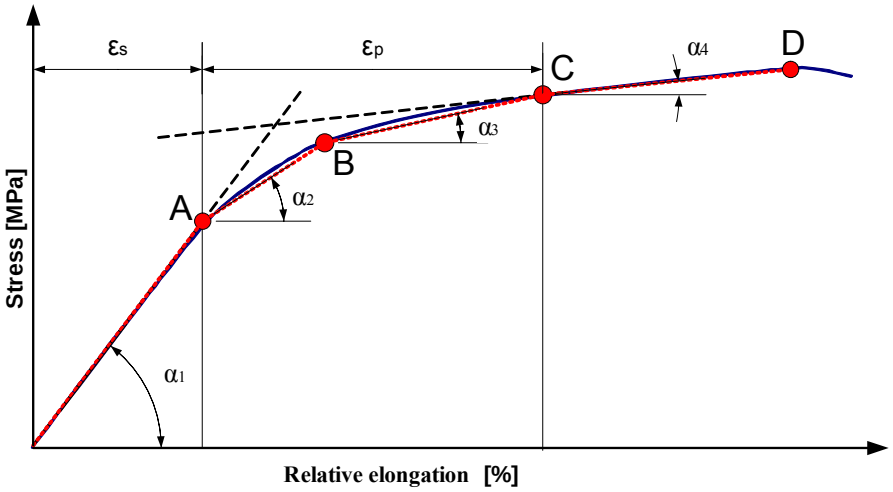

Fig. 4. A graph of stress as a function of strain for a specimen of the TL-T70 adhesive (results of laboratory tests – solid line) and the characteristic adopted for the analysis (line 0-A-B-C-D)

The stress-strain curve for a material of this type is characterized by a significantly smaller slope angle compared with materials in the glassy state and in the state intermediate between glassy and highly elastic, and by high values of maximum relative

strain. In the case of adhesives in the glassy state, this curve goes almost vertically upward to the maximum stress value over a small range of relative strain values to subsequently achieve their maximum values [29].

As stated by R. Sikora [35], materials can have a clearly marked development of high-plastic strains, in which case the yield point is defined by the maximum stress at inflection of the stress-strain curve. Materials, as is the case in Figure 4, can also have a mildly increasing high-plastic strain. In those instances, one speaks of yield strength, which is the stress that causes a small permanent (plastic) deformation in a material, and high-plastic strain is calculated as the sum of elastic strain (ε_s) and plastic strain (ε_p).

When analyzing the strength of adhesive joints under long-term loading or joints manufactured with the use of adhesives exhibiting elastic properties, one must take account of their respective properties in a FEM model. In analyses of adhesive joints, adhesives are commonly assumed to have linear-elastic properties. This, however, encumbers the results with large error. The situation is similar in the case of plastic adhesives, which has a particularly negative effect on the results of their modelling [16]. On account of the above, in the present analysis, interpolation of the stress-strain curve into four straight line segments was adopted (Figure 4), where segment 0-A represents the elastic range of the characteristic of the analyzed material (E = 90 MPa, υ = 0.4), and segments A-B and B-C, with different values of the angle of their depression, model the plastic range, ensuring in this way more precise representation of the strength characteristic of the material in its numerical model. The precision of representation is of particular importance here because it translates into precise modelling of the behaviour of the analyzed material under loading.

Although the problems of rubber materials, their models and the modelling of their behaviours in various structures and conditions have in the recent decade been considered in a number of publications [12, 22, 32, 36–45], still, as pointed out by Diani et al. [22], adequately precise modelling of the behaviour of rubber materials remains an open question. There are several mathematical models describing the behaviour of such materials that had been created since 1940, when Mooney put forward his theory of large elastic deformation, and in subsequent years when Rivlin and Saunders in 1951 studied large elastic deformations of rubber, Blatz and Ko (1993) presented a new form of strain energy function for deformation of rubber materials, Yeoh (1993) proposed a strain energy function characterizing carbon-black-filled rubber vulcanizates, until the end of the 20th century, when Ogden formulated a strain energy function for the description of rubber-like solids capable of nonlinear large elastic deformations based on a strain energy density function. Other constitutive relations are, in turn, based on macromolecular network structure [45], and each of them requires determination of a set of coefficients. The modelling and design of hyperelastic materials, including rubbers, require selection of an appropriate strain energy function and accurate determination of material constants for such a function. In available publications, the hyperelastic materials that are being modelled are, as a rule, selected in an ar-

bitrary way. This is another frequent mistake in FEM analysis which renders modelling results imprecise since rubber is a specific material whose properties are usually quite diverse dependent on its composition or content of special additives [11]. Having at one's disposal data coming from strength tests conducted in the manner described above, one can check experimentally which of the available theoretical models best represents the behaviour of the material being modelled. To that purpose, the available hyperelastic material models had to be tested separately for each constitutive rubber material of the analyzed adhesive joint and the degree of their conformity with experimental data was assessed by analyzing the behaviour of a hyperelastic material in a given case on the basis of the created response curves using selected strain energy potentials for the available test data. Such procedure follows from the fact that hyperelastic materials are characterized in terms of a strain energy potential $U(\varepsilon)$ [11, 36, 43], which defines the strain energy stored in the material per unit of reference volume (volume in the initial configuration).

We have at our disposal a number of forms describing that quantity, which make possible effective modelling of the analyzed grade of materials. These include the Arruda–Boyce form, the Marlow form, the Mooney–Rivlin form, the neo-Hookean form, the Ogden form, the polynomial form, the reduced polynomial form, the Yeoh form, and the Van der Waals form. By assessing the degree of conformity of strength test data with the above-mentioned forms and selecting a model that best represents the measurement data, we can make sure that a reliable numerical model of the analyzed structure is being constructed [11].

6. Conclusion

Correct data concerning the strength features of the constituent materials of a conveyor belt and the adhesives, in particular rubber adhesives, used in joining them are extremely important for accurate development of a FEM model of such structure. As stated in a study by Godzimirski et al. [28], the non-linearity of the $\sigma = f(\varepsilon)$ relation has a significant effect on the strength of adhesive joints and cannot be ignored in the calculations and analysis of joint strength, which also should not use approximate values of mechanical properties as substitutes for their actual values. An accurate description of the strength characteristics of an adhesive also guarantees fewer simplifications or errors in FEM analysis, which are typical of models adopting mean values of the basic strength properties. It is, therefore, important, that identification of the strength features of rubber materials be carried out using strength tests based on a method guaranteeing constant measurement of the cross sectional area of a specimen, for instance in the manner described in the present work.

The laboratory studies described above enabled determination of the exact values of the relevant strength parameters and the appropriate characteristics of the analyzed constituent materials of the conveyor belt and its adhesive-bonded joint to be used in constructing a numerical model.

In the conducted analysis of the strength of the joint, the adhesive was modelled as an elastic-plastic material, assuming the thickness of its layer to be 0.4 mm. Since in many cases natural rubber adhesives are treated as materials with properties similar to rubber, calculations were also made for the adhesive treated as a hyperelastic material conforming to the Mooney–Rivlin model [11, 44–45]. The rubber materials from the external and the interply layers were modelled in accordance with the data determined during the strength tests described above. The results concerning the characteristic points of the tensile test obtained during the laboratory studies are similar to the data cited in the literature and those specified by the manufacturer.

The conducted laboratory studies and the results obtained in them indicate that the data prepared for the numerical modelling of the adhesive joint of a conveyor belt are accurate and provide a basis for developing an adequate numerical model within the framework of the finite element method. In operation of such designed and constructed conveyors we have to solve also several other maintenance and reliability problems [4–6], in which we can be supported by other computer methods including computer based industrial measurement systems and real-time diagnostics [5, 46–47].

Acknowledgement

The research work financed with the means of the State Committee for Scientific Research (Poland) in the years 2007–2010 as a research project.

References

[1] De S.K., White J.R. (eds.): *Poradnik technologa gumy*, Piastów, Instytut Przemysłu Gumowego "Stomil", 2003.
[2] Pękala M., Radkowski S.: *Gumowe elementy sprężyste*, Warszawa, PWN, 1989.
[3] Antoniak J.: *Przenośniki taśmowe w górnictwie podziemnym i odkrywkowym*, Gliwice, Wydawnictwo Politechniki Śląskiej, 2007.
[4] Mazurkiewicz D.: *Monitoring the condition of adhesive-sealed belt conveyors in operation*, Eksploatacja i Niezawodnosc – Maintenance and Reliability, No. 3, 2005, pp. 41–49.
[5] Mazurkiewicz D.: *Computer system for monitoring conveyor belt joints*, Canadian Mining Journal, Vol. 128, No. 4, 2007, pp. 24–24.
[6] Mazurkiewicz D.: *Analysis of the ageing impact on the strength of the adhesive sealed joints of conveyor belts*, Journal of Material Processing Technology, Vol. 208, No. 1–3, 2008, pp. 477–485.
[7] Markiewicz I.: *Projektowanie metodą SADSF i analizy własności sprężystych i zmęczeniowych pasm rozciąganych z otworem*, Eksploatacja i Niezawodnosc – Maintenance and Reliability, No. 1, 2010, pp. 4–14.
[8] Markiewicz I.: *Analiza rozmieszczenia otworów w rozciąganej tarczy z wykorzystaniem metody SADSF oraz szacowanie trwałości zmęczeniowej*, Eksploatacja i Niezawodnosc – Maintenance and Reliability, No. 3, 2009, pp. 24–31.
[9] Ważny M., Jasztal M., Szajnar S.: *CFD-Fastran – narzędzie do numerycznej analizy opływu obiektów przez strumień powietrza*, Eksploatacja i Niezawodnosc – Maintenance and Reliability, No. 4, 2008, pp. 55–62.

[10] Markiewicz I.: *Analiza połączenia spawanego zaprojektowanego metodami nośności granicznej*, Eksploatacja i Niezawodnosc – Maintenance and Reliability, No. 3, 2008, pp. 12–21.
[11] Mazurkiewicz D.: *Problems of numerical simulation of stress and strain in the area of the adhesive-bonded joint of a conveyor belt*, Archives of Civil and Mechanical Engineering, No. 2, 2009, pp. 75–91.
[12] Baldan A.: *Review: Adhesively-bonded joint in metallic alloys, polymers and composite materials*, Mechanical and environmental durability performance, Journal of Materials Science, Vol. 39, No. 15, 2004, pp. 4729–4797.
[13] Dębski H., Rudawska A.: *Analiza rozkładów naprężeń w jednozakładowym połączeniu klejowym*, In: T. Niezgoda (ed.), *Analizy numeryczne wybranych zagadnień mechaniki*, Warszawa, WAT, 2007.
[14] Błażej R.: *Wpływ właściwości mechanicznych rdzenia taśm przenośnikowych tkaninowo-gumowych na wytrzymałość ich połączeń*, Rozprawa doktorska, Wrocław, Politechnika Wrocławska, 2001.
[15] Norma PN-C-94147:1997: *Wyroby gumowe, Połączenia taśm przenośnikowych metodą wulkanizacji*.
[16] Godzimirski J., Rośkowicz M.: *Analiza numeryczna metodą elementów skończonych procesu pełzania spoin połączeń klejowych*, In: T. Niezgoda (ed.), *Analizy numeryczne wybranych zagadnień mechaniki*, Warszawa, WAT, 2007.
[17] Quek M. Y.: *Analysis of residual stresses in a single fibre-matrix composite*, International Journal of Adhesion and Adhesives, Vol. 24, No. 5, 2004, pp. 379-388.
[18] Błażej R., Hardygóra M., Komander H.: *Wpływ wybranych parametrów na trwałość zmęczeniową połączeń wieloprzekładkowych taśm przenośnikowych*, Transport Przemysłowy, No. 3, 2002, pp. 5–9.
[19] Golikov G.F., Ryabov D.V.: *Criteria for assessing the service quality of conveyor belts*, International Polymer Science and Technology, Vol. 2, No. 33, 2006, pp. 59–61.
[20] Kuzmenko V.I., Kiriaz'ev P.M.: *Developing high-strength joints for conveyor belts*, In: Technical, Technological and Economic Aspects of Thin-Seams Coal Mining. (Edit.) E.J. Sobczyk and J. Kicki, London, Taylor & Francis Group, 2007.
[21] Madziarz M.: *Wpływ konstrukcji i technologii wykonywania połączeń tkaninowych, wieloprzekładkowych taśm przenośnikowych na ich wytrzymałość*, Wrocław, Politechnika Wrocławska, 1998.
[22] Diani J., Brieu M., Gilarmini P.: *Observation and modelling of the anisotropic visco-hyperelastic behaviour of a rubberlike material*, International Journal of Solids and Structures, Vol. 43, No. 10, 2006, pp. 3044–3056.
[23] Duncan B.C.: *Test methods for determining hyperelastic properties of flexible adhesives*, CMMT (MN) 054, Published by Crown, 1999.
[24] Gadala M.S.: *Unified numerical treatment of hyperelastic and rubber-like constitutive laws*, Communications in Applied Numerical Methods in Engineering, Vol. 7, No. 8, 1991, pp. 581–588.
[25] Gent A.N.: *Engineering with rubber*, How to design rubber components, Munich, Hanser Publisher, 2001.
[26] Apalak Z.G., Apalak M.K., Davies R.: *Analysis and design of tee joints with double support*, International Journal of Adhesion and Adhesives, Vol. 16, No. 3, 1996, pp. 187–214.

[27] Gładysiewicz L.: *Kierunki optymalizacji transportu taśmowego*, Transport Przemysłowy, No. 1, 2008, pp. 5–9.
[28] Godzimirski J., Kozakiewicz J., Łunarski J., Zielecki W.: Konstrukcyjne połączenia klejowe elementów metalowych w budowie maszyn, Rzeszów, Oficyna Wydawnicza Politechniki Rzeszowskiej, 1997.
[29] Niezgoda T.: *Analizy numeryczne wybranych zagadnień mechaniki*, Warszawa, WAT Publishers, 2007.
[30] Norma PN-EN ISO 283-1:2002: *Metody badań taśm przenośnikowych*, *Oznaczanie wytrzymałości na rozciąganie oraz wydłużenia względnego i wydłużenia trwałego*.
[31] Norma PN-EN ISO 13934-1:2002: *Tekstylia. Właściwości płaskich wyrobów przy rozciąganiu – Część 1: Wyznaczanie maksymalnej siły i wydłużenia względnego przy maksymalnej sile metodą paska*.
[32] Rosłaniec Z., Kwiatkowska M., Kułak W.P., Nastalczyk J., Kwiatkowski K.: *Elastomery termoplastyczne: nowe materiały, właściwości i przetwórstwo*, In: *Elastomery i przemysł gumowy*, Praca zbiorowa, Instytut Przemysłu Gumowego "Stomil", Piastów–Łódź, 2006, pp. 54–84.
[33] Kwon Y., Kwon H., Kim W., Leo S.: *Estimation of rubber material property by successive zooming genetic algorithm*, Journal of Solid Mechanics and Materials Engineering, Vol. 1, No. 6, 2007, pp. 815–826.
[34] Sheppard A., Kelly D., Tong L.: *A damage zone model for the failure analysis of adhesively bonded joints*, International Journal of Adhesion and Adhesives, Vol. 18, No. 6, 1998, pp. 385–400.
[35] Sikora R.: *Tworzywa wielkocząsteczkowe, Rodzaje, właściwości i struktura*, Lublin, Wydawnictwa Uczelniane Politechniki Lubelskiej, 1991.
[36] Ciesielski A.: *An introduction to rubber technology*, Shawbury, Rapra Technology Limited, 1999.
[37] Curley A.J., Hadavinia H., Kinloch A.J., Taylor A.C.: *Predicting the service-life of adhesively-bonded joint*, International Journal of Fracture, Vol. 103, No. 1, 2000, pp. 41–69.
[38] Darwish S.M.: *Analysis of weld-bonded dissimilar materials*, International Journal of Adhesion and Adhesives, Vol. 24, No. 4, 2004, pp. 347–354.
[39] de Moura M.F.S.F., Daniaud R., Magalhaes A.G.: *Simulation of mechanical behaviour of composite bonded joints containing strip defects*, International Journal of Adhesion and Adhesives, Vol. 26, No. 6, 2006, pp. 464–473.
[40] Dorfmann A., Ogden R.W.: *A constitutive model for the Mullins effect with permanent set in particle-reinforced rubber*, International Journal of Solids and Structures, Vol. 41, No. 7, 2004, pp. 1855–1878.
[41] Fung T.C., Soh C.K., Gho W.M., Qin F.: *Ultimate capacity of completely overlapped tubular joints, I – An experimental investigations*, Journal of Constructional Steel Research, Vol. 57, No. 8, 2001, pp. 855–880.
[42] Greve L., Andrieux F.*: Deformation and failure modelling of high strength adhesives for crash simulation*, International Journal of Fracture, Vol. 143, No. 2, 2007, pp. 143–160.
[43] Liljedahl C.D.M., Crocombe A.D., Wahab M.A., Ashcroft I.A.: *Damage modelling of adhesively bonded joints*, International Journal of Fracture, Vol. 141, No. 1–2, 2006, pp. 147–161.
[44] Martins P.A.L.S., Natal Jorge R.M., Ferreira A.J.M.: *A comparative study of several materials models for prediction of hyperelastic properties: application to silicone-rubber and soft tissues*, Strain, Vol. 42, No. 3, 2006, pp. 135–147.

[45] Ruiz M.J.G.M., Gonzales L.Y.S.: *Comparison of hyperelastic material models in analysis of fabrics*, International Journal of Clothing Science and Technology, Vol. 18, No. 5, 2006, pp. 314–325.
[46] Timofiejczuk A.: *Identyfikacja reguł diagnostycznych z zastosowaniem algorytmu ewolucyjnego*, Eksploatacja i Niezawodnosc – Maintenance and Reliability, No. 1, 2008, pp. 11–16.
[47] Batko W., Borkowski B., Głocki K.: *Zastosowanie systemów bazo-danowych w monitoringu diagnostycznym maszyn*, Eksploatacja i Niezawodnosc – Maintenance and Reliability, No. 1, 2008, pp. 7–10.

Problemy identyfikacji właściwości wytrzymałościowych materiałów gumowych na potrzeby analizy numerycznej: przegląd

Odpowiedni dobór elementów przemysłowego połączenia klejowego, składającego się z różnych typów materiałów gumowych, poparty szczegółową analizą zjawisk zachodzących w spoinie, szczególnie w ujęciu zmęczeniowym jest wciąż zagadnieniem bardzo trudnym i nie w pełni rozwiązanym. Tylko pojedyncze prace badawcze wykorzystujące modelowanie numeryczne MES dotyczą prób oceny i analizy zjawisk zachodzących w obszarze złącza gumowej taśmy przenośnikowej. Wynika to z szeregu problemów, uniemożliwiających uzyskanie wiarygodnych i powtarzalnych wyników, jak między innymi zdefiniowanie odpowiednich modeli materiałowych gumy poszczególnych warstw taśmy i złącza, wprowadzających do obliczeń silne efekty nieliniowe. Guma, jako podłoże do klejenia i jednocześnie materiał konstrukcyjny jest specyficznym materiałem, którego właściwości mogą być dość zróżnicowane w zależności od składu, zawartości dodatków itp. Poddawana wulkanizacji mieszanka gumowa składa się, bowiem z jednego lub większej liczby kauczuków oraz różnego rodzaju dodatków kształtujących jej późniejsze właściwości. Dlatego też rozwiązanie problemu prawidłowej identyfikacji właściwości wytrzymałościowych tego typu materiałów w aspekcie budowy poprawnego modelu numerycznego połączenia klejowego jest istotnym zagadnieniem z punktu widzenia przemysłowego zastosowania tej metody łączenia materiałów gumowych. Szczególnie z racji konieczności posiadania wiedzy w zakresie rozwiązywania problemów odpowiedniego użycia właściwego kleju i parametrów połączenia w celu uzyskania optymalnych właściwości i cech eksploatacyjnych złącza. Typowym błędem w przygotowaniu modeli materiałowych dla gumy jest przeprowadzanie prób wytrzymałościowych dla określenia naprężeń i odkształceń w odniesieniu do początkowej wartości przekroju poprzecznego próbki. Duże, nieanalizowane przewężenie próbki w czasie badań wytrzymałościowych w istotny sposób wpływa na niedokładność modelu MES analizowanej konstrukcji. W artykule przeanalizowano ten problem w odniesieniu do modelowania połączenia klejowego materiałów gumowych łączonych klejem kauczukowym, prezentując sposób postępowania przy identyfikacji cech wytrzymałościowych analizowanych materiałów, eliminujący niedokładność modelu MES.

ARCHIVES OF CIVIL AND MECHANICAL ENGINEERING

Vol. X 2010 No. 1

Effect of phosphorus on vacuum carburising depth of iron compacts

K. WIDANKA
Wrocław University of Technology, Institute of Materials Science and Applied Mechanics, Materials Science Division, Wrocław, Poland.

The work was aimed at determining the effect of phosphorus on vacuum carburising of iron compacts with density over 7.2 gcm^{-3}. An attempt was made to determine the effectiveness of phosphorus on carbon diffusion rate into the material of compacts with no additional effect of interconnected porosity. Vacuum carburising of compacts, made with a blend of powders ASC100.29 and PASC60, was carried out at 1050 °C in a laboratory vacuum furnace.

The effect of phosphorus content within 0.1% to 0.6% on the vacuum carburising depth was analysed. It was found that the phosphorus addition up to 0.4% increased the carburising depth by ca. 20% in comparison with the compacts of pure iron.

Keywords: *phosphorus, vacuum carburising, iron compacts*

1. Introduction

In solid structural steels, phosphorus is considered a detrimental impurity. It increases the steel brittleness by increasing the so-called brittle-to-ductile transition temperature. In sintered steel brittleness is mainly caused by pores, so this unfavourable phosphorus effect is invisible. However, other properties of phosphorus are enhanced. It results from the Fe-P equilibrium system that at the sintering temperature it creates with Fe a liquid mixture that intensifies the sintering process. When introducing phosphorus, the sintering process is intensified not only by action of the liquid phase (transition eutectic mixture Fe-Fe_3P), but also by activation of sintering in the created solid solution. At phosphorus concentration over 0.3%, the Fe_α and Fe_γ phases are created at normal sintering temperatures ca. 1150 °C. The α phase, in that the Fe self-diffusion coefficient is ca. 100 times higher than in the γ phase, ensures good sintering of Fe powder grains and the two-phase structure prevents from excessive grain growth occurring in one-phase structure as a result of phosphorus action [1–2]. As a consequence, sinters are obtained with higher strength and ductility in comparison to those of pure iron with identical density. Phosphorus reduces the austenite area and increases ferrite strength by dissolving in it (maximum to 2.8 wt.% at 1050 °C). The phosphorus concentrations most frequently occurring in sintered steels range from 0.3 to 0.6% [3].

Vacuum carburising is very frequently applied to sintered parts because of better control of carburising depth in comparison to traditional gas carburising, which consequently permits obtaining the assumed thickness of the case-hardened layers.
Thanks to its specificity [4–9], this method ensures faster carburisation process, mainly thanks to higher temperature and lower hydrocarbon gas pressure during the process. The carburisation depth depends on carbon diffusion rate into the material. In turn, the carbon diffusion rate depends not only on the process parameters but also to a large extent on the parameters of the processed material. In the case of products made by powder metallurgy, the carburisation depth is decidedly depended, beside chemical composition, on the material density and especially the volume fraction of interconnected porosity.

In this work, an attempt was made to evaluate the effectiveness of phosphorus on vacuum carburising process of iron compacts with density over 7.2 gcm^{-3}. The main purpose was to analyse the sole effect of phosphorus addition on carbon diffusion rate into the material by excluding the effect of interconnected porosity. In the specialist literature, a very small amount of data can be found on phosphorus influence on carbon activity in Fe-C-P alloys. In particular, shortage of experimental data is noticeable. The few existing data, mainly based on theoretical analyses and computer simulations [10–11], seem to confirm increased carbon activity in phosphorus presence. Therefore, it was assumed that increased carbon activity could accelerate its diffusion into the material, resulting in faster and deeper carburisation of iron-based compacts.

2. Material and experimental procedure

Cylindrical test specimens dia. 13 mm × 10 mm were made of mixed powders ASC100.29 and PASC60 (produced by Höganäs AB) by one-side pressing at 800 MPa. 0.6% Kenolube P11 was used as the sliding agent. The 6 lots of specimens (3 ones in each) were prepared, with various phosphorus concentrations within 0.1% to 0.6% P. To compare the results, some specimens of pure iron with density 7.25 gcm^{-3} were prepared. Chemical composition and density of the prepared specimens is given in Table 1. Hardness of the vacuum-carburised specimens was measured using the Vickers method under 1 kG (9.81 N). Microscopic examinations and pearlite content measurements were performed using a computerised imaging system and "Multiscan" software made by Polish company Computer Scanning Systems.

Table 1. Chemical composition and density of examined compacts

Specimen	Chemical composition		Green density [gcm^{-3}]
	wt.% P	wt.% Fe	
Fe-0.1P	0.1	remainder	7.26
Fe-0.2P	0.2		7.25
Fe-0.3P	0.3		7.25
Fe-0.4P	0.4		7.26
Fe-0.5P	0.5		7.25
Fe-0.6P	0.6		7.24

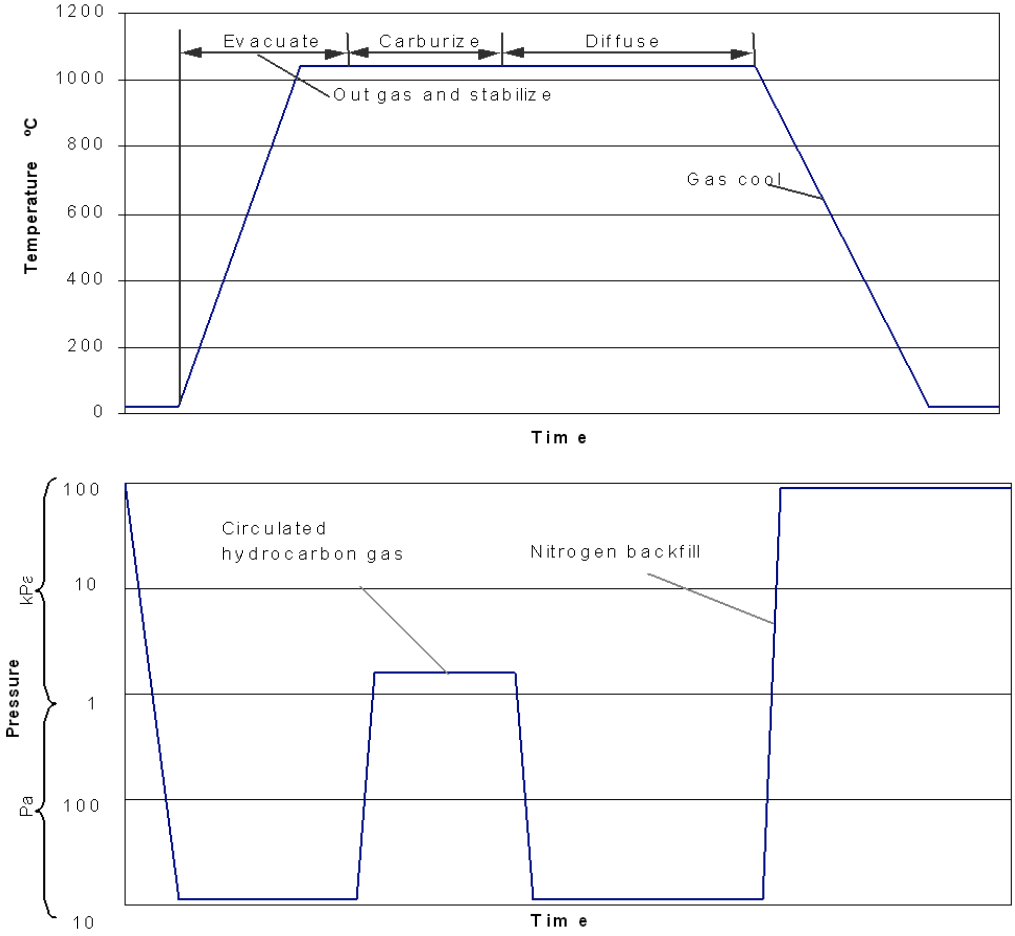

Fig. 1. Vacuum carburising process: a) variation of temperature, b) variation of pressure; (scheme)

The vacuum carburising process was carried out in a laboratory vacuum furnace (Seco/Warwick). The process parameters: temperature and time were 1050 °C and 360 minutes (boost time = 30 min and diffuse time = 330 min).

The carburising atmosphere consisted of propane diluted with nitrogen. Working pressure in the furnace chamber was 20 hPa. Stable working pressure in the chamber during carburising was maintained by cyclical dosing the gas with constant flow rate of 110 dm^3h^{-1}. A schematic diagram of vacuum carburising is shown in Figure 1.

3. Results and discussion

Carburisation depth was determined on the ground of hardness profile in the hardened layer obtained as a result of vacuum carburising. Boundary of the carburised

layer was defined at hardness equal to arithmetic mean of average hardness values of surface layer and core (in the middle of transition zone). The so obtained carburisation depth values and the related hardness values of all the examined specimens are settled in Table 2. The representative hardness profile for Fe-0.4P specimen is shown in Figure 2.

Table 2. Carburisation depth and hardness of phosphorus-containing and pure iron compacts

Specimen	Carburisation depth [mm]	Hardness HV1 (in the centre of transition zone)
Fe-pure	2.8 ± 0.1	101
Fe-0.1P	2.9 ± 0.1	127
Fe-0.2P	3.0 ± 0.1	134
Fe-0.3P	3.2 ± 0.1	145
Fe-0.4P	3.3 ± 0.1	152
Fe-0.5P	3.0 ± 0.1	155
Fe-0.6P	2.8 ± 0.1	152

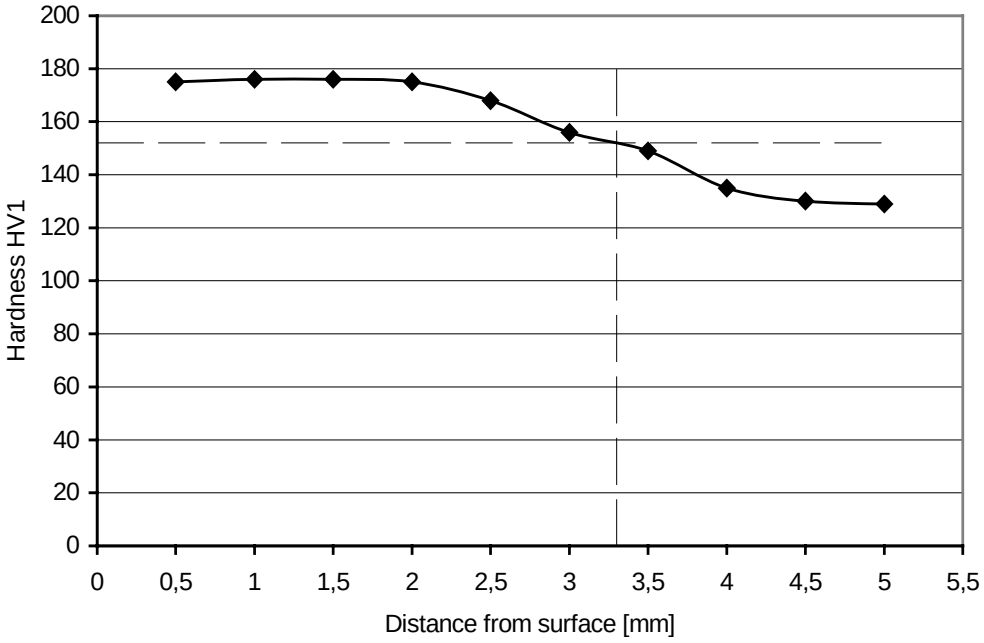

Fig. 2. Hardness profile HV1 for Fe-0.4P specimen

Figures 3 and 4 show representative microstructures of carburised layer and core for the Fe-0.4P specimen. In all the examined specimens, the carburised layer consists of pearlite with ferrite and the core consists of ferrite strengthened with phosphorus only.

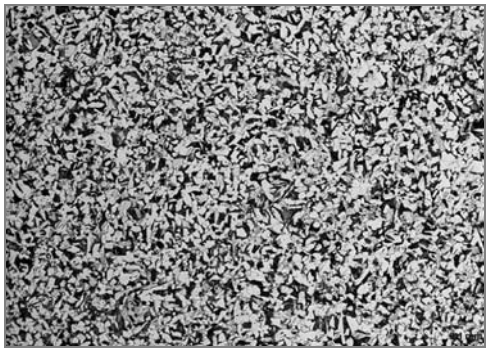

Fig. 3. Case microstructure of specimen Fe-0.4P

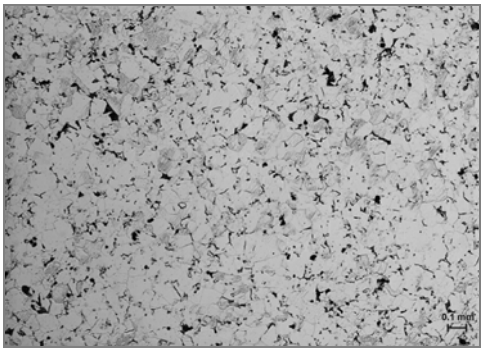

Fig. 4. Core microstructure of specimen Fe-0.4P

Fraction of pearlite in the carburised layer changes gradually with changing phosphorus content from the highest 48% in the Fe-0.1P specimen to the lowest 38% in the Fe-0.6P specimen. The pearlite fractions determined in carburised layers of the examined specimens and their related carbon concentrations are settled in Table 3. The carbon concentrations were calculated accepting 0.77% C in the eutectoidal point and omitting phosphorus effect that shifts it to the left (according to literature data), towards lower carbon concentration. With this effect considered, the calculated carbon concentrations would be slightly lower.

Table 3. Estimated pearlite volume fraction and carbon content in case of examined specimens

Specimen	Pearlite volume fraction [%]	Carbon content [wt. %]
Fe-0.1P	48	0.37
Fe-0.2P	47	0.36
Fe-0.3P	43	0.33
Fe-0.4P	40	0.31
Fe-0.5P	39	0.30
Fe-0.6P	38	0.29

Decrease of pearlite fraction and its related carbon concentration along with increasing phosphorus concentration is a consequence of decreasing carbon solubility in austenite at the carburising temperature of 1050 °C. According to the computed equilibrium diagrams C-Fe-P published in [11], solubility of carbon in austenite at 1050 °C changes from ca. 1.7% for 0.1% P to ca. 1.2% for 0.6% P. In this case, phosphorus behaves like boron, silicon and other elements which intensify carbon activity in austenite and thus reduce surface carbon concentration in the layer during carburisation. Lower surface carbon concentration results in its slower diffusion into the material. The obtained carburisation depths (see Table 2) indicate that, along with phosphorus concentration increasing to 0.4%, thickness of the carburised layer increases in spite of lowering surface carbon concentration in the layer. This increase evidences favourable effect of phosphorus on carbon diffusion rate in austenite, probably by increasing its

diffusion coefficient. Above 0.4% P, thickness of the carburised layer declines. Those results from decreasing surface carbon concentration in the layer due to lower and lower carbon solubility in austenite as well as ferrite that appears beside austenite in the compacts structure. It results from the Fe-P equilibrium diagrams that at the carburisation temperature (1050 °C) within 0.3 to 0.6% P, the two-phase structure consists of austenite and ferrite whose fraction gradually increases along with increasing phosphorus concentration. In the structure containing over 0.3% P, the present ferrite effects probably on slower surface saturation in carbon during carburisation and in consequence reduces carbon stream that should diffuse into the material. The declining carbon solubility in austenite during carburisation (1050 °C) at over 0.3% P can be also evidenced by smaller size of pearlite colonies in comparison to compacts of pure iron and with 0.1 to 0.3% P, as observed in microstructure. In spite of higher phosphorus concentration (conductive to grain growth), less intensive growth of austenite grains at the carburisation temperature in these specimens results probably from lower carbon concentration. Differences in grain size of former austenite are presented in Figures 5 and 6, showing microstructure of carburised layers of the specimens Fe-0.1P (0.1% P) and Fe-0.5P (0.5% P), respectively.

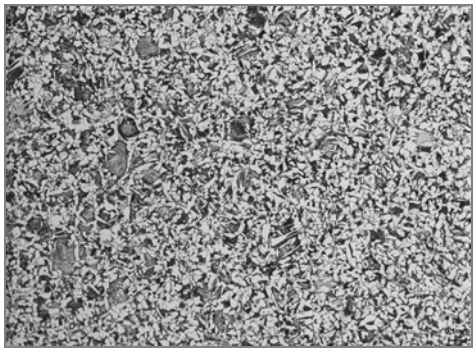

Fig. 5. Case microstructure of Fe-0.1P specimen

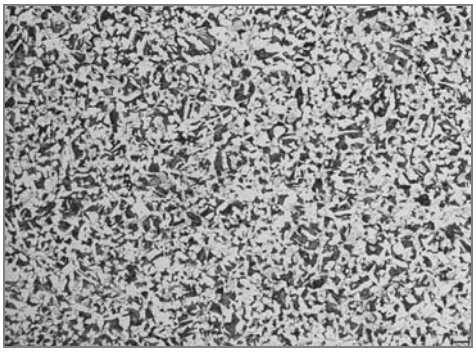

Fig. 6. Case microstructure of Fe-0.5P specimen

4. Conclusions

The obtained results indicate that phosphorus addition up to 0.4% results in deeper carburisation of iron compacts. The largest thickness of carburised layer, ca. 18% more than in pure iron, was found for 0.4% P (specimens Fe-0.4P).

Larger thickness of carburised layer in the phosphorus-containing specimens in comparison to those of pure iron can result from higher carbon diffusion coefficient in austenite, probably as a consequence of higher activity of carbon in the presence of phosphorus.

Analysis of carburised layer thickness depending on phosphorus concentration indicates that it increases till 0.4% P and declines above this value.

This thickness decrease is probably caused by lower and lower surface carbon content in the layer due to higher phosphorus concentration, which is confirmed by gradual increase of ferrite content in carburised layer of the examined compacts.

References

[1] Dautzenberg N.: *Properties of sintered steels made of water atomised prealloyed and alloyed steel powders*, Archiv Eisenhuttennw, 1969, Vol. 40, No. 4, pp. 351–357.
[2] Lindskog P., Carlsson A.: *Sintered alloys on matrix of sponge iron powder with ferro-phosphorus addition*, Powder Metallurgy (polish edition), 1975, Vol. 8, No. 1, pp. 9–15.
[3] Beiss P., Ruthardt R., Warlimont H.: *Powder metallurgy data*, Landolt–Börnstein Online, Vol. 2A1, 2003, Springer Berlin Heidelberg.
[4] Herling D.H., Hansen P.T.: *Heat treating ferrous P/M parts*, Advanced Materials & Processes, 1998, Vol. 153, No. 4, pp. 44CC–44GG.
[5] Herring D.H.: *Pros and cons of atmosphere and vacuum carburizing*, Industrial Heating, 2002, January, pp. 45–48.
[6] Weber R.G.: *Vacuum carburizing and carbonitriding of P/M ferrous alloys*, Int. J. of Powder Metall., 1983, Vol. 15, No. 2, pp. 383–391.
[7] Kula P., Pietrasik R., Dybowski K.: *Vacuum carburizing-process optimisation*, Journal of Materials Processing Technology, 2005, Vol. 164–165, pp. 876–881.
[8] Preisser F., Seemann R., Zenker W.R.: *Update on vacuum-based carburizing*, Advanced Materials & Processes, 1998, Vol. 153, No. 6, pp. 84II–84LL.
[9] Beauchensne D., Kenosha, Wis, Doussot X.: *Vacuum carburizing: A technology whose time has come,* Industrial Heating, 2003, January, pp. 29–33.
[10] Larsen R.M.: *On phosphorus as additive in iron based soft PM magnets*, Powder Metallurgy, 2004, Vol. 47, No. 4, pp. 332–334.
[11] Raghaven V.: *C-Fe-P(carbon-iron-phosphorus)*, Journal of Phase Equilibria and Diffusion, 2004, Vol. 25, No. 6, pp. 541–542.

Wpływ fosforu na głębokość nawęglania próżniowego wyprasek żelaznych

Celem pracy było określenie wpływu fosforu na przebieg nawęglania próżniowego wyprasek żelaznych o gęstości powyżej 7,2 gcm^{-3}. Podjęto próbę oceny efektywności oddziaływania fosforu na szybkość dyfuzji węgla w głąb materiału wyprasek bez dodatkowego wpływu porowatości otwartej. Nawęglanie próżniowe wyprasek, wykonanych z mieszanki proszków żelaza ASC100.29 i PASC60, przeprowadzono w temperaturze 1050 °C, w laboratoryjnym piecu próżniowym. Analizowano wpływ dodatku fosforu, o zawartości z zakresu 0,1–0,6%, na głębokość nawęglania próżniowego badanych wyprasek.

Wykazano, że fosfor dodany do proszku żelaza w ilości 0,4% zwiększa głębokość nawęglania wyprasek o ok. 20% w porównaniu do wyprasek z czystego żelaza.